APPLICATIONS OF TRANSPARENT CONDUCTIVE INDIUM TIN OXIDE FILMS IN AUTOMOTIVE AND VITRIFICATIONS INDUSTRIES

A Thesis submitted to
the graduate school of engineering and science of
İzmir Institute of Technology
in partial Fulfillment of the Requirement for the Degree of

MASTER OF SCIENCE

in Physics

by
Öcal TUNA

June 2009
İZMİR

We approve the thesis of **Öcal TUNA**

Assist. Prof. Yusuf SELAMET
Supervisor

Assoc. Prof. Lütfi ÖZYÜZER
Commitee Member

Assoc. Prof. Metin TANOĞLU
Commitee Member

25 June 2009

Prof. Durmuş Ali DEMİR
Head of the Physics Depertment

Prof. Hasan Böke
Dean of the Graduate
School of Engineering and Sciences

ACKNOWLEDGEMENT

I would like to express my gratitude to all those who gave me the possibility to complete this thesis. Firstly, I would like to thank to my supervisor, Yusuf Selamet for his instructive guidance, stimulating suggestions and encouragement helped me during my master thesis education. I want to thank Dr. Lütfi Özyüzer for his great contribution to impruve my experimental skill and everything for my thesis. I would like to thank Dr. Gülnur Özyüzer for ellipsometry measurement and her attributes during my thesis. I am indebted to the staff of Center for Material Research of IYTE for their patients at my detailed characterizations. This research was supported by Ministry of Industry of Turkey and Teknoma Company so I would like to thank them to let us to study this great research. I also extend my thanks to all former colleagues from Izmir Institute of Technology for their supporting, discussing and comments. I can't find better words to explain my family contribution to my education and explain their love and express my thanks for their helps.

ABSTRACT

APPLICATIONS OF TRANSPARENT CONDUCTIVE INDIUM TIN OXIDE FILMS IN AUTOMOBILE AND VITRIFICATIONS INDUSTRIES

Due to its unique electrical and optical properties, highly doped n-type Indium tin oxide used for various applications such as smart glass, LCDs, OLEDs, solar cells and car windows. In this study Indium Tin Oxide (ITO) thin films were grown by both DC and RF magnetron sputtering techniques. To know deposition rate of ITO, system was calibrated for both DCMS and RFMS and then ITO were grown on glass substrate with the thickness of 70 nm and 40 nm by changing substrate temperature. The effect of substrate temperature, film thickness and sputtering method on structural, electrical and optical properties were investigated. Wan der Pauw method was used for electrical characterization and to use this method properly, we patterned ITO thin films by photo-lithography and Ion beam etching techniques. The results show that substrate temperature and film thickness substantially affects the film properties, especially crystallization and resistivity. The thin films grown at the lower than 150 ^{o}C showed amorphous structure. However, crystallization was detected with the further increase of substrate temperature. Substrate temperature and film thickness increment were lead to increase band gap of ITO which can be explained by BMS. Band gap of ITO was calculated to be about 3.64 eV at the substrate temperature of 150 ^{o}C, and it widened with substrate temperature increment. From electrical measurements the resistivity at room temperature was obtained 1.28×10^{-4} and 1.29×10^{-4} Ω-cm, for DC and RF sputtered films, respectively. We also measured temperature dependence resistivity and the Hall coefficient of the films, and we calculated carrier concentration and Hall mobility.

ÖZET

İNDİYUM KALAY OKSİT İLETKEN SAYDAM FİLMLERİNİN OTO VE VİTRİFİYE SANAYİSİNDEKİ UYGULAMALARI

Yüksek oranda kalay atomunun empose edilmesi ile elde edilen İndiyum kalay oksit ince filmleri kendine özgü elektriksel ve optik özelliklerinden dolayı birçok alanda kullanılmaktadır örneğin; akıllı cam, LCD ekranlarda geçiş elektrodu, güneş enerji sisteminde geçiş elementi, OLED' lerde ve araba camlarında. Bu çalışmada İndiyum kalay oksit ince filmleri DC ve RF sıçratma yöntemleri kullanılarak 1 mm kalınlığa sahip cam üzerine büyütüldü. Her iki sistem içinde büyüme hızının tayini yapıldı ve 70 nm ve 40 nm kalınlığa sahip filmler altlık sıcaklığını değiştirerek büyütüldü. Altlık sıcaklığının, film kalınlığının ve kullanılan sistemin (DC/RF) filmin kristallenmesi, elektriksel ve optiksel özellikleri üzerine etkisi çalışıldı. Elektriksel ölçümler van der Pauw yöntemi kullanılarak yapıldı ve bu yöntemin uygun bir şekilde kullanılması için filmler şekillendirildi bunun için photo-lithography ve ion beam etching teknikleri kullanıldı. Elde edilen sonuçlardan altlık sıcaklığının ve filmin kalınlığının filmin özelliklerini büyük oranda etkilediği özellikle kristallenme ve özdirenç üzerine etkisinin çok olduğu gözlendi. Altlık sıcaklığının 150 ^{o}C daha düşük olduğu durumlarda filmin amorf yapıya sahip olduğu ve artan sıcaklıkla birlikte kristallenmelerin başladığı gözlendi fakat kullanılan sisteme göre (DC/RF) kristallenmenin yönünün farklı olduğu gözlendi. Altlık sıcaklığı ve film kalınlığındaki artış ITO ince filimlerinde band aralığının artışına neden olduğu gözlendi örneğin altlık sıcaklığının 150 ^{o}C olduğu durumda band aralığı 3.64 eV olarak hesaplanırken sıcaklığının artması bu değerin artmasına neden oldu ve bu durum burstain-moss shift ile açıklanmaktadır. Elektriksel ölçümlerin sonucunda oda sıcaklığında özdirenç değerleri sırasıyla DC ve RF sıçratma yöntemleri için 1.28×10^{-4} ve 1.29×10^{-4} Ω-cm bulundu. Bu çalışmada sıcaklığa bağlı özdirenç ölçümleri ve Hall katsayısı ölçümleri de yapılarak film içerisindeki taşıyıcı yoğunluğu ve taşıyıcı hızı hesaplandı.

TABLE OF CONTENTS

LIST OF FIGURES ix

LIST OF TABLES xii

CHAPTER 1. INTRODUCTION 1

1.1. Indium Tin Oxide (ITO) 1

1.2. Material Types 3

1.2.2. Insulators 4

1.2.3. Semiconductors 4

1.2.3.1. Intrinsic Semiconductors 6

1.2.3.2. Extrinsic Semiconductors 6

1.2.4. Degenerate and non-degenerate semiconductors 8

1.2.5. Doping concentration 8

1.2.6. Bandgap widening and narrowing 11

1.2.7. Scattering machanism in semiconductors 12

1.3. Aplications of ITO 14

1.3.1. Solar Cell 14

1.3.2. Smart Glasses 16

1.3.3. Organic Light Emitting Diodes 18

1.3.4. Liquid Crystal Displays 19

CHAPTER 2. BACK GROUND OF ITO 21

2.1. Background of ITO 21

2.2. Thin Film Deposition Methods 25

2.2.1. Direct Current Magnetron Sputtering 25

2.2.2. Radio Frequancy Magnetron Sputtering 26

2.2.3. Thermal Evaporation 26

2.2.4. Chamical Vapor Deposition 27

2.2.5. Ion Beam Sputtering 27

CHAPTER 3. EXPERIMENTAL 28

3.1. Purpose 28

3.2. Growth of Indium Tin Oxide 28

3.3. Large Area Coating Magnetron Sputtering 32

3.4. Patterning of Films 35

3.5. R-T and Hall Effect Measurements 39

CHAPTER 4. RESULT AND DISCUSSION 45

4.1. XRD Results 45

4.2. Scanning Electron Microscopy and Atomic Force Microscopy Results 49

4.3. Electrical Results 50

4.3.1. Substrate Temperature Dependence Resistivity 50

4.3.2. Measurend Temperature Dependence Resistivity 52

4.3.3. Variation of Hall Coefficient with Temperature 54

4.3.4. Substrate Temperature Dependence of Carrier Concentration and Hall Mobilities 55

4.4. Optical Results 58

4.4.1. Optical Transmission of Indium Tin Oxide Thin Films 58

4.4.2. Bandgap of Indium Tin Oxide Thin Films 61

4.5. Large Area Coating Magnetron Sputtering Results 67

4.5.1. X-Ray Diffiraction Result of Annealed LA-ITO Samples 67

4.5.2. Electrical Results 68

4.5.2.1. Room Temperature Resistivity versus Annealing Temperature 68

4.5.2.2. Temperature Dependence Resistivity 68

4.5.2.3. Temperature Dependence Hall Coefficient 69

4.5.2.4. Carrier Concentration and Hall Mobilities versus Annealing Temperature 70

4.5.3. Optical Results 71

4.5.3.1. Optical Transmission of LA-ITO Thin Films 71

4.5.3.2. Annealing Temperature Dependence Band Gap of LA-ITO Thin Films 72

CHAPTER 5. SUMMARY AND CONCLUSION 74

REFERENCES 76

LIST OF FIGURES

Figure **Page**

Figure 1.1. In_2O_3 crystal structure 2
Figure 1.2. a,b) two indium sites of ıto films and c)combination of these two sites 3
Figure 1.3. The band structure of conductor, semiconductor and insulator 5
Figure 1.4. Intrinsic semiconductor, n type semiconductors and p type extrinsic semiconductors, respectively. 7
Figure 1.5. the experimental and calculation of the carrier concentration as a function 10
Figure 1.6. Schematic band structure of tin oxide which has a parabolic conductionand valance bands separated by the band gap e_g after heavy doping there is a bandgap widening due to filling lowest energy state of conduction band by carriers, band gap narrowing is occur due to further increased of carrier concentration. 12
Figure 1.7. Figure of scattering mechanism in semiconductor grain boundary scattering and ionized impurity scattering, respectively. 13
Figure 1.8. Schematic of solar cell: 1. solar, 2. n-type semiconductor (generally ıto), 3. p-type semiconductor, 4. holes, 5. basic circute 16
Figure 1.9. Basic configuration of smart glass. 17
Figure 1.10. Schematic of a 2-layer oled: 1. cathode (−), 2. emissive layer, 3. emission of radiation, 4. conductive layer, 5. anode (+)..............................18
Figure 1.11. Schematic of a lcd: 1. polarizer, 2. glass substrate, 3. seal, 4. spacer, 5. ıto, 6. hard coat, 7. polyimide, 8. tft 20
Figure 3.1. The schematic_representation of sputtering process 30
Figure 3.2. The schematic represantation of growth chamber 31
Figure 3.3. Large area coating magnetron sputtering system 31
Figure 3.4. Ito coated large area glass substrate 31
Figure 3.5. The various mask shapes for van der pauw method 35
Figure 3.6. The schematic representation of photolithographic processes 37
Figure 3.7. Ion beam system 37

Figure 3. 8. After etching process, After coating gold by thermal evaporation, Taking contact on gold pallete with high purity In and thin Cu wire, respectively. 38
Figure 3. 9. Evaporation system 38
Figure 3. 10. The schematic represantation of our Cryostat system.. 39
Figure 3. 11. The Hall effect as it is used for the van der Pauw configuration 41
Figure 3. 12. Schematic represantation of our experimental method for resistivity and Hall effect measurement.. 42

Figure 4. 1. The X-ray diffraction patterns of 70 nm thick ITO films grown by RF sputtering at various substrate temperatures……………………………........46
Figure 4. 2. The X-ray diffraction patterns of 70 nm thick ITO films grown by RF sputtering at various substrate temperatures (T_s is substrate temperature, *t* isthe film thickness). 47
Figure 4. 3. The X-ray diffraction patterns of 40 nm thick ITO films grown by DC sputtering at various substrate temperatures (T_s is substrate temperature, the film thickness). 47
Figure 4. 4. The X-ray diffraction patterns of 40 nm thick ITO films grown by RF sputtering at various substrate temperatures (T_s is substrate temperature, *t* is the film thickness). 48
Figure 4. 5. Comparision of thickness effect on crytallization both for DCMS and RFMS samples. 48
Figure 4. 6. SEM cross-section image of ITO (80 nm)/SiO_2.. 49
Figure 4. 7. AFM image of ITO (80nm) /SiO_2 50
Figure 4. 8. Variation of DSMS grown samples electrical resistivity with respect to substrate temperature 51
Figure 4. 9. Variation of RFMS grown samples electrical resistivity with respect to substrate temperature. 52
Figure 4. 10. Variation of electrical resistivity of ITO thin film with respect to temperature (resistivity values were normalized with respect to the measured values of 286 K).. 53
Figure 4. 11. Variation of electrical resistivity of ITO thin film with respect to temperature (resistivity values were normalized with respect to the measured values of 286 K).. 54

Figure 4. 12. Variation of hall coefficient of to thin films with respect to temperature 55
Figure 4. 13. Variation of carrier concentration and hall mobilities of dc sputtered to thin films with respect to the substrate temperature........ 57
Figure 4. 14. Variation of carrier concentration and hall mobilities of rf sputtered to thin films with respect to the substrate temperature........ 57
Figure 4. 15. Transmittance spectrum of 70 nm and 40 nm thick dc sputtered to thin films grown at different substrate temperatures (*t* is thickness). 59
Figure 4. 16. Transmittance spectrum of 70 nm and 40 nm thick rf sputtered to thin films grown at different substrate temperatures (*t* is thickness). 60
Figure 4. 17. Plot of α^2 versus $h\upsilon$ for dcms samples with thickness of 70 nm and 40 nm grown at various substrate temperatures (*t* is thickness). 63
Figure 4. 18. Plot of α^2 versus $h\upsilon$ for rfms samples with thickness of 70 nm and 40 nm grown at various substrate temperatures (*t* is thickness). 64
Figure 4. 19. Variation of band gap with respect to substrate temperature dcms samples, rfms samples 65
Figure 4. 20. X-Ray Diffiraction Results of LA-ITO Thin Films 67
Figure 4. 21. Annealing temperature dependence resistivity of LA-ITO thin films 68
Figure 4. 22. Temperature dependence resistivity of annealed LA-ITO 69
Figure 4. 23. Temperature Ddependence Hall Coefficient of LA ITO Thin Films........ 70
Figure 4. 24. Variation of carrier concentration and Hall mobilities with annealing temperature 71
Figure 4. 25. Transmission spectrum of LA-ITO thin films........ 72
Figure 4. 26. Absorption coefficient versus energy gap of LA-ITO samples 73
Figure 4. 27. Variation of bandgap of LA-ITO thin films versus annealing temperature........ 73

LIST OF TABLES

Table **Page**

Tablo 2. 1. Typical electrical and optical properties of ITO deposited by various techniques 22

Tablo 3. 1. Growth parameters for DC and RF magnetron sputtering 32

Tablo 3. 2. Crosspoint Summary for Resistivity Measurement...................................... 43

Tablo 3. 3. Crosspoint Summary for Hall Voltage Measurement 44

Tablo 5. 1. Properties of the DCMS/RFMS sputtered ITO thin films. (T_s substrate temperature, E_g band gap, ρ resistivity, n carrier concentration, μ Hall mobility, d grain size. Note that : The results are for 70 nm thick samples... 66

CHAPTER 1

INTRODUCTION

1.1. Indium Tin Oxide (ITO)

When the first reports of transparent and conductive cadmium oxide films first appeared at 1907, studying on transparent conductors has rapidly increased (Jianming 2005) Among the various transparent conductors such as zinc oxide, cadmium oxide, cadmium tin oxide, indium oxide, Tin doped Indium Oxide shows better properties in terms of electrical and optical properties. In nature Indium Oxide (In_2O_3) is a very interesting semiconductor materials due to it behaves as a insulater in its stoichiometric form and as a highly conducting semiconductor with a wide direct optical band gap nearly 3-4 eV in its non-stoichiometric form which is providing high transparency in the visible light range and higly reflectivity in the infraret light range (Chrisa 1998). After doping In_2O_3 with tin atoms, both electrical and optical properties increased and these two unique combination has led numerous researcher to a thorough investigation of the growth and characterization of transparent semiconducting indium tin oxide and also due to its unique properties, it is used so many areas such as transparent electrodes in LCDs (Brauer 1999), organic light emitting diodes (Reddy, et al. 2006), solar cells (Zhou, et al. 2005), plasma display panels (Whang, et al. 2005), transparent heat reflecting windows as well as surface heating for cameras, lenses, mirrors and car windows (Brauer 1999), gas sensors (Comini, et al. 2001), ohmic contact to surface-emitting diodes. (Matin, et al. 1994, Tang. et al. 2003). I will mention some of these aplications in the next chapter.

The unique properties of ITO come from its structure and composition. As I said above, ITO can be obtained doping In_2O_3 with tin (S_n) atom as extrinsically. In this porpuse the structure of Indium Oxide should be explained. The structure of Indium Oxide is cubic bixbyte shown in figure 1.1. One unit cell of ITO include 16 units of

In_2O_3 and therefore 32 metalic atoms and 48 oxygen atoms with respect to 2/3 cation/anion ratio and hence 80 atoms located in per unit cell. There are two types of localization occur in Indium Oxide structure which are called b-site crystallization and d-site crystallization which was carried out by Marezio 1965. It is shown in figure 1.2a, oxygen atoms are positioned at the corner of the cube with two body-diagonally corner unoccupied. In figure 1.2b, oxygen atoms occupy positions at the corner of the cube with two face-diagonally opposite corners unoccupied. In figure 1.2c the combination of these two types of structures are shown. X-ray diffraction analysis which was carried out by Marezio 2005. on single crystal of In_2O_3 showed that the separations of In-O are 2.18 Å for b-site and 2.13, 2.19 and 2.23 Å for d-side crystal structure shown in figure 1.2 (a). and figure 1.2b, respectively and the lattice parameter of In_2O_3 is 10.12 Å. The reason of this difference is repulsive forces that come from the two unoccupied corners of the lattice (Chrisa 1998). It is obviously can be explained that both indium sites can be viewed as an incomplete body centered cubic structure with an indium atom located in the center and oxygen atoms at the corners.

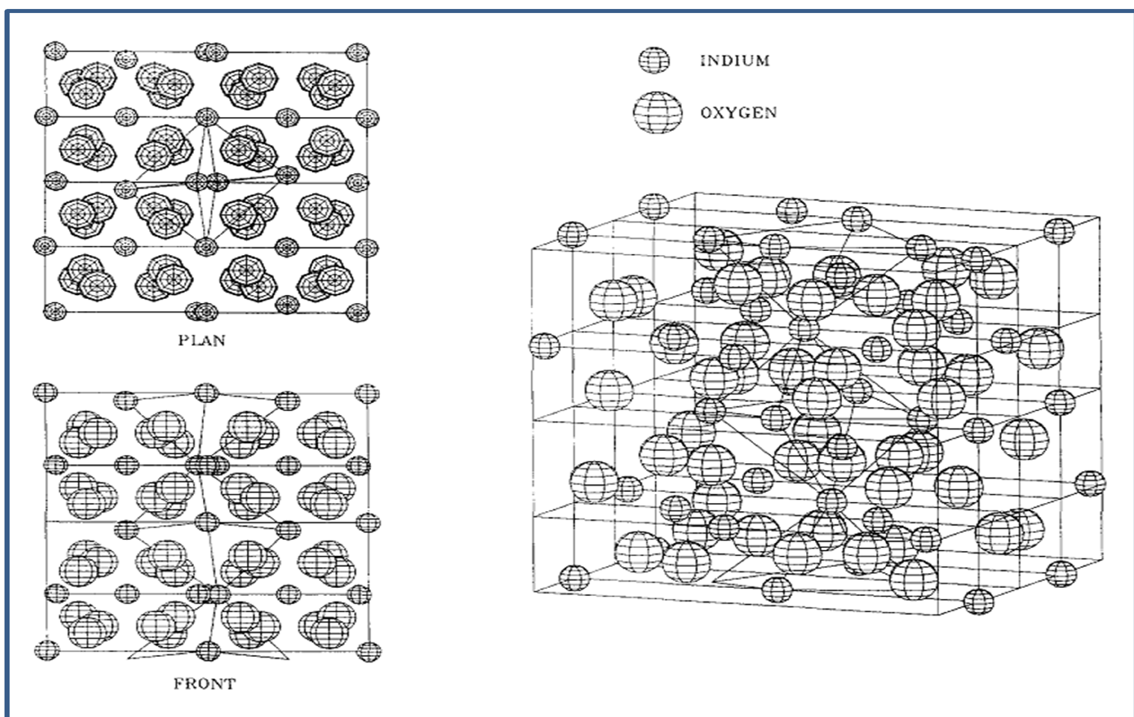

Figure 1. 1. In_2O_3 Crystal structure
(Source : Jianming 2005)

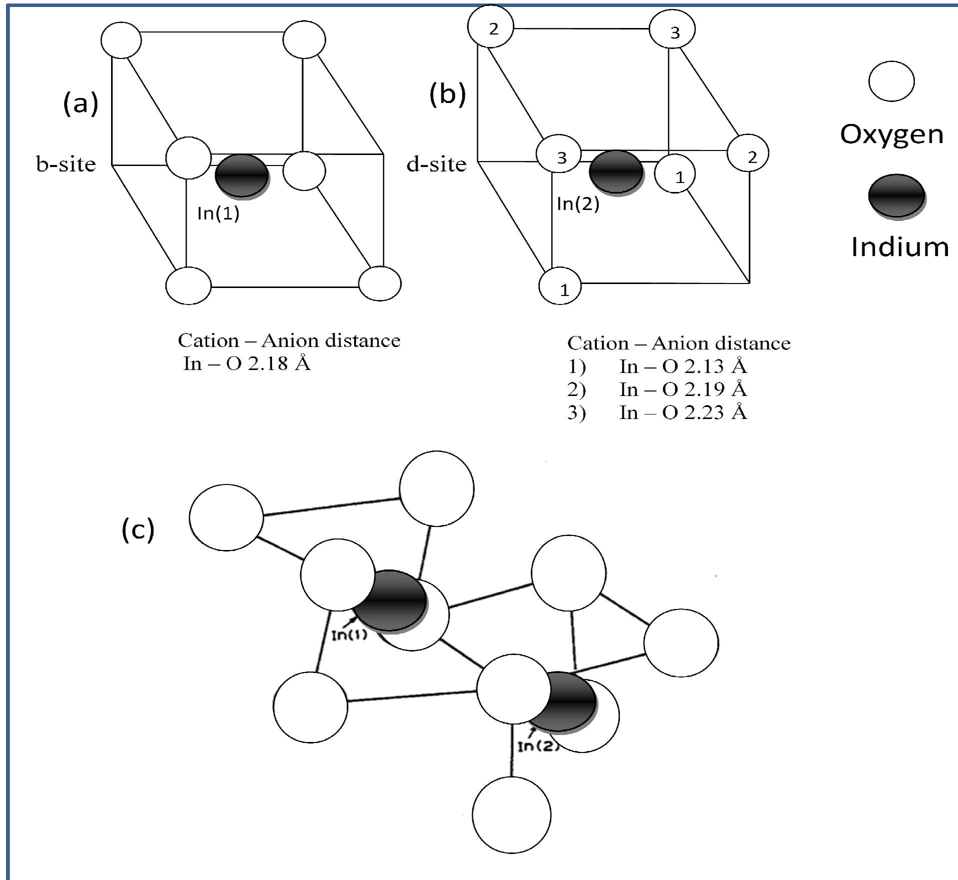

Figure 1. 2. Two indium sites of ITO films (a,b) and combination of these two sites (c) (Source : Marezio 1965)

1.2. Material Types

As I mentioned before Indium Oxide (In_2O_3) is a semiconductor and semiconductors are materials which have intermediate electrical conductivity between conductors and insulators. I will give a brief explanation of conductors, insulators and semiconductors.

1.2.1. Conductors

An electrical conductor which is permit electrons to flow through easily it means that there is no resistivity against electrons motion. Such as metals are very good conductor due to the fact that the energy level between the conduction and valans band is very close and in most cases the conduction and valans band is overlapped. The band gap of conductor is shown figure 1.3a.(Kittel 2004).

1.2.2. Insulators

Insulator is a material opposed to conductor because of the fact that it is genarally made of non metals that have very few or no free electron and it has very high band gap between conduction and valans bad which is in the range of 4 - 5.5 eV. The band gap of insulator is shown figure 1.3c. (Kittel 2004).

1.2.3. Semiconductors

Semiconductor is a material which has electrical properties between insulator and conductor. In semiconductors the electrons can be easily excited from valans band to conduction band due to the fact that it has small band gap energies less than 3 eV between valans and conduction band. In semiconductors as electrons excited conduction band from valans band it leads to icreasing conductivity and directly decreasing resistivity which is in the range of 10^{-2} - 10^{-4} Ω-cm. In fact in semi conductors there is a limited free electrons and it depends on the crystal structure of material used. The band gap structure of semiconductor is shown in figure 1.3b. (Kittel 2004).

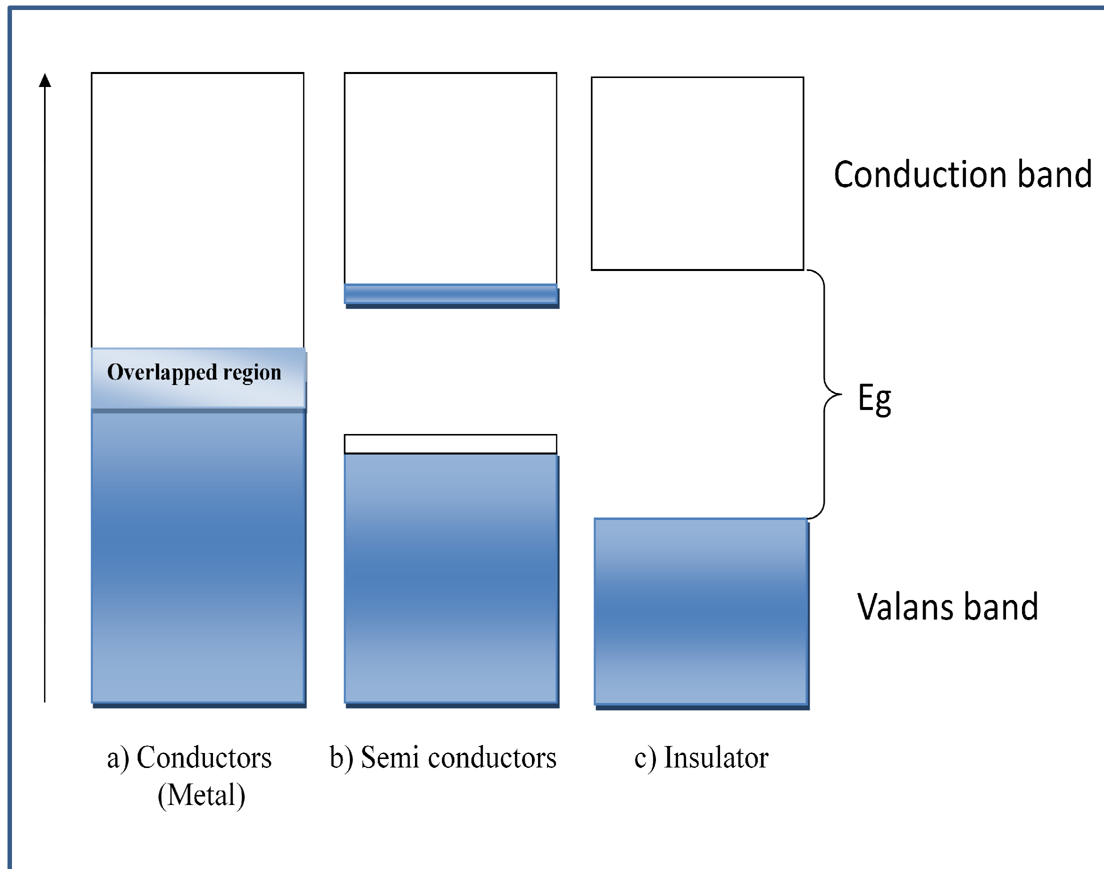

Figure 1. 3. The band structure of conductor, semiconductor and insulator

The most important diferences between semiconductor and conductor is that at absulute zero temperature in semiconductor the uppermost filled elecron energy band is fully filled but in conductor it is partially filled. The reason of this difference may be due to there is no enough number of electrons to fill the number of energy bands in conductor or the highest occupied energy band overlaps the next higher band without an intervening energy gap. At absolute zero temperature, the electrons occupy starting from the lowest possible energy state with the restriction of only two electron with the opposite spin may be in the same energy level. In addition to this semiconductor is distinguished with conductor and insulator with respect to band gap widening. The band gap of conductors are as small as electrons can be populated in conduction band at room temperature but for insulators it seems impossible due to large band gap. At low temperature conducticvity of semiconductors approach insulator while at high temperature it acts as a metal because at low temperature energy of electrons in valans

band gain the enough energy to be raised to the conduction band easily hence it behaves as a conductor.

The important thing for semiconductors is that the electrical properties of it can be changed in a controllable way by adding small amount of impurities which are called dopants. In this purpose I will explain two types of semiconductors that the first one is intrinsic semiconductor and the second one is extrinsic semiconductor.

1.2.3.1. Intrinsic Semiconductors

Intrinsic semiconductor is called as an undopped semiconductor due to it is pure semiconductor. Its all properties come from the material which are made by such as the number of charge carriers depends on the material properties. The conductivity supplied in this semiconductor by thermally excitated electrons from valance band to conduction band and when the electron exceed conduction band it leaves behind a vacancy which may be filled be a another electron. This vacancy which is called as hole also support conductivity but it moving the opposite direction with electrons when apply an electric field. As it can be clearly communicable that if there is an electron in the conduction band there should be a hole in the valance band hence the number of electrons and the number of holes are equal in intrinsic semiconductors. The basic figure is shown in figure 1.4a.

1.2.3.2. Extrinsic Semiconductors

An extrinsic semiconductors can be explained in the manner of doped atoms. Doping is the prosess that change an intrinsic semiconductor with an extrinsic one. During doping extrinsic atoms displace the intrinsic atoms or make a compound with it. Depend on the number of valans electron of doped atoms which is different from

intrinsic atoms, it change the dominant carrier concentration in an extrinsic semiconductor and classify carrier charge either an n type or p type. If the number of valans electron of doped atoms higher than intrinsic atoms valans electrons, the extrinsic semiconductors charge cerriers are electrons and that type of semiconductor called as n type semiconductor and mojority carriers are electrons. It is shown in figure 4b that there is a free electron not bound intrinsic atoms valans electrons. On the contrary, if valans electrons number of doped atoms are lower than intrinsic atoms valans electrons, the extrinsic semiconductor charge carriers are holes and that type of semiconductors are called as p-type semiconductors and majority carriers are holes. In fact holes are not move in semiconductor but neighboring electron move to fill the hole and leaving a new hole behand where it comes hence this way holes appear to move. There is a hole seen in figure 1.4c. that one unbound band in doped intrinsic semiconductor.

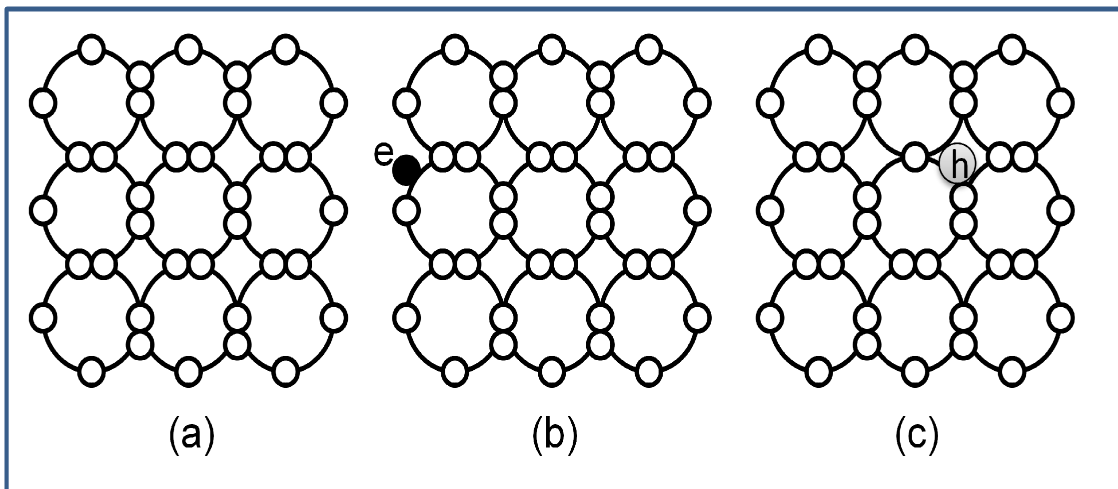

Figure 1. 4. Intrinsic semiconductor, n type semiconductors, p-type extrinsic Semiconductors, respectively.

1.2.4. Degenerate and Non-Degenerate Semiconductors

Depends on the doping concentration, semiconductors can be saperated into two group. The first one is nondegenerate semiconductor and the other is degenerate semiconductor. In the first case, if the doping concentration of impurity atoms is small when we compare it with host atoms or semiconductor atoms, it calls as non-degenerate semiconductors. When the doping concentration is small, the dopands are spread far enough so there is no interaction between donor electrons and they are discrete. Due to the fact that the levels are noninteracting and discrete, this semiconductor laballed as nondegenerate semiconductors. If the doping level increased the discrete of impurity atoms decrease and the donor electrons will interact with each other. When this occur the single discreate donor energy will split into a hand of energies. With the further increase of impurity atoms, the donor state widen and may overlaps the bottom of the conduction band. The overlaps occur when the concentration of impurities comparable with the density of states. If fermi level lies within the conduction band due to high level of electron concentration, this type of semiconductor called as n-type degenerate semiconductors. In a similar way, as the acceptor doping concentration increases in a p-type semiconductor, the discrete acceptor energy states will split into a band of energy and with the further increase of doping it may overlap the top of the valence band. The fermi level will lie in the valence band, when the concentration of the holes exceed the density of states. This type semiconductor called as a p-type degenerate Semiconductors (Donald 1997).

1.2.5. Doping Concentration

Finding a material with the properties of good transparancy and high conductivity simultaneously is difficult. The only way to have these properties are creating electron degeneracy with a wide band gap greater than 3eV by controllably

doping with suitable dopants (Shabbir 1998). For the point of wiev In_2O_3 doped with tin atoms. This extrinsic doping change the electrical properties of indium oxide significantly and the crystal structure is not change and it keep its structure as cubic bixybyte. During doping tin atoms will replace indium atoms and form tin oxide in either SnO and SnO_2 depending on valans of +2 and +4, respectively. These valence state is directly contribute to the conductivity of ITO. When it is form as SnO, it behaves as an acceptor because it accept electron. In the second case it may form SnO_2 and for this stuation it behaves as a donor due to it gives of electron. In the first case there are same hole create and these holes leads to reducing electron concentration due to vacancies traps electrons. The second case is the main source of electron concentration in ITO because of it gives off electrons in the conduction band. It can be conclude that the second case is dominant ionization state of Sn in ITO. This is to be expected since SnO_2 is more stable than SnO and the lattice parameter of SnO_2 (10.330 Å) is larger than of In_2O_3 (10.118 Å), the replacement of In^{+3} by Sn^{+4} is leading to expantion of lattice (Akkad, et al. 2000) After combining Tin atoms with Indium oxide atoms the new materials occured expressed as $In_{2-x}Sn_xO_{3-2x}$. (Shabbir 1998). As I said before doping rate is critical for electrical properties of ITO and the most suitable doping concentration is 10:90 SnO_2 and In_2O_3, respectively. The carrier concentration as a function of tin doping level is well illustrated in figure 1.5. which is showed by Elfallal and Hill 1993.

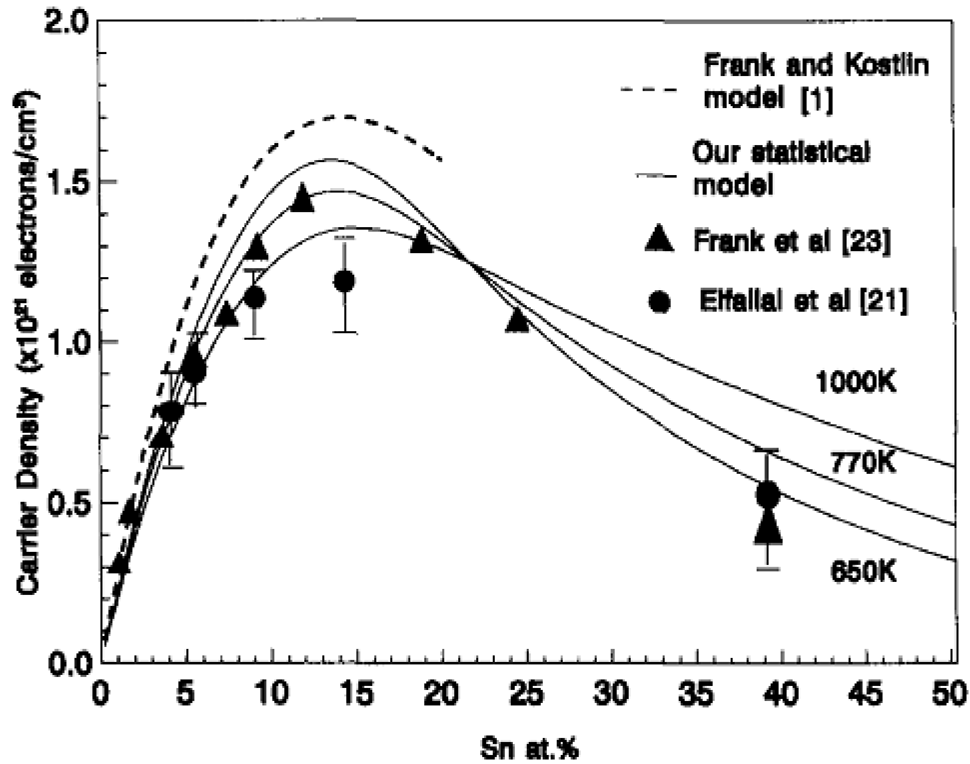

Figure 1. 5. The experimental and calculation of the carrier concentration as a function of tin doping level (Elfalla 1993)

It is obviously seen in figure 1.5 that as the tin concentration increases, the carrier concentration increase until a saturation level about 10% tin atoms. An increase in the tin concentration above this saturation level leads to decreasing free carrier concentration. Its reason is that the probability of occupation of adjacent cation positions by two or more tin atoms which can deplate the active tin concentration and also distort the lattice structure due to extra tin atoms may penetrate into the lattice structure. This doping level will produced degenerative ITO which is contribute highly to conductivity of ITO (Gupta, et al. 1998, Sanon, et al. 1991)

1.2.6. Bandgap Widening and Narrowing

Bandgap of a semiconductors are changed by highly doping it with a suitable dopant and bandgap of a semiconductor gives information about its electrical and optical properties. Increasing of bandgap is explained by Burstain Moss Shift (Sanon, et al. 1991) which is proposed that increased carrier concentration leads to filling the lowest energy states of conduction band by these carriers so it results in increasing bandgap which is shown in figure 1.6b. Figure 1.6a shows the band gap of tin oxide for undoped stuation. The bandgap widening (figure 1.6b) can be expresssed mathematically that

$$E_g^{BM} = \left[E_c^0(k_f) - E_v^0(k_f)\right] - E_{g_0} \quad (1.4)$$

Where $$E_c = \frac{\hbar k_f^2}{2m_e^*} \quad \text{and} \quad E_v = \frac{\hbar k_f^2}{2m_h^*} \quad (1.2)$$

and $$\Delta E_g^{BM} = \frac{\hbar k_f^2}{2m_{vc}^*} \quad (1.3)$$

where $m_{vc} = \left[\frac{1}{m_c} + \frac{1}{m_h}\right]^{-1}$ and fermi wave number $k_f = (3\pi^2 n_e)^{\frac{1}{3}}$ put these relation in equation 1.3 and

$$\Delta E_g^{BM} = \frac{\hbar}{2m_{vc}}(3\pi^2 n_e)^{\frac{2}{3}} \quad (1.4)$$

Where ħ is Planck constant, n_e electron concentration, Ec is lowest level of conduction band energy and Ev is upper level of valans band energy, m_e and m_h are mass of electron and hall, respectively.

As it is seen in equation 1.4 that bandgap widening directly depends on the carrier concentration. With the further increase of carrier concentration band gap is being narrow due to electron - electron and electron - impurity interactions. When these interactions happen, conduction band level is decline and valans band level is increase which is seen in figure 1.6c.

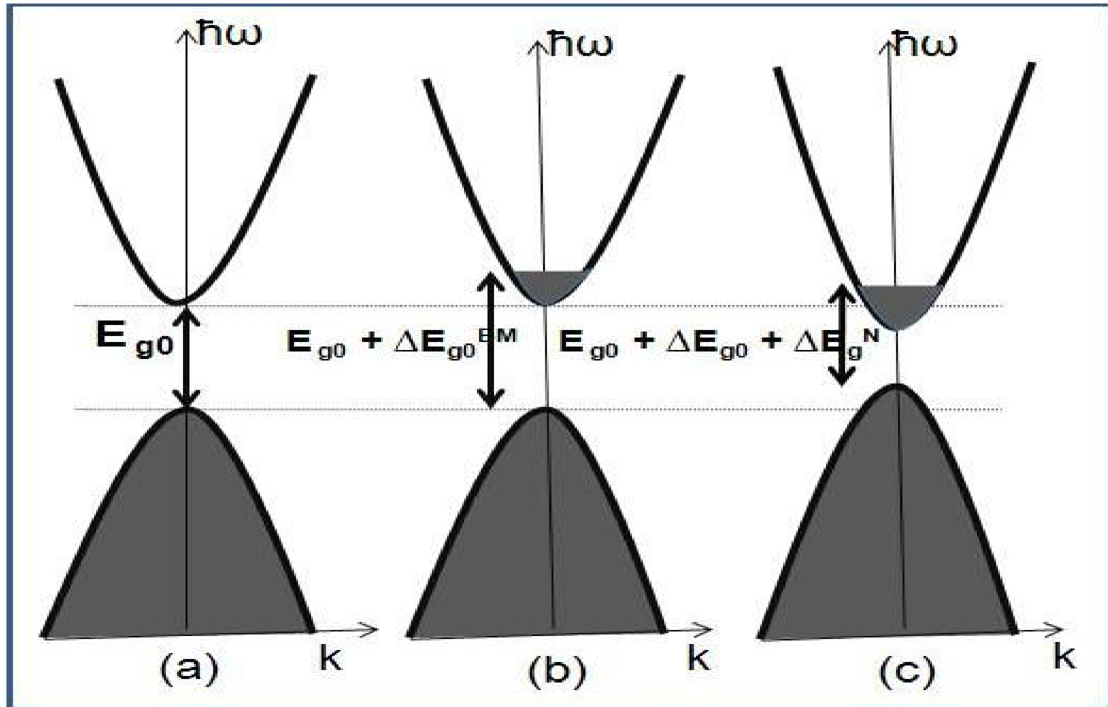

Figure 1. 6. Schematic band structure of Indium Oxide which has a parabolic conduction and valance bands separated by the band gap E_{g0}, after heavy doping there is a bandgap widening due to filling lowest energy state of conduction band by carriers. band gap narrowing is occur due to further increased of carrier concentration, respectively.

1.2.7. Scattering Machanism in Semiconductors

There are several scattering occur in semiconductors and I will explain the more dominant scattering machanisms here such as grain boundary, ionized impurity and lattice scattering.

Grain boundary scattering : Grain baundary scattering is dominant when structure of film is amorphous (Figure 1.7a) and also if grain size of thin films are small, number of grains will be much therefore scattering from these grain boundaries are effective. (Lee and Park 2004)

Ionized impurity scattering : Impurity scattering is dominant at high degree of crystallinity and also high carrier concentration (Figure 1.7b). Impurity scattering is occur when carriers traveling near the impurity center and the probability of scattering from there increased with increased carrier concentration. At low temperatures impurity scattering is more effective because of the fact that when the mean velocity of carriers are high, the probability of scattering from impurity center is low due to carriers remain shorter time near the impurity center. (Lee and Park 2004).

Lattice scattering : Lattice scattering results from thermal vibrations of lattice atoms at any temperature above absulute zero. At high temperature the probability of encountering carriers with lattice atoms are much.

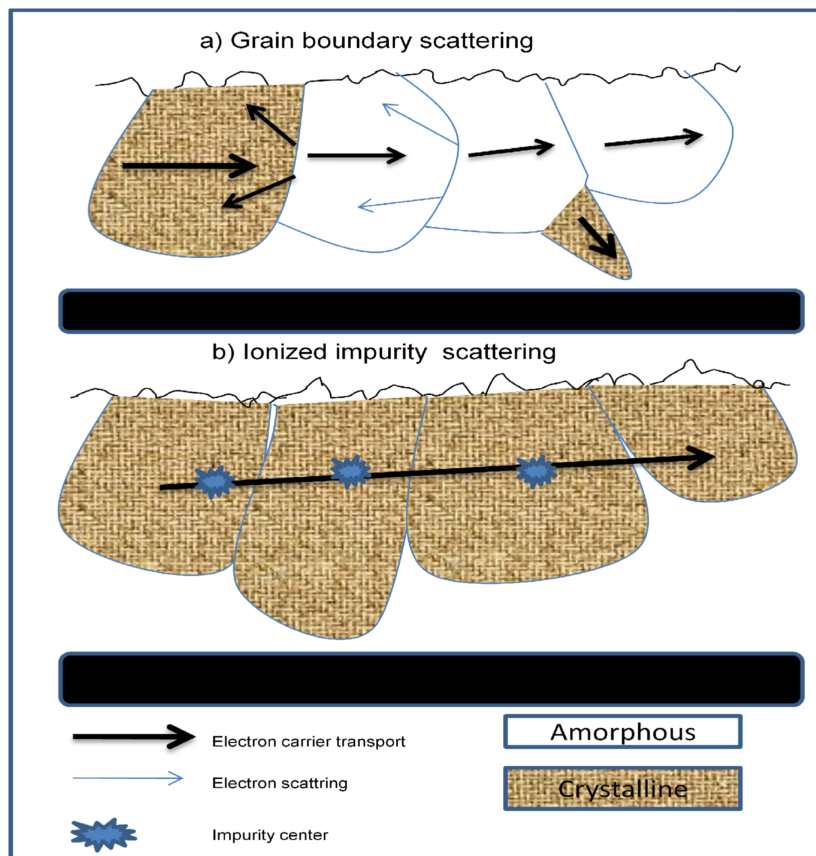

Figure 1. 7. Figure of scattering mechanism in semiconductor grain boundary scattering and ionized impurity scattering, respectively.(Source : Lee and Park 2004)

1.3. Aplications of ITO

Due to unique electrical and optical properties ITO have been used so many areas ranged from transparent of car windows, antistatic coatings over electronic instruments, display panel, heat reflecting mirrors, antireflection coating and high temperature sensor. Early electro-optic devices using ITO such as liquid crystal display. ITO is also used as a transparent contact in advanced optoelectronic devices such as solar cell and organic light emitting diodes. I will explain some of important aplications here.

1.3.1. Solar Cell

Solar energy is quite simply the energy produced directly by the sun and collected elsewhere, normally the Earth. Due to the nature of solar energy, two components are required to have a functional solar energy generator. These two components are a collector and a storage unit. The collector simply collects the radiation that falls on it and converts a fraction of it to other forms of energy (either electricity and heat or heat alone). The storage unit is required because of the non-constant nature of solar energy; at certain times only a very small amount of radiation will be received. At night or during heavy cloudcover, for example, the amount of energy produced by the collector will be quite small. The storage unit can hold the excess energy produced during the periods of maximum productivity, and release it when the productivity drops. Just like the cells in a battery, the cells in a solar panel are designed to generate electricity; but where a battery's cells make electricity from chemicals, a solar panel's cells generate power by capturing sunlight instead.

A solar cell is a sandwich of two different layers of silicon that have been specially treated or doped so they will let electricity flow them in a particular way. The lower layer is doped so it has slightly too few electrons. It's called p-type or positive-type silicon. The upper layer is doped the opposite way to give it slightly too many

electrons and generally ITO is used. It's called n-type or negative-type silicon. When we place a layer of n-type silicon on a layer of p-type silicon, a barrier is created at the junction of the two materials (Figure 1.8). No electrons can cross the barrier so, even if we connect this silicon sandwich to a flashlight, no current will flow: the bulb will not light up. But if we shine light onto the sandwich, something remarkable happens. As photons enter our sandwich, they give up their energy to the atoms in the silicon. The incoming energy knocks electrons out of the lower, p-type layer so they jump across the barrier to the n-type layer above and flow out around the circuit. The more light that shines, the more electrons jump up and the more current flows. The working process of solar cell can be given as and shown in Figure 1.8

1. When sunlight shines on the cell, photons (light particles) bombard the upper surface.
2. The photons (yellow blobs) carry with carriers of ITO and conduct energy down through the cell.
3. The photons give up their energy to electrons (green blobs) in the lower, p-type layer.
4. The electrons use this energy to jump across the barrier into the upper, n-type layer and escape out into the circuit.
5. Flowing around the circuit, the electrons make the lamp light up

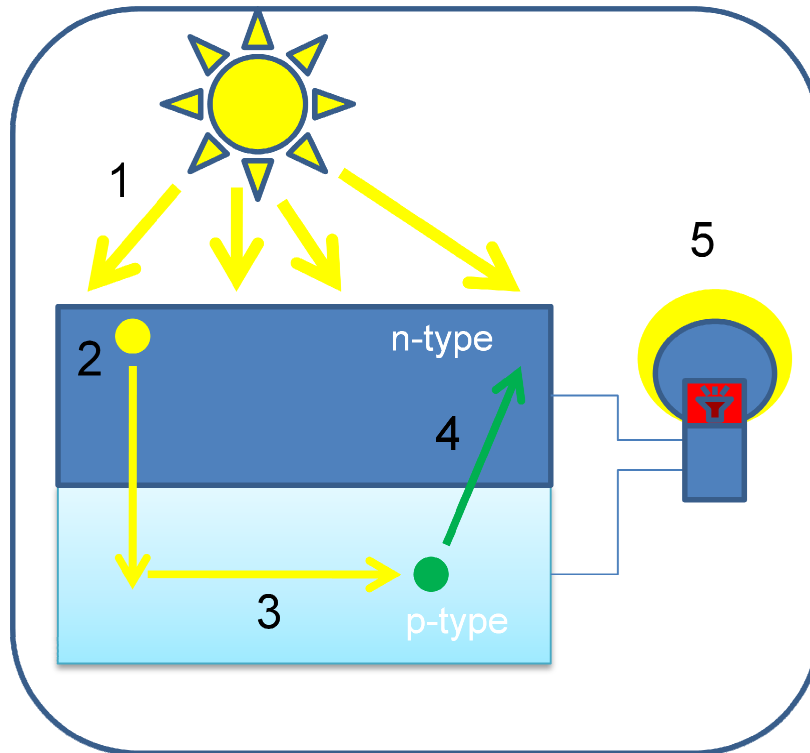

Figure 1. 8. Schematic of solar cell: 1. Solar, 2. N-type semiconductor (generally ITO), 3. P-type semiconductor, 4. Holes, 5.

1.3.2. Smart Glasses

The smart glasses can be used so many places such as buildings (commercial and residental), vehicles (land, sea and air), skylights, interior partitions and structures, eyewar and indoor display and signs. These windows consist of up to seven layers of materials. The basic figure of these glasses are shown in figure 1.9.

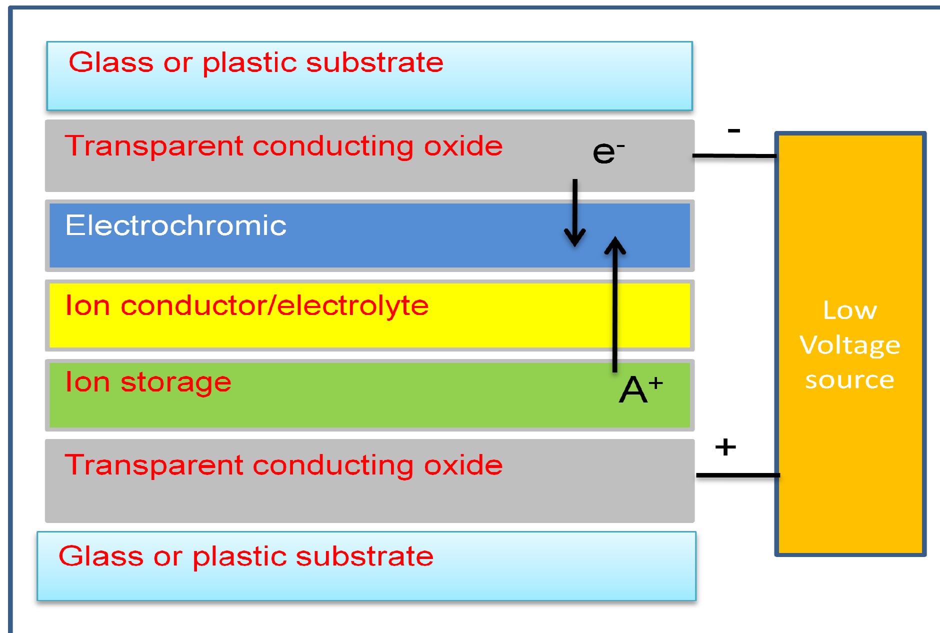

Figure 1. 9. Basic configuration of smart glass.

The most important layer of the smart glass is electrocromic layer that is generally tungsten oxide (WO_3). The central three layers are sandwiched between two layers of a transparent conducting oxide material which is generally indium tin oxide (ITO). To protect the five layers of materials, they are further sandwiched between two layers of glasses. The essential function of the device is that the transport of hydrogen or lithium ions from an ion storage layer and through an ion conducting layer, injecting them into an electrochromic layer. The presence of the ions in the electrochromic layer changes its optical properties, causing it to absorb visible light. The large-scale result is that the window darkens. All of the layers, of course, are transparent to visible light.

To darken the windows, a voltage is applied across the two transparent conducting oxide layers. This voltage drives the ions from the ion storage layer, through the ion conducting layer and into the electrochromic layer. To reverse the process, the voltage is reversed, driving the ions in the opposite direction, out of the electrochromic layer, through the ion conducting layer, and into the ion storage layer. As the ions migrate out of the electrochromic layer, it lightens, and the window becomes transparent again. The benefits of this technology range from reduced energy consumption for heating and cooling, increased control over the work environment,

increased worker productivity. A unique benefit or feature of the smart glass is it is self-powering, it does not need to be connected to a buildings electrical system in order to operate. (Azens and Granqvist 2003, Licciulli and Lisi 2001).

1.3.3. Organic Light Emitting Diodes

Organic Light Emitting Diodes are composed of an emissive layer, a conducting layer, a substrate and anode and cathode terminal. ITO is generally used as a conducting layer. The layers are made of special organic molecules that conduct electricity. Their levels of conductivity range change from insulators to conductors, and so they are called organic semiconductors. The basic configuration is shown in Figure 1.10.

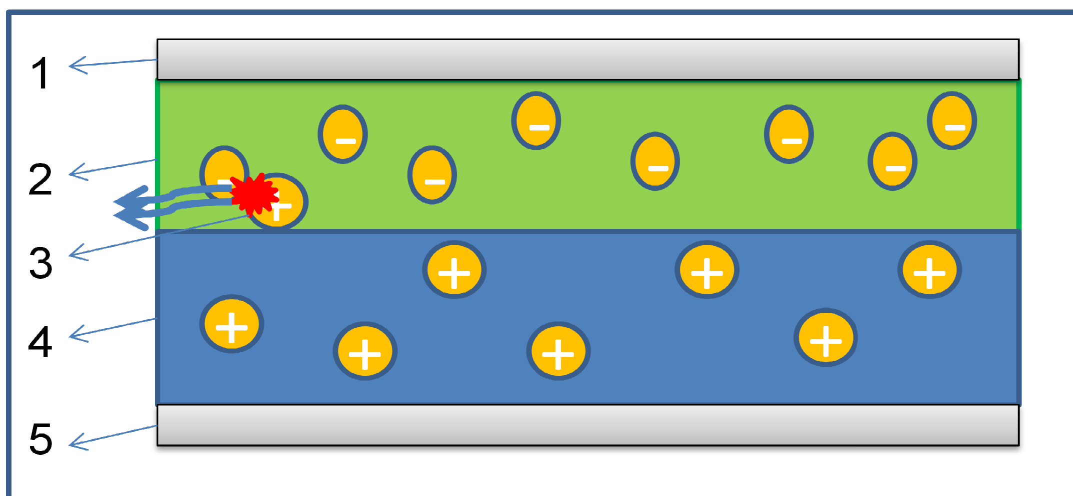

Figure 1. 10. Schematic of a 2-layer OLED: 1. Cathode (−), 2. Emissive Layer, 3. Emission of radiation, 4. Conductive Layer, 5. Anode (+)

Indium tin oxide is commonly used as the anode material. It is transparent to visible light and has a high work function which promotes injection of holes into the

polymer layer. Metals such as aluminium and calcium are often used for the cathode as they have low work functions which promote injection of electrons into the polymer layer. When a voltage applied across the oled, it is positively charged with respect to the cathode so this leads to flowing electrons through the divice from cathode to anode. In other words cathode gives electrons to the emissive layer and anode take these electrons from conductive layer so the emissive layer becomes negatively charged and conductive layer higly charged positively holes. Due to these charged interaction an electric forces occur toward each other. This happens closer to the emissive layer, because in organic semiconductors holes are more mobile than electrons. The recombination causes a drop in the energy levels of electrons, accompanied by an emission of radiation whose frequency is in the visible region. That is why this layer is called emissive. (Piromreun, et al. 2000, Ammermann, et al. 1995, Friend, et al. 1999).

1.3.4. Liquid Crystal Displays

Liquid crystals are organic molecules that have crystal-like properties but that are liquid at normal temperatures. Because the intermolecular forces are weak, the molecules can be oriented by weak electromagnetic fields. The liquid crystal molecules used in LCDs also have an optical anisotropy (different indices of refraction for different axes of the molecule) that is used to create visible images. Depending on the orientation of the molecules, the panel is either transparent or dark.

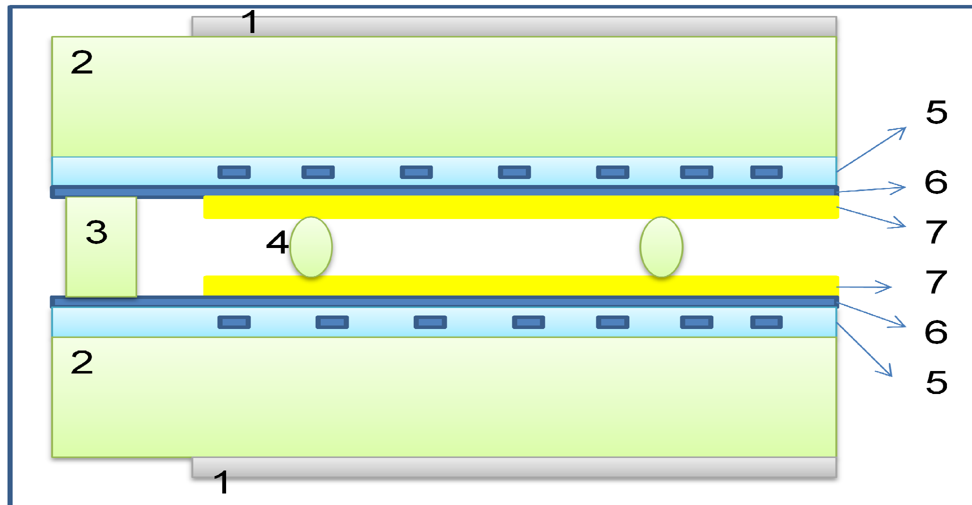

Figure 1. 11. Schematic of a LCD: 1. Polarizer, 2. Glass substrate, 3. Seal, 4. Spacer, 5. ITO, 6. Hard coat, 7. Polyimide, 8. TFT

A passive matrix LCD is composed of several layers (Figure 1.11). The main parts are two glass plates, connected by seals. The polarizer is applied to the front glass plate in order to polarize the incoming light in a single direction. The light then passes through the front glass sheet. An Indium Tin Oxide (ITO) layer is used as an electrode. A passivation layer, sometimes called hard coat layer, based on SiO_x is coated over the ITO to electrically insulate the surface. Polyimide is printed over the passivation layer to align the liquid crystal fluid. The liquid crystal fluid is sensitive to electric fields and changes orientation when an electric field is applied. The liquid crystal is also optically active and rotates the polarization direction of the incoming light. The thickness of this layer is determined by spacers, which keep the two glass plates in a fixed distance. When there is no electric potential from the front piece of glass to the rear piece of glass, the polarised light is rotated 90° as it passes through the liquid crystal layer. When an electric potential is applied from one plate to the other plate the light is not rotated. After the light has passed through the liquid crystal, it passes through another polyimide layer, another hard coat layer, the rear ITO electrode, and the rear glass. When it reaches the rear polarizer it is either transmitted through or absorbed, depending on whether or not it has been rotated 90°.

CHAPTER 2

BACKGROUND OF ITO

2.1. Background of ITO

There are many techniques have been used to grow Indium Tin Oxide thin film on glass substrate and as a results of these studies it can be said that deposition techniques are remarkable effective on film properties especially electrical and optical properties. In Table 2.1 I give some deposition techniques used by some reserchers and their important results on electrical and optical properties of ITO thin film.

Tablo 2. 1. Typical electrical and optical properties of ITO deposited by various techniques

Deposition techniques	**Thickness (Å)**	**Hall mobility($cm^2\ V^{-1}s^{-1}$)**	**Carrier concentration (cm^{-3})**	**Resistivity (Ω-cm)**	**Transmittance (%)**	**Ref.**
r.f. sputtering	2200	18	17×10^{19}	2.05×10^{-3}	80	Jayaraj et al. 2005
d.c. sputtering	3200	43	9×10^{20}	-	85	Lee 2004
Ion beam sputtering	-	5.56	6.31×10^{21}	1.77×10^{-4}	85	Ding, et al. 2005
Thermal evaporation	4400	42	29×10^{19}	5×10^{-4}	90	Chen et al.2007
Electron beam evaporation	1500	39	4.93×10^{21}	2.8×10^{-4}	82	Ali, et al. 2005
Pulsed laser ablation	1000	45	3×10^{21}	1.75×10^{-4}	87	Adurodija et al. 1999

These results founded after some pre- and post-deposition treatment and also different deposition techniques. For instance substrate temperature was increased before deposition (Das and Benerjee 1986) and different reactive gases was used by some worker (Lee and Park 2004 , Meng and Santos 1998). In addition to growth conditions that metioned above, some workers also used different target composition with respect to tin oxide and indium oxide weigh ratio and it is really affect film properties. (Adorodija, et al. 1999). In all above mentioned growth techniques, dc or rf sputtering methods have been mostly used due to some advantages such as the possibility of growing on different substrate and different area i.e. large and small and deposition rate

can be change easily by changing pressure or power. Because of these adventages I will mention here some results of ITO thin films grown by dc or rf magnetron sputtering.

Saveral workers were growth ITO by changing substrate temperature or applying post annealing treatment to improve structural, optical and electrical properties. Das and Banerjee 1986 used both substrate temperature increament and annealing method to grow tin oxide films and found out that crystallization is increased both with substrate temperature and annealing. The peaks of SnO phase appeared at the substrate temperature of 250 ^{o}C in their study. They showed that crystallization direction change from (222) to (444) with increased substrate temperature and as they explained that its reason was mobility of sputtered atoms which were increased with substrate temperature. Similar crystallization behaviour observed by Diao, et al. 2004 and Reddy, et al. 2006 at different substrate temperature. All these workers have support that resistivity of ITO thin films decreased with increasing substrate temperature due to increasing carrier density. Nisha, et al. 2005. decleared that increament of substrate temperature leads to decreasing resistivity till a critical temperature which is about 350 ^{o}C. Increament of substrate temperature above this critical temperature may leads to deminish substrate structure and release some substrate atoms through thin film. These substrate atoms behaves as impurity in thin films and therefore it results in increasing resistivity of ITO. Meng and Dos 1988. reported resistivity of ITO thin film was 3.7×10^{-4} Ω-cm with the film thickness of 900 nm at the substrate temperature of 400 ^{o}C and Reddy, et al. 2006. reported resistivity value of ITO thin film was 1.5×10^{-3} Ω-cm with the film thickness of 400 nm at the substrate temperature of 300 ^{o}C. Both Meng, et al. 1998 and Reddy, et al. 2006 used rf magnetron sputtering and same target with regart to SnO_2 doping ratio. Due to the thickness of the samples, Mengs' results are better. Also Dutta and Ray 1988 studied on ITO thin film changing substrate temperature. They changed substrate temperature from 250 ^{o}C to 450 ^{o}C and they found lowest resistivity at the substrate temperature of 450 ^{o}C with the value of 1.8×10^{-4}. When we compare Reddy, et al 2006 and Dutta and Ray 1988 work, it can be conclude that the reason of lower resistivity of Dutta and Ray 1988's work is higher carrier concentration and higher hall mobility which are about 1.2×10^{21} cm^{-3} and 31.4 cm^{2} V^{-1}s^{-1}, respectively, at substrate temperature of 450 ^{o}C. These values are really higher than Reddy, et al. 2006 results which are 6.2×10^{20} cm^{-3} and 6 cm^{2}V^{-1}s^{-1} carrier concentration and hall mobility, respectively. There are some

studies about growth of ITO thin films using oxygen (Lee and Park 2004, Guillen and Herroro 2006) and hydrogen as a reactive gases. Lee and Park 2004 and also Guillen and Herroro 2006 mentioned that used reactive oxygen atoms fill the oxygen vacancies which are contribute to the carrier density. Oxygen atoms incorparate with Sn atoms which are responsible for conductivity and deactivate it by forming $Sn^{+}O^{-}$ complexes so decreased carrier concentration and also oxygen concentration decreased from 48.5 cm^{-3} to 47.7 cm^{-3} with increasing oxygen parial pressure from 0 % to 5 % in all gases in chamber (Lee and Park 2004). In cotrast to carrier concentration, carrier mobility first increase till a critical oxygen rates and with increasing oxygen concentration above this critical region carriers mobility decreasing. Mobility increase firstly from 38 $cm^2 V^{-1}s^{-1}$ to 46 $cm^2 V^{-1}s^{-1}$ with the oxygen flow rate from 0 % to 1.25% O_2/Ar vol% and than decresed till 42 $cm^2V^{-1}s^{-1}$. The distinct behaviour of the carrier mobility with the oxygen flow rate is closely related to the scattering machanism; i) ionized impurity scattering in the first region untill 1.25% O_2/Ar vol% ii) neutrol defect scattering and negetively charged oxygen scattering in the axcess oxygen region above 1.25% O_2/Ar vol%. (Lee and Park 2004). Decreasing carrier concentration is consistent with increasing transmittance in the near infrared region due to decreasing carrier concentration leads to decreasing scattering of light from carriers (Lee and Park 2004, Guillen and Herroro 2006). It was reported by Guillen and Herroro 2006 that in the near infrared region transmittance increase from 68% to 77% with increasing oxygen-argon partial pressure from 0.002 to 0.008. There are also some workers used hydrogen as reactive gas to sputter (Zhang, et al. 2000). Zhang, et.al. 2000 growth ITO thin film used hydrogen as a reactive gas and there did not apply any thermal treatment on thin film such as annealing or substrate temperature. They found that with increased hydrogen partial pressure from 0 to 7×10^{-6} and 2×10^{-5} torr, roughness of ITO thin films decreased from 1.44 nm to 1.13 nm and 0.92 nm, respectivelly. It shows that the addition of hydrogen in the sputtering mixture results in decreasing roughness and according to Zhang, et al. 2000. it is reason was reducing effect of oxide. Effect of hydrogen on electrical properties of ITO thin films is good till a crytical hydrogen partial pressure which is about 7.5×10^{-6} torr. Untill this pressure resistivity decreased from 5.2×10^{-4} to 4.66×10^{-4} Ω-cm and carrier concentration increased from 3.5×10^{20} to 4.59×10^{20} cm^{-3}. The effect of substrate temperature on energy band gap was also studied and it is connected with carrier concentration. The highest band gap 3.92 eV at T_s of 500 °C, 3.88 eV at T_s of 250 °C and 3.84 eV without T_s measured by Meng and Santos 1988, Nisha, et al. 2005.

and Zhang, et al. 2000, respectively. Burstain Moss Shift explained band gap widening with increasing carrier concentration (Meng and Santos 1988, Nisha, et al. 2005). In addition to effect of substrate temperature, some worker studied effect of film thickness on properties of ITO thin film. (Akkad, et al. 2000, Lee and Park 2004). Grain size, crytallinity, carrier concentration and hall mobilities increased with thickness. (Akkad, et al 2000). Grain size of the ITO thin films increased from 9 nm to 28 nm with film thickness increament from 90 nm to 850 nm. This grain size increament explained with well devoloped grains and full width at half maximum (FWHM) value which is decreased with increased thickness. Carrier concentration n is in the range 7.34×10^{20} cm^{-3} – 1.41×10^{21} cm^{-3} and hall mobility is μ in the range 7.60 – 14.5 cm^2/Vs and these increament depends on the thickness of films increased from 90 nm to 850 nm. Hall mobility increament was interpreted as the result of grain size increament by (Akkad 2000) so relatedly decreasing grain boundary scattering and carrier concentration increament was stated as rising of Sn_{In} defects.

2.2. Thin Film Deposition Methods

There are several methods to grow ITO thin film on various substrates. I am going to mention some of important methods here.

2.2.1. Direct Current Magnetron Sputtering

As the name suggest in that system a DC power supply is used to create the plasma. Direct current sputtering allow high deposition rate. Only conductive targets can be sputtered Using conventional DC sputtering. When we apply power the flux of electrons from DC supply causes charged build up on the surface of the a conductive target. These electrons collide with argon (Ar) atoms and ionized it. Ionized Ar atoms accelarates through the negatively charged target and transfer their energy to the target

atoms and dislodged them then deposited on the surface of substrate. One method used to sputter conductive targets using pulsed DC source. When using a pulsed DC source, the voltage is periodically pulsed positive for a very short time to remove the charged on the conductive target. The positive pulse duration is a very small fraction of the entire period, leading to a higher sputtered rate.

2.2.2. Radio Frequancy Magnetron Sputtering

The main difference between DC and RF magnetron sputtering is power supply. Radio frequency power supply is used for RF sputtering that is operating at 13.56 MHz, to generate plasma. Similarly with DC sputtering, the generated ions accelerates towards the target by a negative DC bias on the target due to the flux of the electrons. The ions hit the target with enough energy and transfer their energy to the target atoms and dislodged it. Both DC and RF sputtering performed under vacuum, between 1 mTorr and 50 mTorr, to improve the quality of films and to increase deposition rate by increasing mean free part that is explain the distance between collisions.

RF sputtering can be used to sputter both insulating and conducting targets, due to charge does not build up on the surface of the target. The major disadvantages of RF sputtering are cost and lower deposition rate.

2.2.3. Thermal Evaporation

Thermal evaporation is a phsical vapor deposition (PVD) method used to deposit materials with relatively low melting points. Evaporations take plase under high vacuum condition lower than 5×10^{-6} Torr. The evaporation is uccur as current passed through a flament or a boat, containing the materials to be evaporated. While current flows through, the boat is heating up because of resistive heating untill material either melts and evaporates. In this work we evaporated gold under vaccum condition. We send about 165 Amper to heating up a boat and evaporate gold on the patterned films.

2.2.4. Chamical Vapor Deposition

Chemical vapor depositions depends on a chamical reactions rather to deposit the film using a physical process. In this techniques there are several reactive gases are used and the reaction takes place within these used gases and film occurs on the heated substrate.

2.2.5. Ion Beam Sputtering

Ionized Ar ions beam focuses on the target surface with a degree and transfer their energy to the target atoms and dislodged them. This deposition takes place under vacuum condition. The energy of argon ions are important for this deposition techniques therefore applied voltage is critical for accalerating argon ions through the substrate surface.

CHAPTER 3

EXPERIMENTAL

3.1. Purpose

The main purpose of this work is growth of ITO thin film on small glass substrate and investigate its structural, electrical and optical properties and then apply our experience to grow ITO on large area . In this aim, we growth ITO thin film using various deposition techniques including DC, RF for coating small area and pulsed DC magnetron sputtering for coating large area. The structural characterizations including XRD (X-Ray diffiraction), AFM (Atomic Force Microscopy), SEM (Scanning Electron Microscopy) and the electrical characterizations including Hall measurement, R-T and R-T_s measurement were performed. In this chapter, the all of experimental procedure including from growth to all characterization will be described step by step.

3.2. Growth of Indium Tin Oxide

In this study 1 mm thick microscope glass slides were used as substarte to grow ITO films on it. They were cleaned in an ultrasonic bath in the order of acetone, alcohol and de-ionized water, ten minutes in each, prior to introducing them into the growth chamber. Target to substrate distance was kept at 7.5 cm for each deposition. The system was evacuated down to the base pressure of about 2 x 10^{-6} Torr using rough and turbo pump, respectively, prior to growth. After avecuated chamber pressure, 40 sccm Ar gases was send into the chamber using mass flow controller and applied DC and RF

power to occur plasma on the ITO target. When the power apply Ar gases were ionized because of collitions between electrons and argon atoms. There are some magnets located under target and these magnets hold the electrons, which are coming from power supply, on the surface target to increase collision and to continuou plasma. Due to target was charged negatively, argon ions accelarete through the target and gives their energy to the ITO atoms and leads to dislodged them with as enough as energy stick the surface of the glass substrate. (Figure 3.1). For DC sputtering it is only a power supply enough to generate plasma however for RF sputtering the mathching network is need to deminish reflecting power. We applied 15 W DC power and 40 W RF power, operating 13.56 MHz, to generate plasma. These power values are the lowest value to start initial plasma.

The important point part of this study is substrate temperature differences for each growth. For this purpose we used IR heater. Before starting deposition, we increased the substrate temperature and fixed the temperature with the 1% accuracy and also before deposition five minutes pre-sputtering was applied before each growth to get rid of any contamination on the surface of the target therefore there is a shutter used between target and substrate during pre-sputtering. All growth paremeters are shown in Table 3.1. and the schematic representation of growth chamber is shown in Figure 3.2.

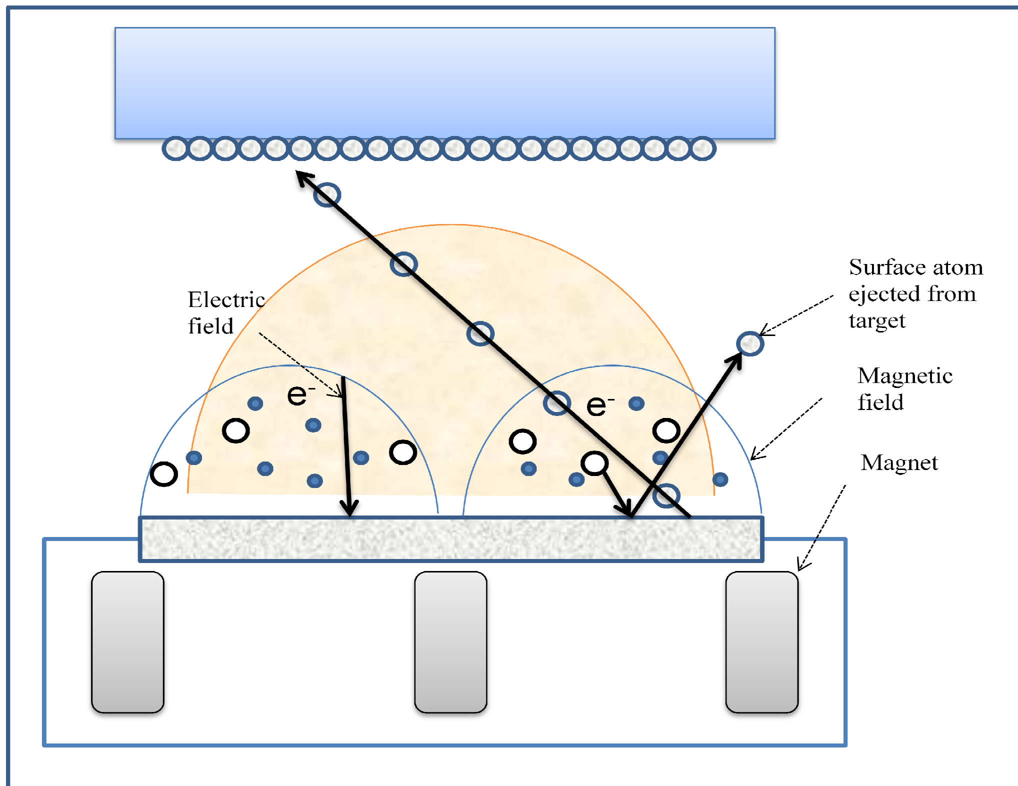

Figure 3. 1. The schematic representation of sputtering process

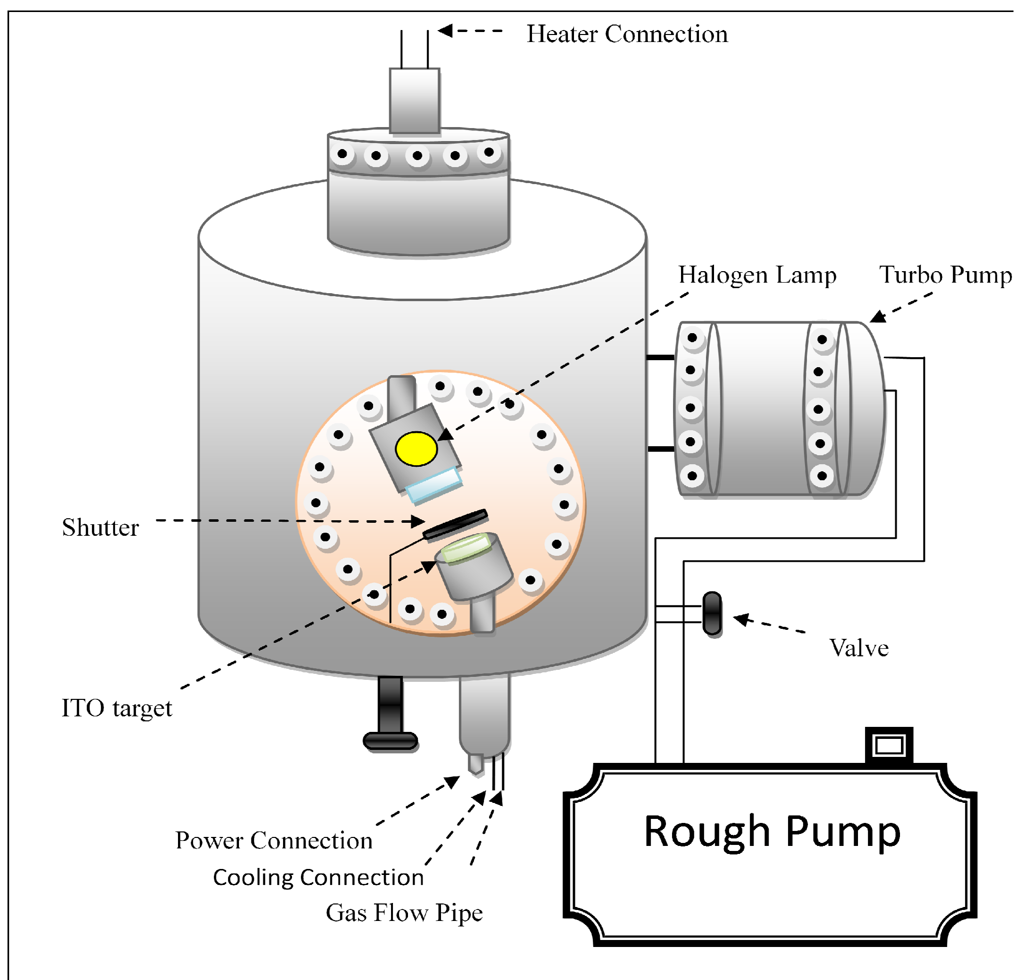

Figure 3. 2. The schematic represantation of growth chamber

Tablo 3. 1. Growth parameters for DC and RF magnetron sputtering

Growth method	**Sample code**	**Thickness (Å)**	**Power (W)**	**Substrate temperature (^{o}C)**	**Argon gas (sccm)**
DCMS	ITO1	700-400	15	150	40
DCMS	ITO2	700-400	15	200	40
DCMS	ITO3	700-400	15	250	40
DCMS	ITO4	700-400	15	300	40
DCMS	ITO5	700-400	15	350	40
DCMS	ITO6	700-400	15	400	40
RFMS	ITO1	700-400	40	150	40
RFMS	ITO2	700-400	40	200	40
RFMS	ITO3	700-400	40	250	40
RFMS	ITO4	700-400	40	300	40
RFMS	ITO5	700-400	40	350	40
RFMS	ITO6	700-400	40	400	40

3.3. Large Area Coating Magnetron Sputtering

In this study we also grew ITO on large area glass substrate. For this purpose we used large area coating magnetron sputtering system shown in figure 3.3. This system designed to coat 60×90 cm^2 glass substrate. This system includes there part. The first part is substrate loading part, second part is ITO coating area and the thirt part is used to

take out ITO coated glass substrate. There are many paremeters affect film properties in this system. The important think for us is to find thinner film by changing sample motion velocity under target, sending Ar gas value and applied power. In this system substrate holder are slowly moved under target with feet through system and depends on the applied power and angular velocity of the feet through mechanism film thickness is changed. To grow ITO films using this system we send 40 sccm fixed Ar gas for all sample and we pushed sample holder with the velocity of 7.2 cm/min again for all sample. We only changed applied power value to changed film thickness. To evacuate the system pressure untill 2.5×10^{-6} torr that is base pressure for this system, we used used rough pump and turbo molecular pump, respectively. By changing applied power, we grew samples with different thicknesses shown in figure 3.4. For the first film we applied 50 W, for second film we applied 40 W and for the third film we applied 35 W DC power and the thicknesses of the films were 125nm, 95nm and 70nm, respectively. For all this films we used 40 sccm Ar and we moved the sample holder with 7.2 cm/min.

After growing large area ITO glass, in order to improve the quality of the films we annealed the samples with different temperature changing from 200 to 450 ^{o}C under vacuum condition. At first we cut the large area samples into some pieces and locate that samples in our small area magnetron sputtering system and then evacuate system pressure untill 2.5×10^{-6} torr. In order to anneale the samples we used halogen lamp and after recieving a certain temperature we kept the temperature constant and annealed samples at one hour. We controlled the annealing temperature with thermocouple during annealing.

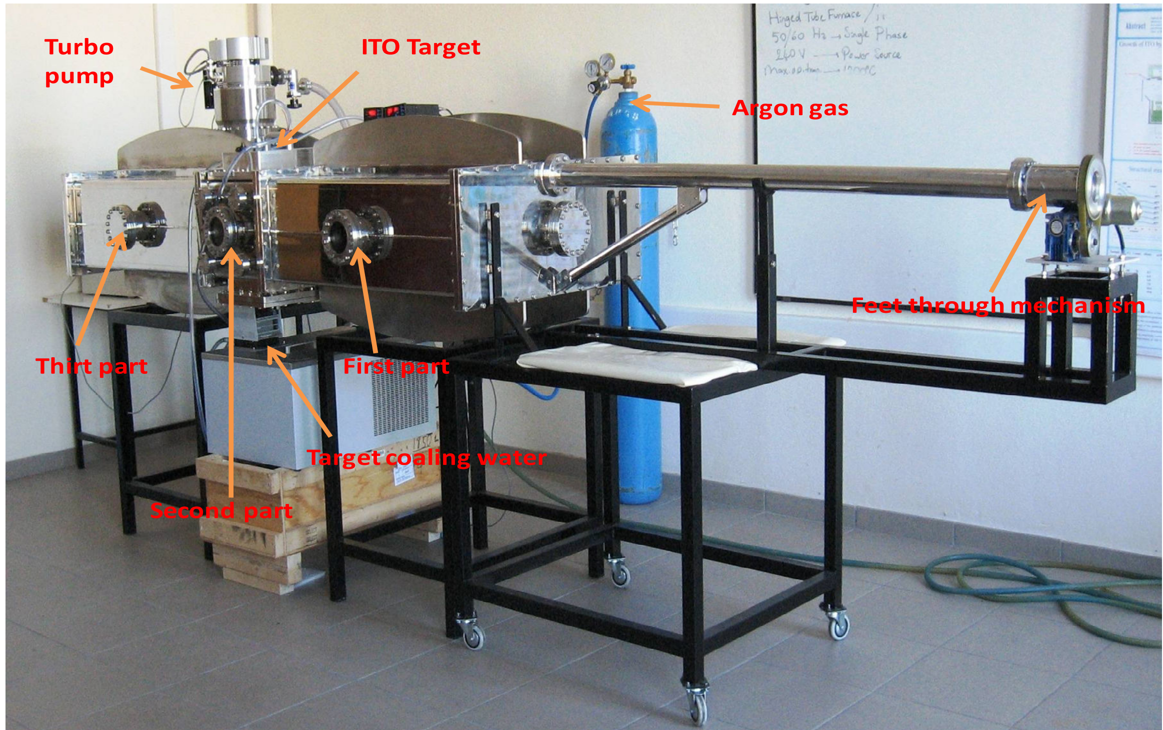

Figure 3.3. Large Area Coating Magnetron Sputtering System

Figure 3.4. ITO coated large area glass

3.4. Patterning of Films

After structural characterization of grown ITO thin films, they were patterned for electrical measurement. General photolithograpy mathod used for patterning of the films and the important thing in this process was used mask. Clover-leaf shape was used as mask. There are some mask figures shown in Figure 3.5 for van der Pauw method. In order to apply van der Pauw method properly, the shape of mask must be symmetric so we choose the first mask shape whichs' lenght and width are 3×3 cm^2 seen in Figure 3.5.

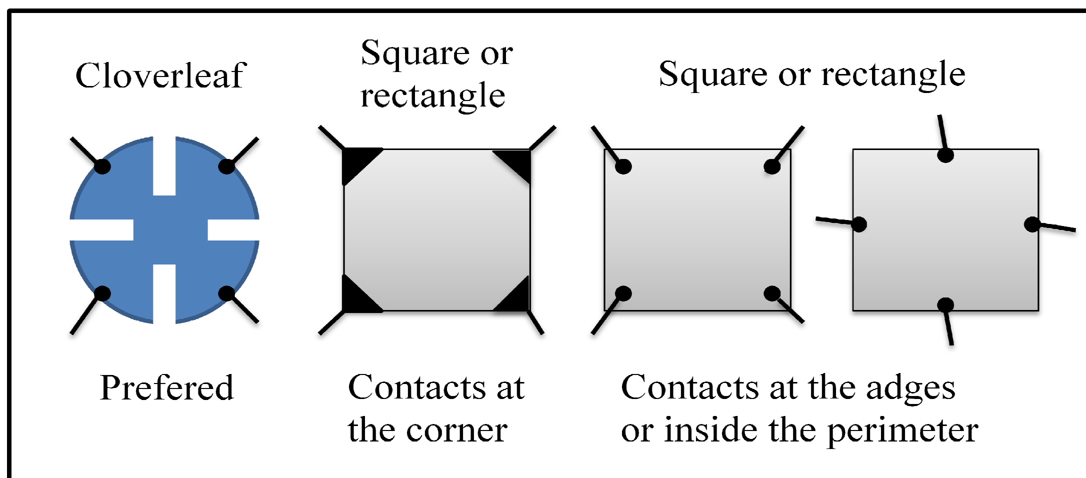

Figure 3. 5. The various mask shapes for van der Pauw method

Because of Photoresist (PR) is sensitive to light, the lithograpy process are done in dark room. The first step is that the sample is covered with PR by spin coater. (Figure 3.6). To provide uniform smooth PR layer and also enables to adjust thickness of the PR on ITO, the rotating valocity and the coating time of the spin coater is important and we apply 4.5V to rotate spin coater and allow it to rotate about 15 second and at the end of this process we achieve about 40nm thick photo resist on ITO films. To get rid of the

excess solvent in PR, soft bake process is done at process temperature of 85 ^{o}C for 30 minutes (Figure 3.6). After soft bake viscous PR layer obtained on ITO thin films. We used positive PR which means that when it exposed to UV light under a mask, exposed area where UV light passes through the mask is removed by developer solution that is sodium hydroxide (NaOH) with 0.2 M concentration. Thus we obtain PR pattern whose sizes are same with mask patterns in which are not allowed to passing of the UV light (Figure 3.6.). The last process is hard bake that is aneble the remained photo resist part during ion beam etching. Hard bake process last 30 minutes at 115 ^{o}C.

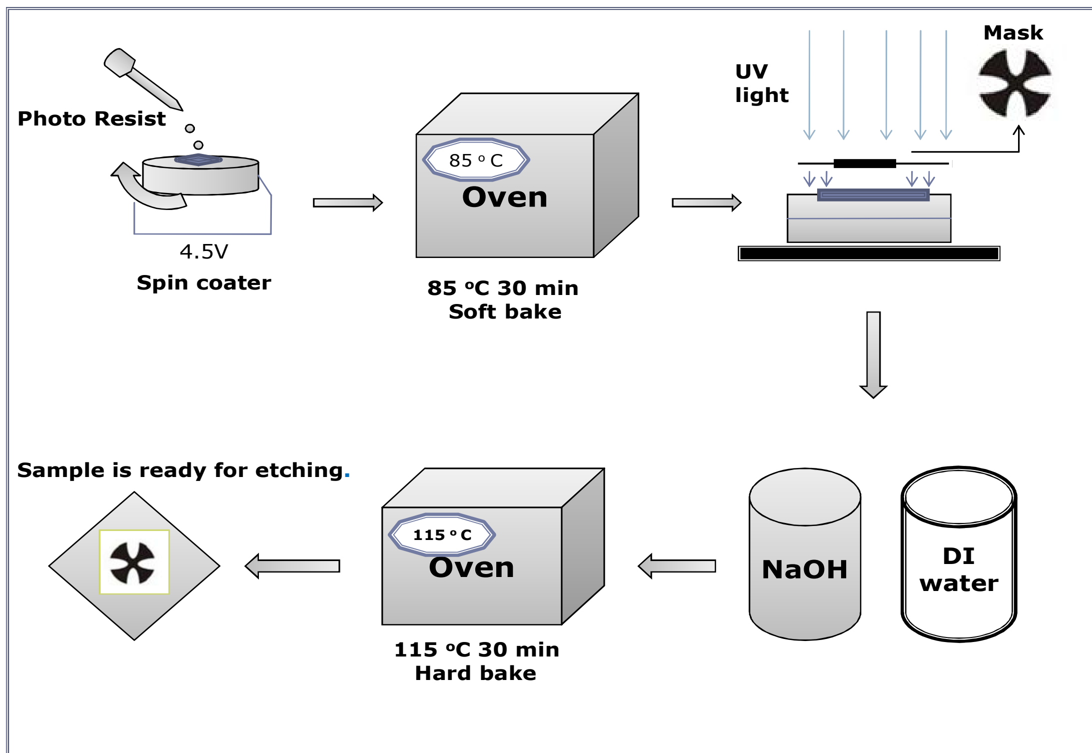

Figure 3. 6. The schematic representation of Photolithographic processes

After photolithograph process, samples are located in ion beam system which produce accelareted ions through the surface of the sample to etch some unprotected PR part of the films. In ion beam source on the chamber (Figure 3.7.) ionizes the inert argon gases whose quantity adjusted by gas flow controller and accelerated them towards the sample holder. High vacuum is necessary to eliminate colliding between ions and some

gases in chamber and thus increase mean free path of ion beam. Therefore turbo molecular pump with back pump is used to reach the high vacuum value of 4×10^{-6} torr for our system (Figure 3.7.). The angle between incident ion beam and sample surface is 45°. To ionize Ar gas we apply 35 W and to accelarate Ar ions we apply 700 V. The etch rate of ITO is about 2.33 nm for per minutes so we etch 70 nm thin film for 30 min.

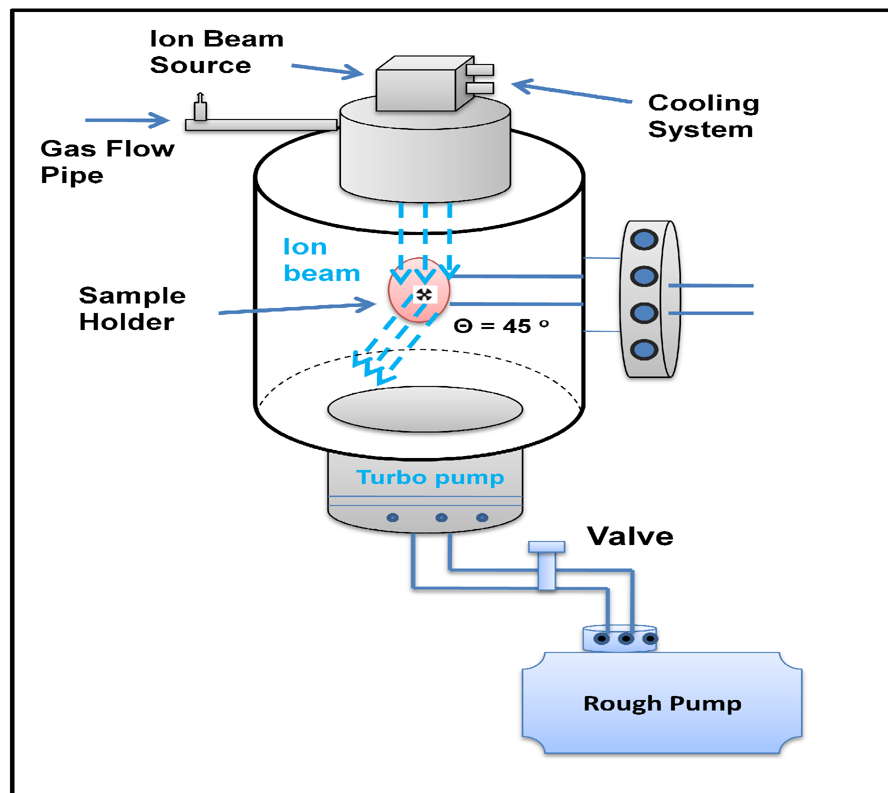

Figure 3. 7. Ion beam system

After etching we found photoresist coated ITO thin film on glass substrate with cloverleaf shape shown in Figure 3.8a. To get rid of photoresist on ITO thin film, we etch it with acetone and dry blown with high purity nitrogen gas. For electrical measurement as a said before we used van der Pauw method and so we have to take four contact on the sample. To avoid non-ohmic contact problem on patterned films, 20 nm-thick gold film was deposited by thermal evaporation to the corners of the patterned samples (Figure 3.8.b). Wiring to the gold pads were done by high purity In and 80 µm

thick Cu wires (Figure 3.8c). The evaporation system is shown in Figure 3.9. Prior to evaporation we pump down pressure to 10^{-6} torr by rough pump and turbo pump in order to eliminate chamical and physical interraction between atmospheric gas atoms and gold atoms. After reaching the base pressure, we apply high current as much as 170 A on flament boat and evaporate gold through the our samples (Figure 3.9).

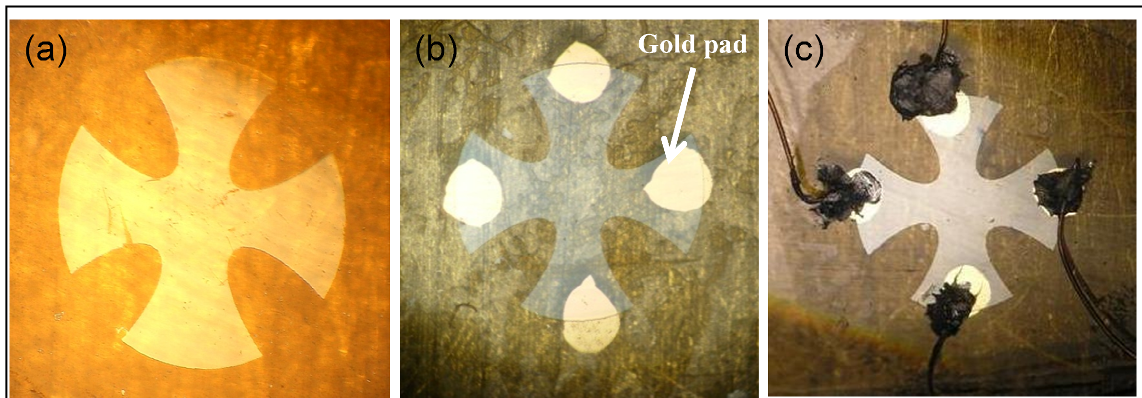

Figure 3. 8. After etching process, After coating gold by thermal evaporation, Taking contact on gold pallete with high purity In and thin Cu wire, respectively.

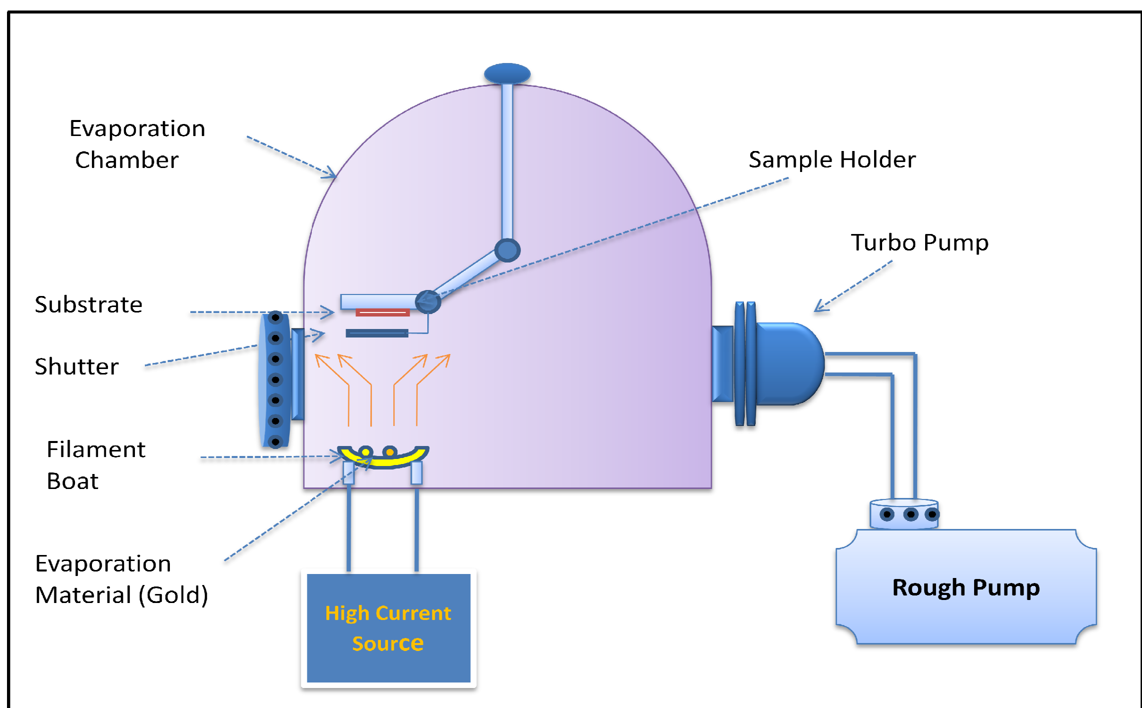

Figure 3. 9. Evaporation system

3.5. R-T and Hall Effect Measurements

The cryostat system seen in Figure 3.10. is used to measure sheet resistance at room temperature, temperature dependence resistivity and Hall effect. Liquid nitrogen is used to decrease temperature of the cryostat from room temperature 300 K to 78 K. 320 G permanent magnetic field is applied for Hall effect measurement. The thickness of the film is very important parameter for van der Pauw method and it must be much less than width and lenght of the sample. In order to reduce the errors in calculations, it is preferable that the sample is symetrical. There must be no isolated holes within the sample.

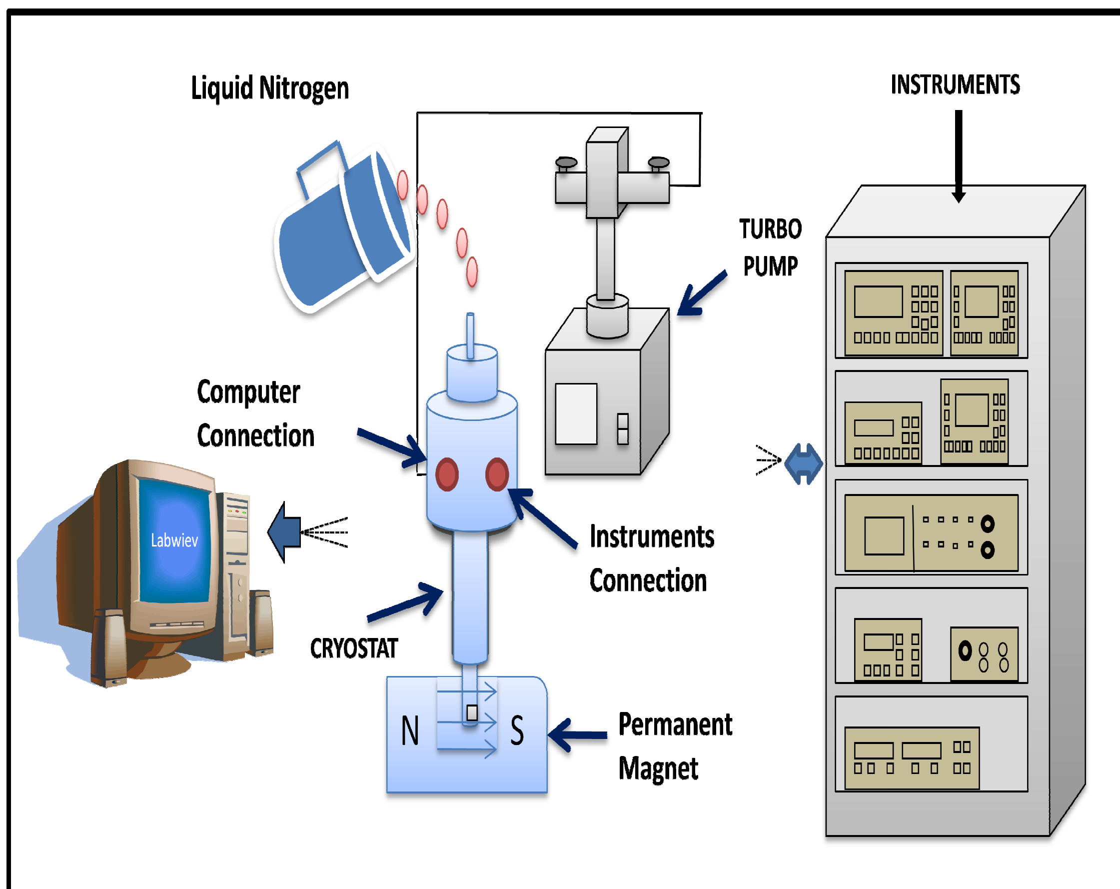

Figure 3. 10. The schematic represantation of Cryostat system

A Labview program-controlled set-up consisted of Keithley 2200 Programmable Current Source, Keithley 2182 Nanovoltmeter, a Keithley Hall effect card and a temperature controller was used for the electrical measurements (Figure 3.10). For resistivity and Hall effect measurements, we apply 0.1 mA and 1 mA current, respectively. Prior to cooled down cryostat temperature to 78 K, we measured room temperature sheet resistance by sending 0.1 mA through the contacts with respect to order of given in Tablo 3.2 that is related to Figure 3.12. The values of voltages from V_1 to V_8 are measured (Tablo 3.2.) and the ratio of voltage and applied current give us sheet resistance values. A further improvement in the accuracy of the resistance values can be obtained by repeating the resistance measurements after switching polarities of both the current source and the voltage meter. Since this is still measuring the same portion of the sample, just in the opposite direction, the values of $R_{vertical}$ and $R_{horizontal}$ that is given in equ. 3.1 and 3.2 can still be calculated as the averages of the standard and reversed polarity measurements. The benefit of doing this is that any offset voltages, such as thermoelectric potentials due to the Seebeck effect, will be cancelled out. Resistivity of the films are calculated by multiplying sheet resistance with thickness of the films given in equ 3.4.

$$R_{vertical} = \frac{R_{12,34} + R_{34,12} + R_{21,43} + R_{43,21}}{4} \tag{3.1}$$

and

$$R_{horizontal} = \frac{R_{23,41} + R_{32,14} + R_{41,23} + R_{14,32}}{4} \tag{3.2}$$

The avarege of these value is given in equ. 3.3.

$$R_{avarege} = \frac{R_{vertical} + R_{horizontal}}{2} \tag{3.3}$$

As a result resistivity of the films can be written as

$$\rho = R_{avarege}\, t \tag{3.4}$$

Where $R_{avarege}$ is sheet resistance of the films and t is the thickness of the films.

To understand Hall measurement clearly I will give brief explanation about Hall effect. When a charged partical such as an electron is placed in a magnetic field, it experiences a Lorentz force proportional to the strength of the field and the velocity at which it is travelling through it. That force is strongest when the direction of motion is

perpendicular to the direction of the magnetic field, and it can be explained mathematically as

$$F_L = QvB \tag{3.5}$$

Where Q is the charge on the partical, υ is the velocity travelling at centimeters per second and B is the strenght of the magnetic field (Wb/cm^2).

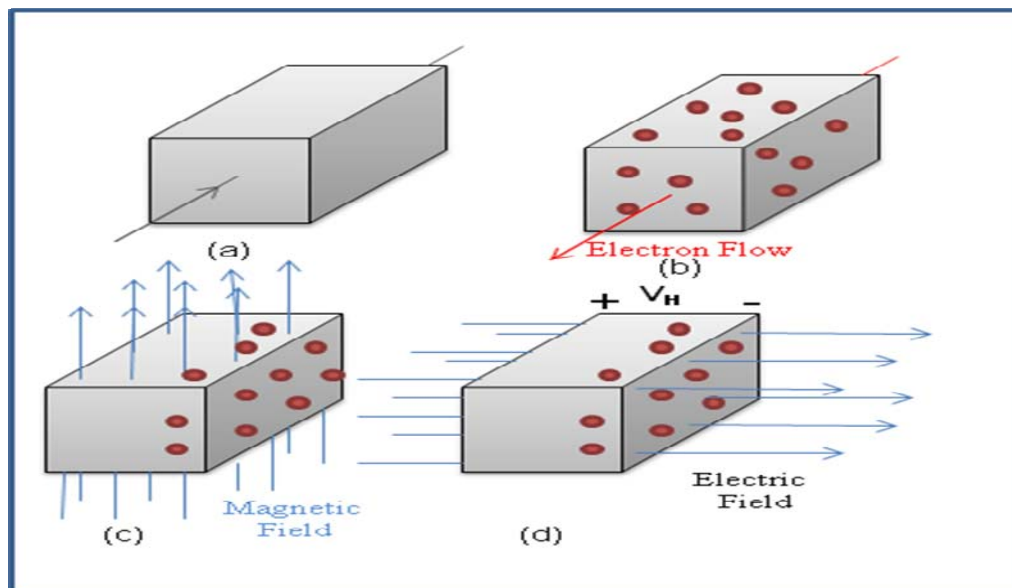

Figure 3. 11. The Hall effect as it is used for the van der Pauw configuration

When a current is applied to a piece of semiconducting material, this result in a steady flow of electrons through the material shown in Figure 3.11a and b. The velocity of the electrons are travelling at

$$V = \frac{1}{nAq} \tag{3.6}$$

Where n is electron charge density, A is the cross sectional area of the material and q is the elementary charge (1.602×10^{-19} coulombs). If an external magnetic field is applied perpendicular to the direction of the current flow, the occuring Lorenz force will

cause the electrons to accumulate at one edge of the sample seen part c of Figure 3.11. If we combine the equation 3.5 and 3.6, we can write Lorenz for experienced by an electron that

$$F_L = \frac{IB}{nA} \tag{3.7}$$

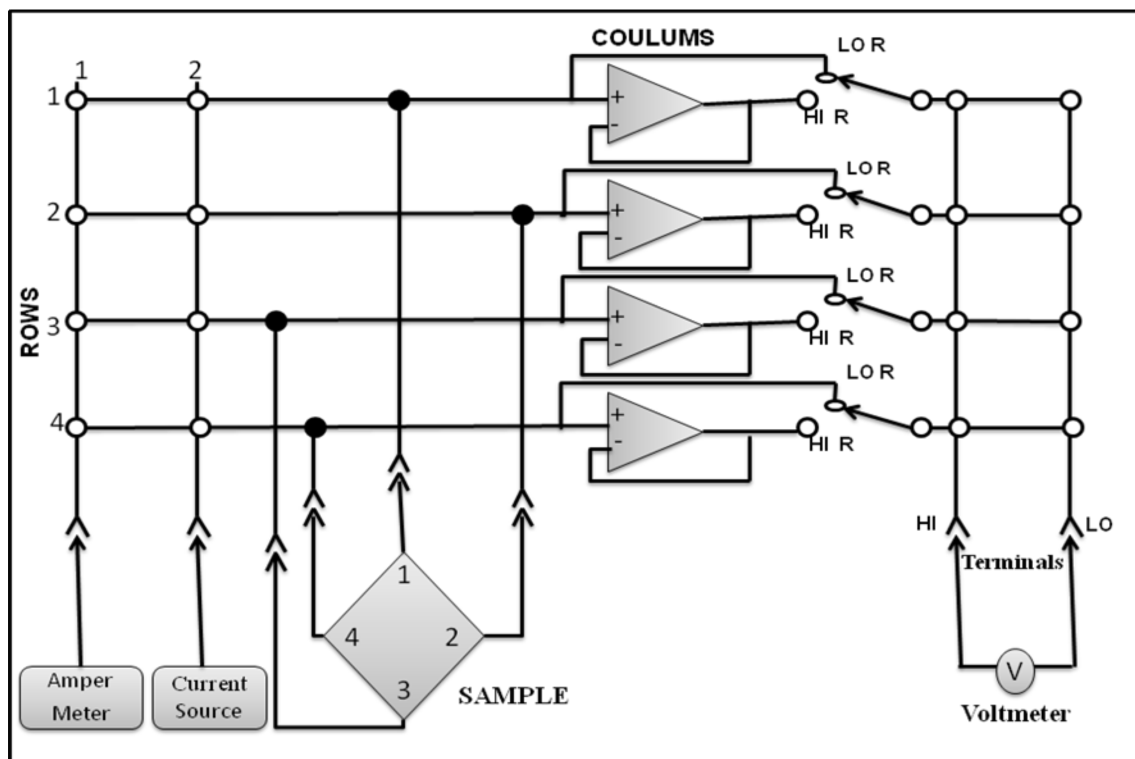

Figure 3. 12. Schematic represantation of our experimental method for resistivity and Hall effect measurement

Tablo 3. 2. Crosspoint Summary for Resistivity Measurement

Voltage Designation	Crosspoints Closed				Current Applied Between	Voltage Measured Between
V_1	1,2	2,1	3,3	4,4	1-2	3-4
V_2	2,2	1,1	3,3	4,4	2-1	3-4
V_3	2,2	1,3	3.4	4,1	2-3	4-1
V_4	2,3	1,2	3,4	4,1	3-2	4-1
V_5	2,3	1.4	3,1	4,2	3-4	1-2
V_6	2,4	1,3	3,1	4,2	4-3	1-2
V_7	2,4	1,1	3,2	4,3	4-1	2-3
V_8	2,1	1,4	3,2	4,3	1-4	2-3

To evaluate carrier concentration and Hall mobility of the films, we measure Hall coefficient of the them firstly. Hall coefficient can be calculated by these formulations:

$$R_{HC} = \frac{2.5\times10^{7} t_s}{BI} \left(V_2 - V_1 + V_5 - V_6\right) \qquad (3.8)$$

$$R_{HD} = \frac{2.5\times10^{7}\ t_s}{BI} \left(V_4 - V_3 - V_7 - V_8\ \right) \qquad (3.9)$$

Once R_{HC} and R_{HD} have been calculated, the average Hall coefficient, R_{Havg} can be determined as follows:

$$R_{H_{avg}} = \frac{R_{HC} + R_{HD}}{2} \qquad (3.10)$$

Where R_{HC} and H_{HD} are Hall coefficients in cm^3/C, R_{Havg} is the average of the Hall coefficient measured for each magnetic field direction +B and -B, t is the sample thickness in cm, B is the magnetic flux in gauss and I is the applied current. Voltage values which are starting from V_1 to V_4 measured by applying magnetic flux +B direction and other values starting from V_5 to V_8 by changing magnetic flux direction opposite of first direction (Tablo 3.3.). In the first situation magnetic flux goes inside the sample but in the second situation magnetic flux turn just vise versa of the first

situation. To measure these voltage values, we applied 1 mA current through the crosspoint contact given in Tablo 3.3.

Tablo 3. 3. Crosspoint Summary for Hall Voltage Measurement

Voltage Designation	Flux	Crosspoints Closed	Current Applied Between	Voltage Measured Between
V_1	+B	2,1 1,3 3,4 4,2	1-3	4-2
V_2	+B	2,3 1,1 3,4 4,2	3-1	4-2
V_3	+B	2,2 1,4 3,1 4,3	2-4	1-3
V_4	+B	2,4 1,2 3,1 4,3	4-2	1-3
V_5	-B	2,1 1,3 3,4 4,2	1-3	4-2
V_6	-B	2,3 1,1 3,4 4,2	3-1	4-2
V_7	-B	2,2 1,4 3,1 4,3	2-4	1-3
V_8	-B	2,4 1,2 3,1 4,3	4-2	1-3

Hall mobility can be calculated using already known resistivity and Hall coefficient values. Hall mobility explained mathematically:

$$\mu_H = \frac{\left|R_{H_{avg}}\right|}{\rho_{avg}} \tag{3.11}$$

Where μ_H is Hall mobility in cm^3/V-s, R_{Havg} is the average of the Hall coefficient in cm^3/C, ρ_{avg} is the average resistivity in Ω-cm.

CHAPTER 4

RESULT AND DISCUSSION

In this study Indium Tin Oxide (ITO) thin films have been grown by DC and RF magnetron sputtering and their stuructural, electrical and optical properties have been studied. In this part of thesis I will explain all results in detail.

4.1. XRD Results

XRD diffraction results shows that ITO thin films has polycrystalline structure and its crystalline structure substentially affected by substrate temperature and film thickness. The analysis of XRD pattern also demonstrates that ITO thin films grown at low substrate temperatures (lower than 150 ^{o}C) are amorphous. The crystallization detected in (222) plane with the preferentially oriented [111] direction for both DC and RF samples with increasing substrate temperature up to 300 ^{o}C. Since Indium has a face-centered tetragonal structure, [111] direction is the most densely packed and, consequently, it is the lowest energy plane (Chen, et al. 2007). While the substrate temperature was increased above 300 ^{o}C up to 400 ^{o}C, crystallization planes slowly changed from (222) to (400) and (440) for DCMS samples shown in Figure 4.1. It also changed from (222) to (211) and (440) for RFMS samples shown in Figure 4.2. Similar changes in crystallization plane with increased substrate temperatures was detected and, similarly to what we did not talk about mobility yet, reported as the increment in the mobility of the ad-atoms and cluster by Chen et al. 2007 and Jayaraj, et al.2005. Figure 4.3. and Figure 4.4. show X-ray diffraction patterns of 40 nm thick DCMS and RFMS samples, respectively. The comparision of thickness effect on crystallization is shown in Figure 4.5 clearly. In this figures all samples were grown at substrate temperature of 350°C which is the best substrate temperature to attain optimum electrical properties. It

is clear seen that detection of crystallization is decreased with decreasing thickness of samples. Increasing thickness yields more distinguished X-ray peaks. Similar findings were reported by Lee, et al.(2004) that as the thickness of ITO film is increased, the crystallinity degree of the films are observable (Lee and Park 2006). Using X-Ray diffraction peaks of ITO and Debye-Scherrer' formula given in equation 4.1, grain size of RFMS and DCMS grown thin films were calculated and listed in Table 4.1.

$$D = \frac{K\lambda}{BCos\theta_B} \tag{4.1}$$

Where the value of constant K is 0.9 and D is defined as full width at half maximum (FWHM) of the diffraction peak (Akkad, et al. 2000), λ is the wavelength of CuK_α and θ is the Bragg diffraction angle.

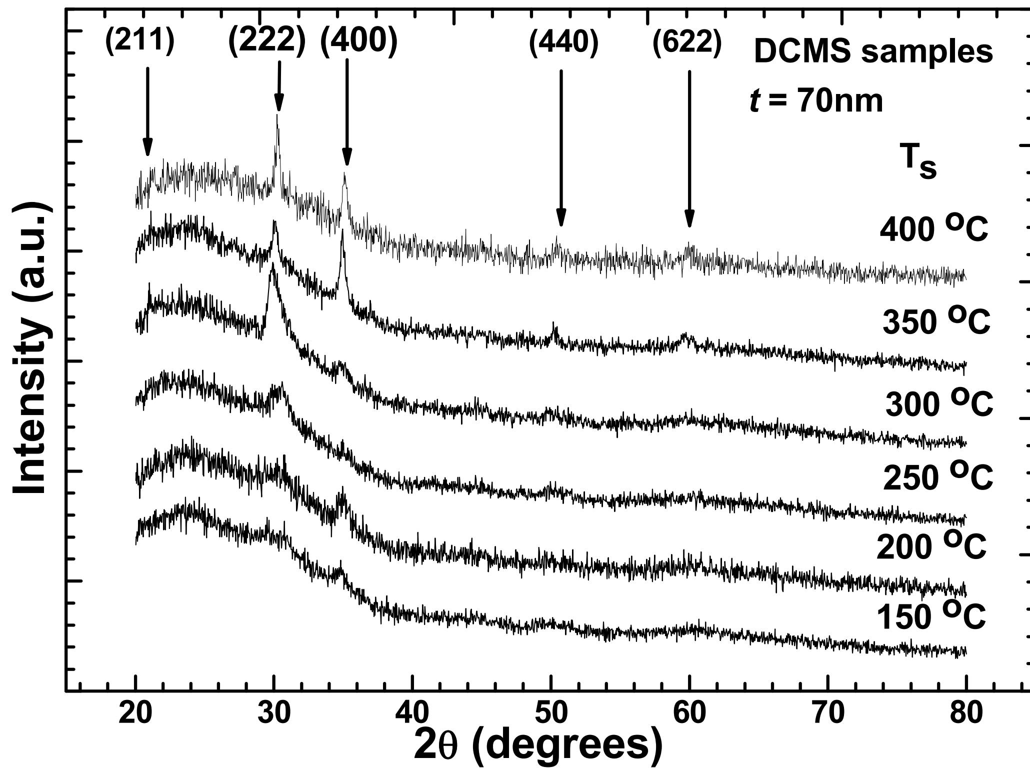

Figure 4. 1. The X-ray diffraction patterns of 70 nm thick ITO films grown by RF sputtering at various substrate temperatures (T_s is substrate temperature, t is the film thickness).

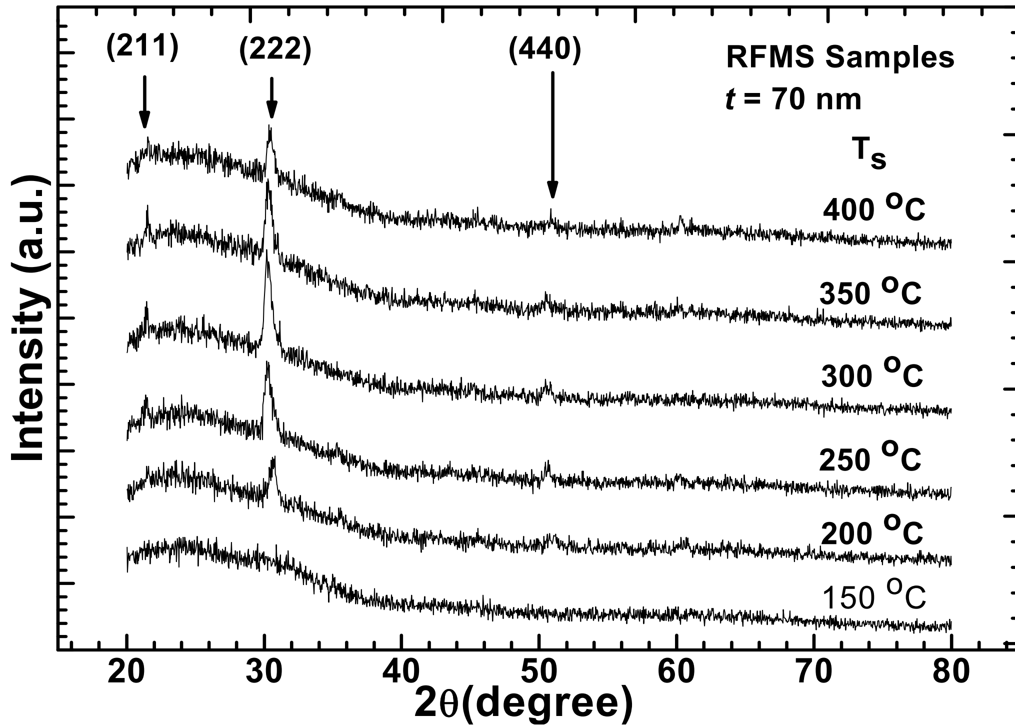

Figure 4. 2. The X-ray diffraction patterns of 70 nm thick ITO films grown by RF sputtering at various substrate temperatures (T_s is substrate temperature, t isthe film thickness).

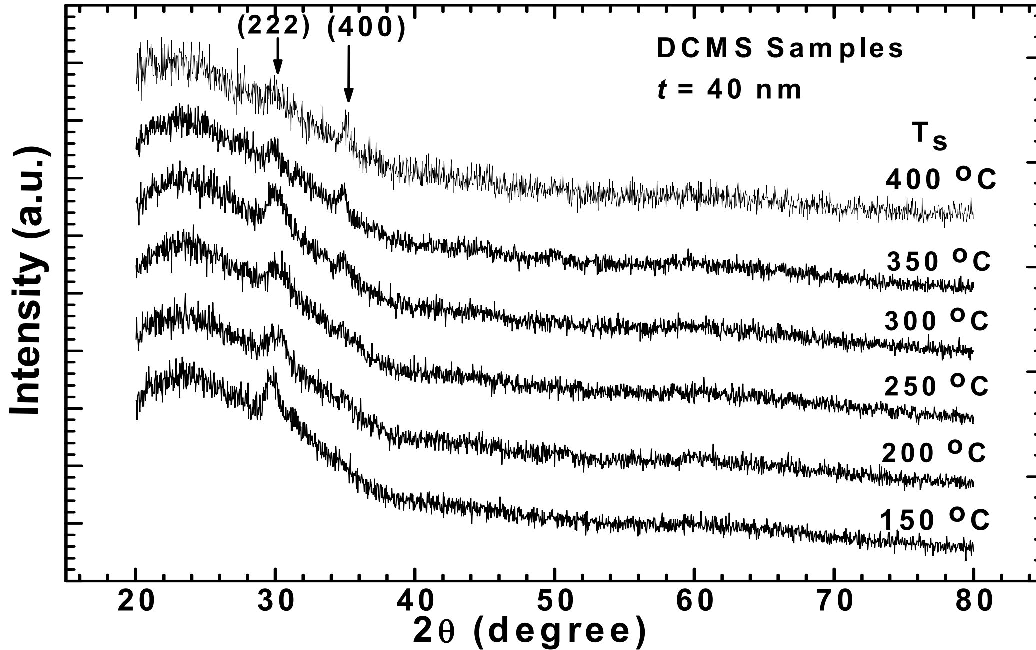

Figure 4. 3. The X-ray diffraction patterns of 40 nm thick ITO films grown by DC sputtering at various substrate temperatures (T_s is substrate temperature, the film thickness).

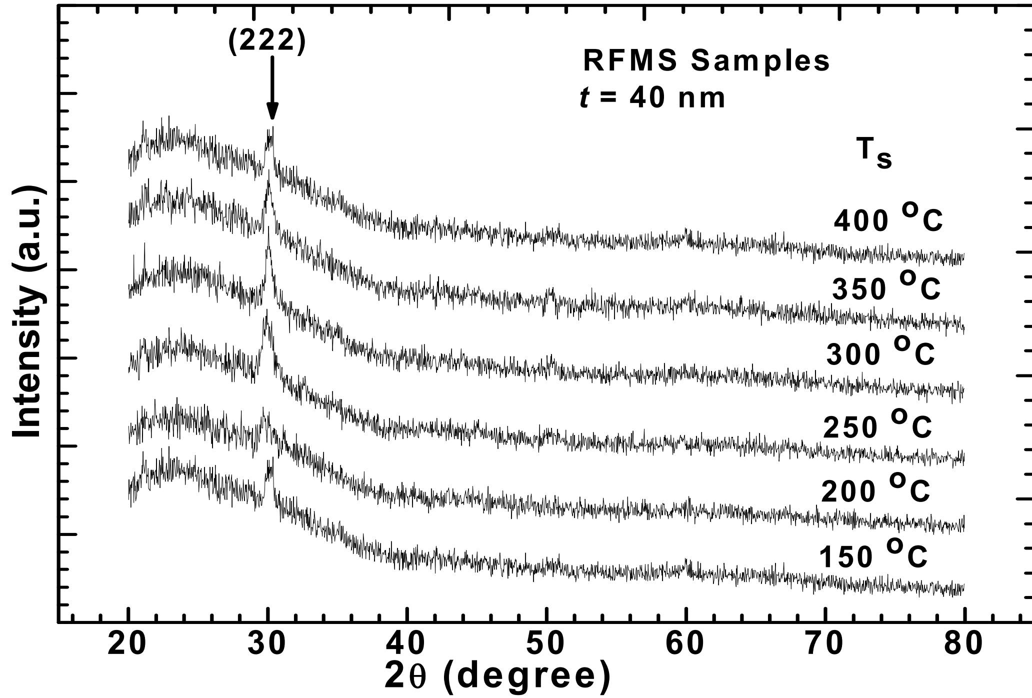

Figure 4. 4. The X-ray diffraction patterns of 40 nm thick ITO films grown by RF sputtering at various substrate temperatures (T_s is substrate temperature, t is the film thickness).

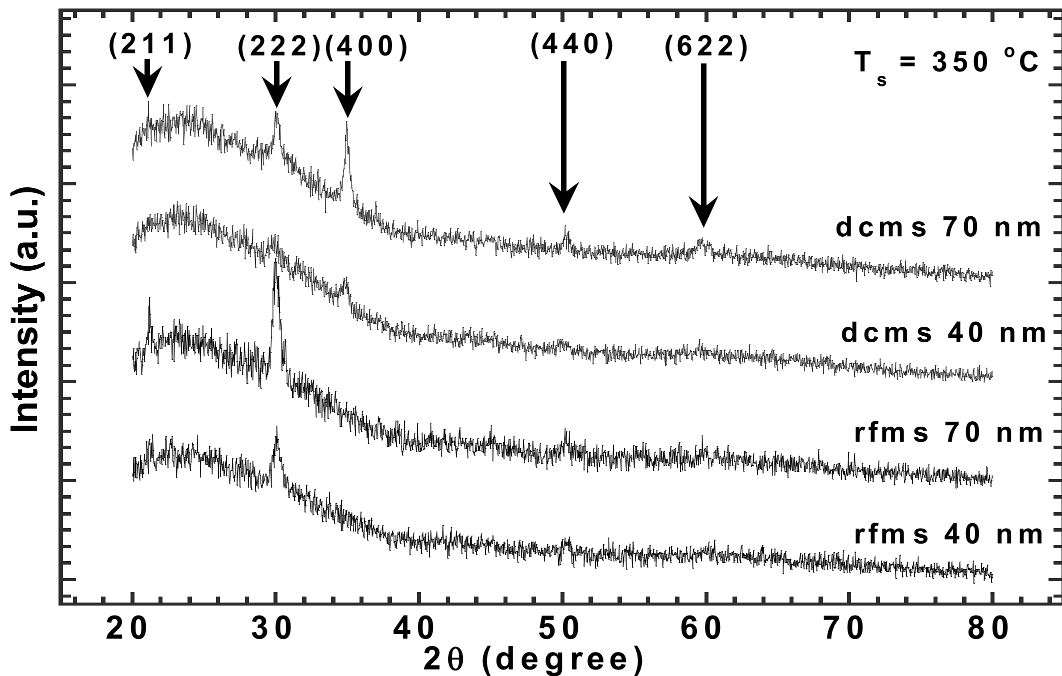

Figure 4. 5. Comparision of thickness effect on crytallization both for DCMS and RFMS samples.

4.2. Scanning Electron Microscopy and Atomic Force Microscopy Results

SEM cross-section image of ITO on glass substrate is illustrated in Figure 4.6. ITO thin film grown on amorph SiO_2 substrate as columnar structure shown in Figure 4.7. and from this graph, thickness of ITO thin layer was found to be about 70 nm for 10 minutes deposition.

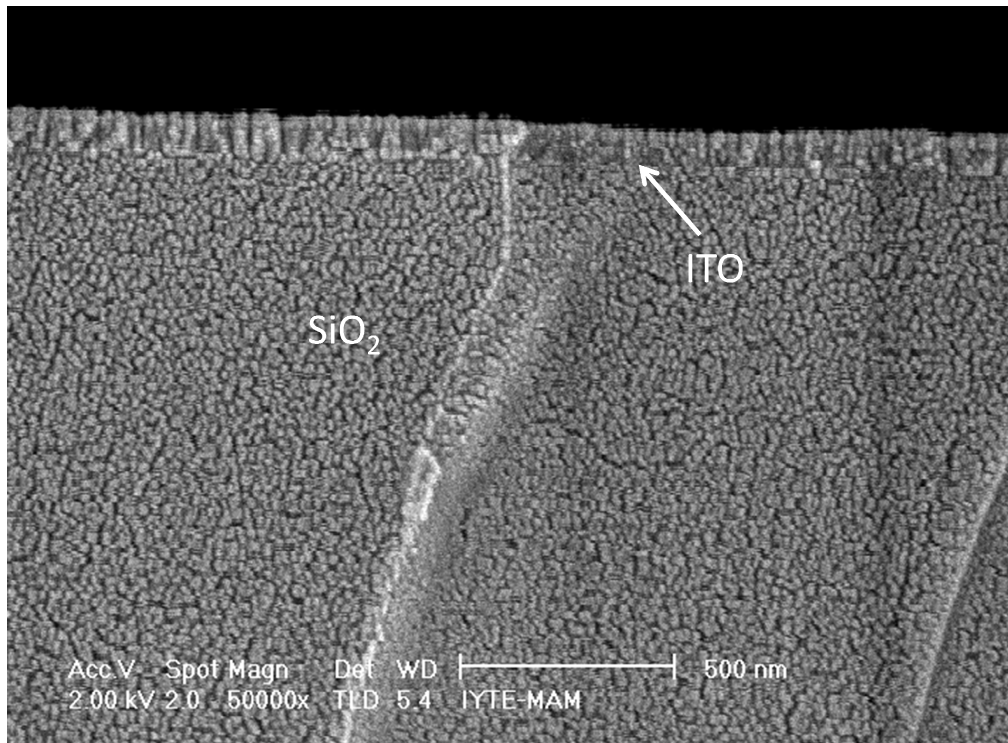

Figure 4. 6. SEM cross-section image of ITO (80 nm)/SiO_2

Atomic Force Microscopy image and the figure shows thickness value of ITO thin films grown on glass substrate illustrated in figure 4.7. As it is shown in figure thickness is about 80 nm and the roughness value of the films is about 3 nm.

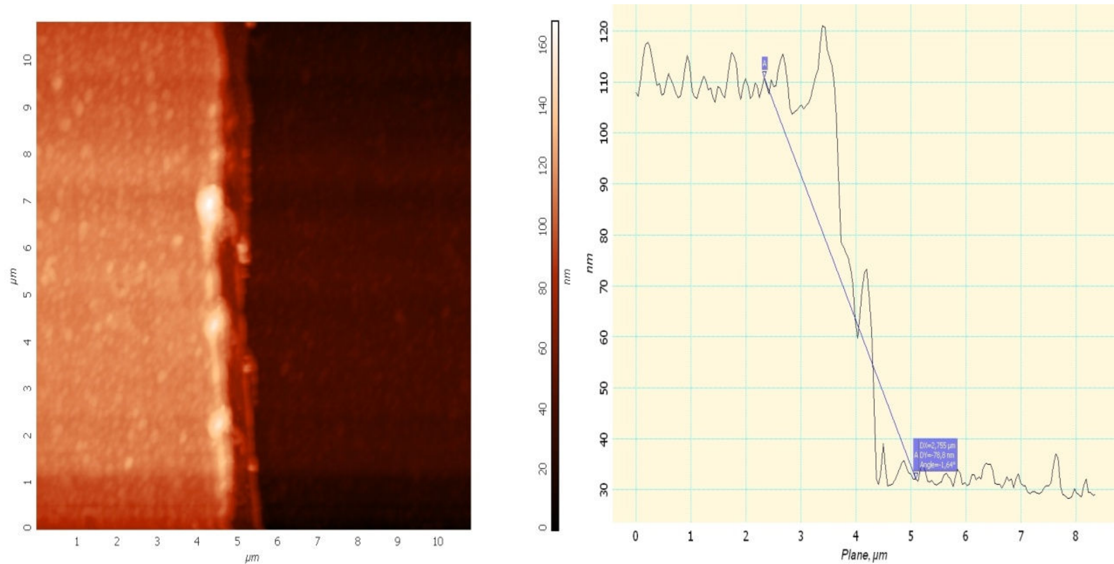

Figure 4. 7. AFM image of ITO (80nm) /SiO_2

4.3. Electrical Results

4.3.1. Substrate Temperature Dependence Resistivity

We used van der Pauw configuration for sheet resistance and Hall effect measurements. For these measurements we used 80 μm thick cupper wire and high purity indium to take contact on gold coated patterned films. (Figure 3.6c). Actually Hall effect measurement be done under low temperature as low as 78 K but sheet resistance measured by sending 0.1 mA current through the contact in the order of given in Tablo 3.2. before cooling down the cryostat temperature. We observed that the resistivity decreases as the substrate temperature increases. This may be due to in an increment in the number of carrier concentration, crystallization and grain size with the increasing substrate temperature (Tablo 5.1.) of ITO thin films. The lowest resistivity for 70 nm thick films grown at the substrate temperature of 350 ^oC were measured as 1.28×10^{-4} Ω-cm for DCMS (Figure 4.8.) and 1.29×10^{-4} Ω-cm for RFMS (Figure 4.9.).

The resistivity is inversely proportional to the carrier concentration and grain size of the film which was calculated using Debye-Scherrer formula. Since the grain size is increased with substrate temperature (Tablo 5.1.), the number of grains, hence, are decreased. Therefore, probability of scattering from grain boundaries decreased.

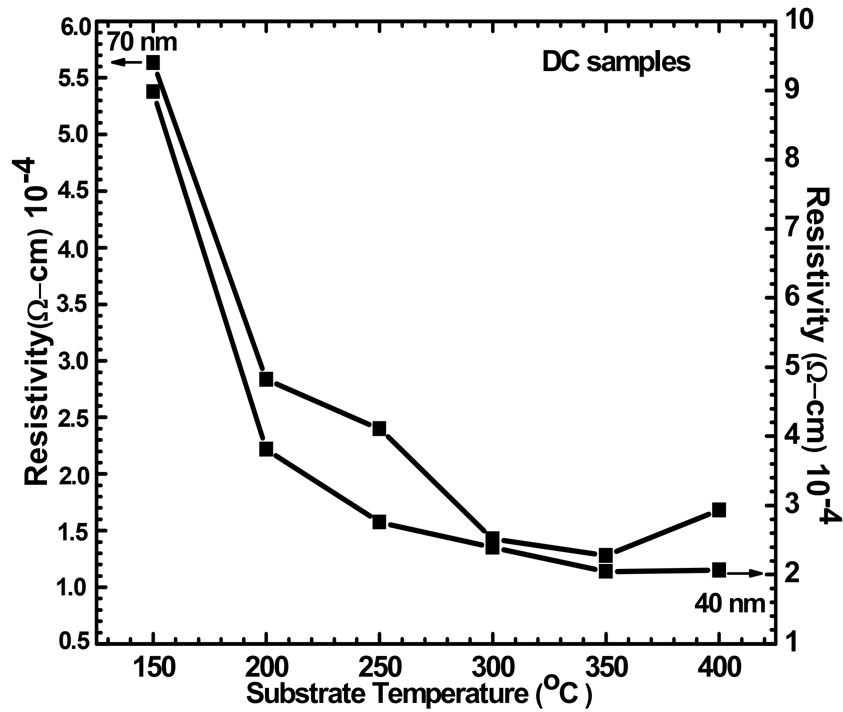

Figure 4. 8. Variation of DSMS grown samples electrical resistivity with respect to substrate temperature

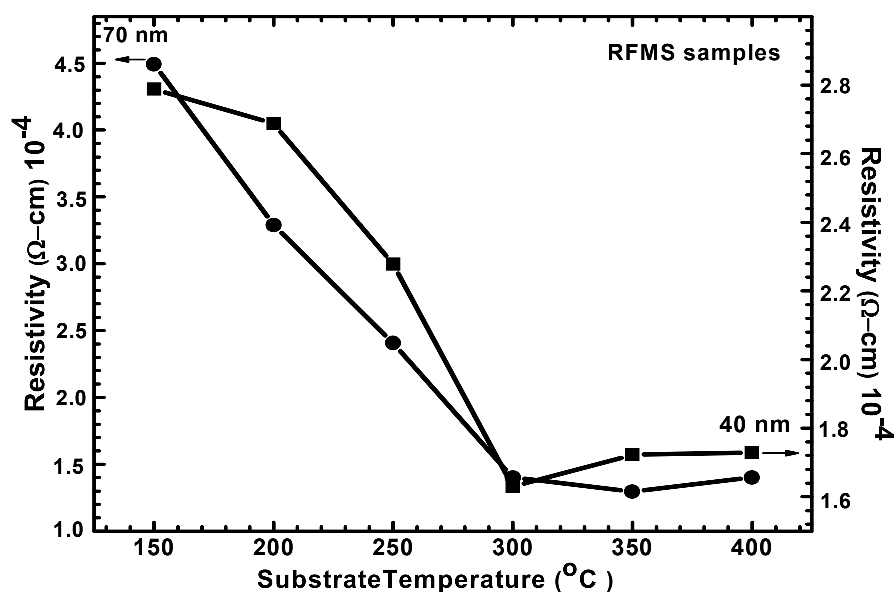

Figure 4. 9. Variation of RFMS grown samples electrical resistivity with respect to substrate temperature.

The resistivities of the films grown at 400 ^{o}C were found to be slightly higher than those grown at 350 ^{o}C for both RFMS and DCMS (Figure 4.8 and Figure 4.9.). The stoichiometry of deposited films might be adversely affected due to increased oxygen vacancies with the increased substrate temperature. On the other hand, as previously reported, some alkali ions might probably diffuse into the film structure from glass substrate at relatively higher growth temperatures (Jayaraj, et al. 2005). Therefore, it is preferable to grow films substrate temperature close to 350 ^{o}C to attain optimum electrical properties.

4.3.2. Measurend Temperature Dependence Resistivity

Due to ITO is composed highly with Sn atoms, we have expect that it is temperature dependence resistivity should be similar to metals namely its resistivity should be increase with temperature because of in metals, when temperature is increased the vibration of atoms in crystal are raised and then they released phonons.

Due to the scattering of electrons from these phonons, resistivity is increase. From our analysis we found that for all films resistivity versus temperature curve shows the expected metallic behavior and as it is also reported by Campet et al. 1991. The resistivity of 70 nm-thick films grown at 350 ^{o}C substrate temperature changed from 1.28×10^{-4} to 1.16×10^{-4} Ω-cm for DC and from 1.29×10^{-4} to 1.16×10^{-4} Ω-cm for RF sputtered while the temperature decreased from 295 to 78 K Figure 4.10. The resistivity of 40 nm-thick films grown at 350 ^{o}C substrate temperature changed from 2.04×10^{-4} to 1.9×10^{-4} Ω-cm for DC sputterred and grown at 300 ^{o}C substrate temperature changed from 1.62×10^{-4} to 1.5×10^{-4} Ω-cm for RF sputtered as temperature changed from 295 K to 78 K shown in Figure 4.11. The room temperature resistivity of DCMS and RFMS grown samples were nearly same and their resistivity versus temperature behaviours were very similar.

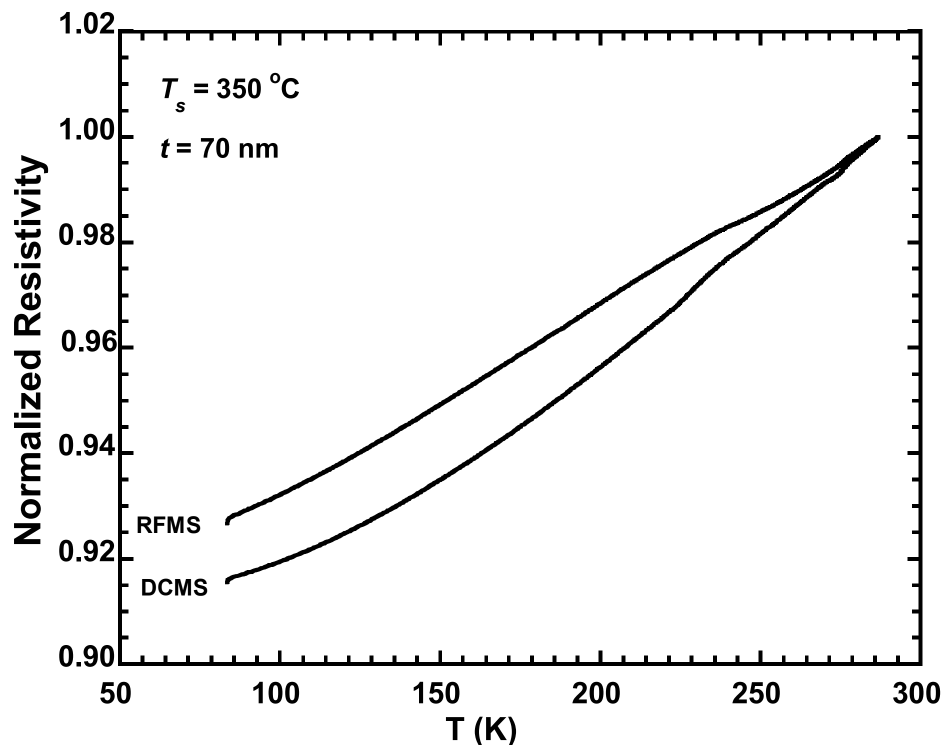

Figure 4. 10. Variation of electrical resistivity of ITO thin film with respect to temperature (resistivity values were normalized with respect to the measured values of 286 K).

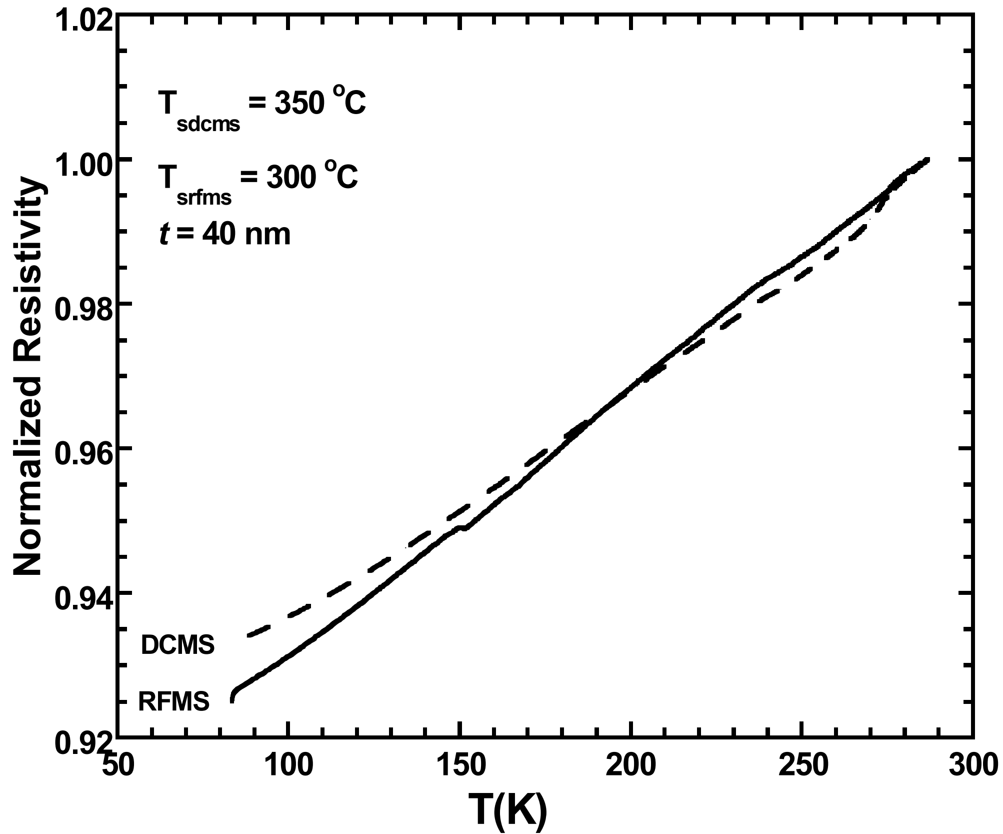

Figure 4. 11. Variation of electrical resistivity of ITO thin film with respect to temperature (resistivity values were normalized with respect to the measured values of 286 K).

4.3.3. Variation of Hall Coefficient with Temperature

As I said before ITO is a highly doped degenerate n-type semiconductors and due to it is doping concentration, it shows nearly metalic behavior with temperature. In order to figure out temperature dependence of ITO thin films we measure Hall coefficient by changing temperature from 78K to room temperature using van der Pauw configuration. We observed that the Hall coefficient slowly increased with the measured temperature. (Figure 4.12). Since ITO thin films are highly degenerate *n*-type semiconductors, the variations of electrical properties with temperature is small as similarly reported by Campet et al. 2005.

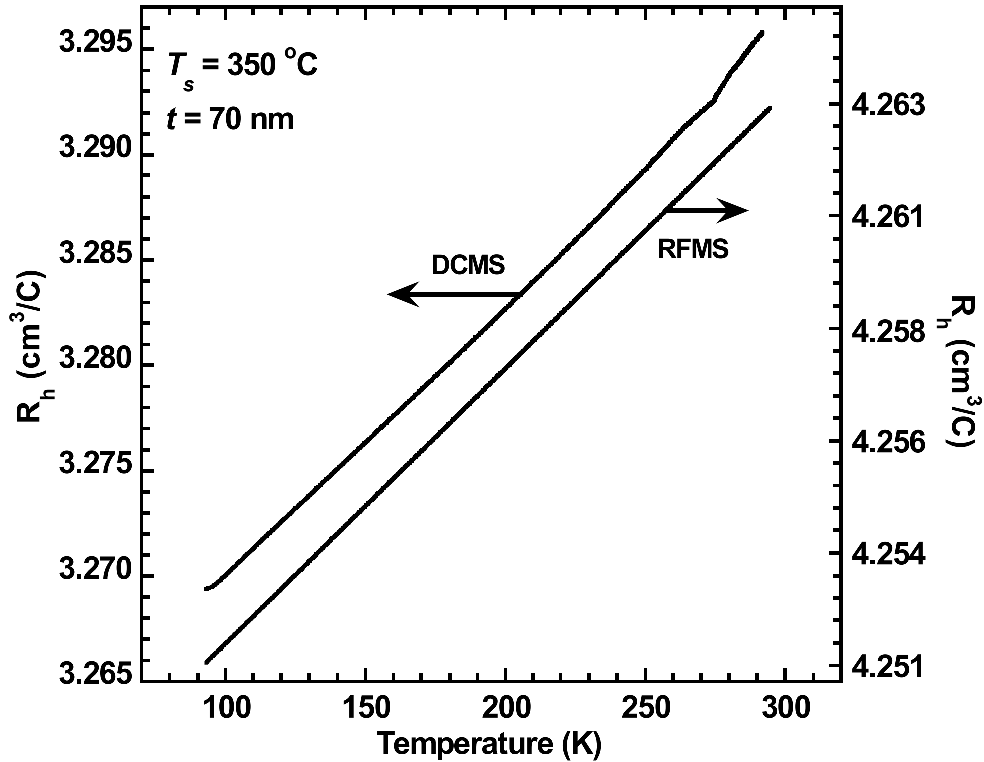

Figure 4. 12. Variation of Hall Coefficient of ITO Thin Films with respect to Temperature

4.3.4. Substrate Temperature Dependence of Carrier Concentration and Hall Mobilities

Hall mobilities and carrier concentration of ITO thin films calculated using results of Hall coefficient measurement for 70 nm thick samples. The carrier concentration was calculated using the formulation of $N_e = \frac{1}{n\,R_h}$ where R_h is hall coefficient and n is an electron charge which is 1.602×10^{-19} Coulomps. It was observed that the carrier concentration increases with increasing substrate temperature seen in Figure 4.13. and Figure 4.14. for DCMS and RFMS sputtering, respectively. In ITO thin films oxygen vacancy and the activated Sn in In site are the two main sources of the free electrons. As discussed above the crystallinity of ITO film increased with substrate temperature. This higher degree of crystallinity results in the lessen oxygen vacancy

and, therefore, Sn atoms would have a higher possibility to produce free electrons as suggested by (Lee and Park 2004). Our findings point out that increase in carrier concentration with increasing substrate temperature may also be due to increase in the diffusivity of tin atoms with four valance electrons in interstitial locations and grain boundaries, replacing In atoms with three valance electrons as reported earlier by Reddy et al. 2006. It is also observed that as the substrate temperature increased, Hall mobility of ITO thin films consistently decreased for DCMS samples which is expected (Figure 4.13). However, for RFMS grown samples, even though carrier concentration show similar increase, mobilities show different behavior with substrate temperature (Figure 4.14). This might be due to different scattering mechanism limiting mobility in RFMS grown samples. The increase in the mobility for temperatures higher than 250 ^{o}C can be attributed to the higher crystallinity of ITO films, which higher crystallinity was observed also in XRD data. There is a rapid decrease in mobility above 350 ^{o}C, which might be due to large increase in carrier concentration, which then reduced the mobility. Similarly, for DC sputtered samples we saw very slow decrease in mobility around 200 -300 ^{o}C region, where, again improvement in crystal quality might be playing a role, however, this time not strong enough to see increase in the mobility. Having different scattering mechanisms play an important role in the variation between carrier concentration and Hall mobility for DC samples (Figure 4.13). There are several scattering mechanism in ITO effectively limiting mobility, such as grain boundary, lattice, ionized impurity, dislocation scattering as mentioned in chapter 2. At low substrate temperatures, the grain sizes are small leading to large number of grain boundaries. Hence, the scattering from these grains boundaries effective limiting mechanism. On the other hand, at high temperature the carrier concentration is in the order of 10^{20}-10^{21} cm^{-3}, so that the mobility mainly limited by the ionized impurity scattering.

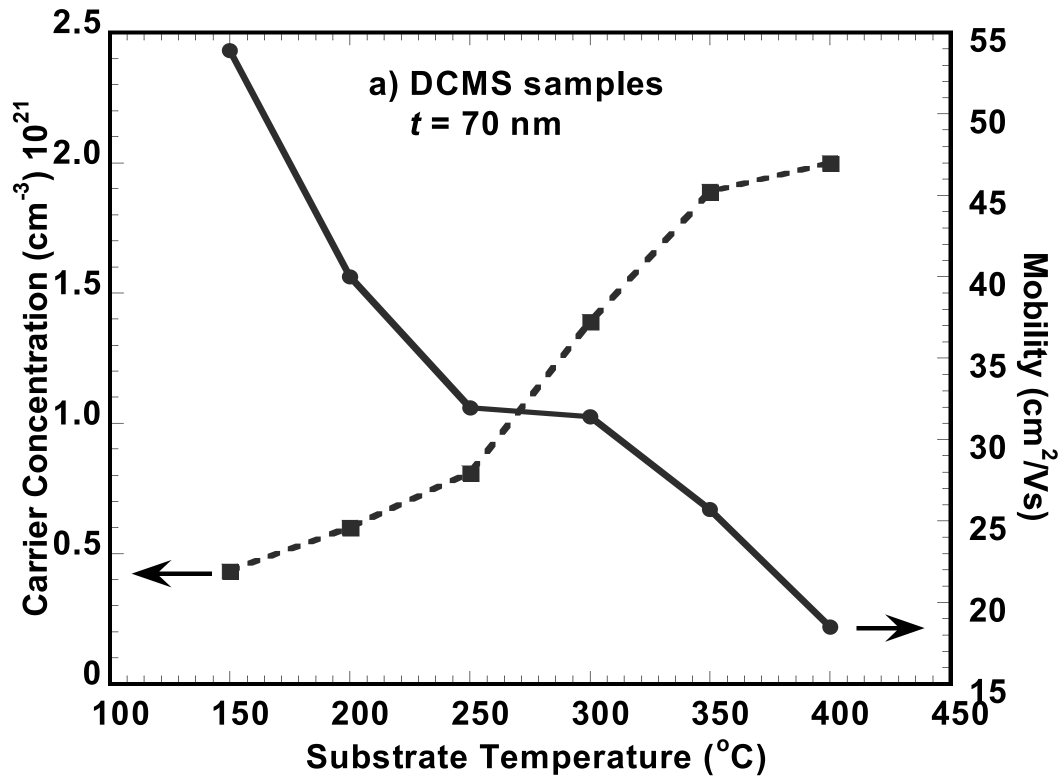

Figure 4. 13. Variation of carrier concentration and Hall mobilities of DC sputtered ITO thin films with respect to the substrate temperature.

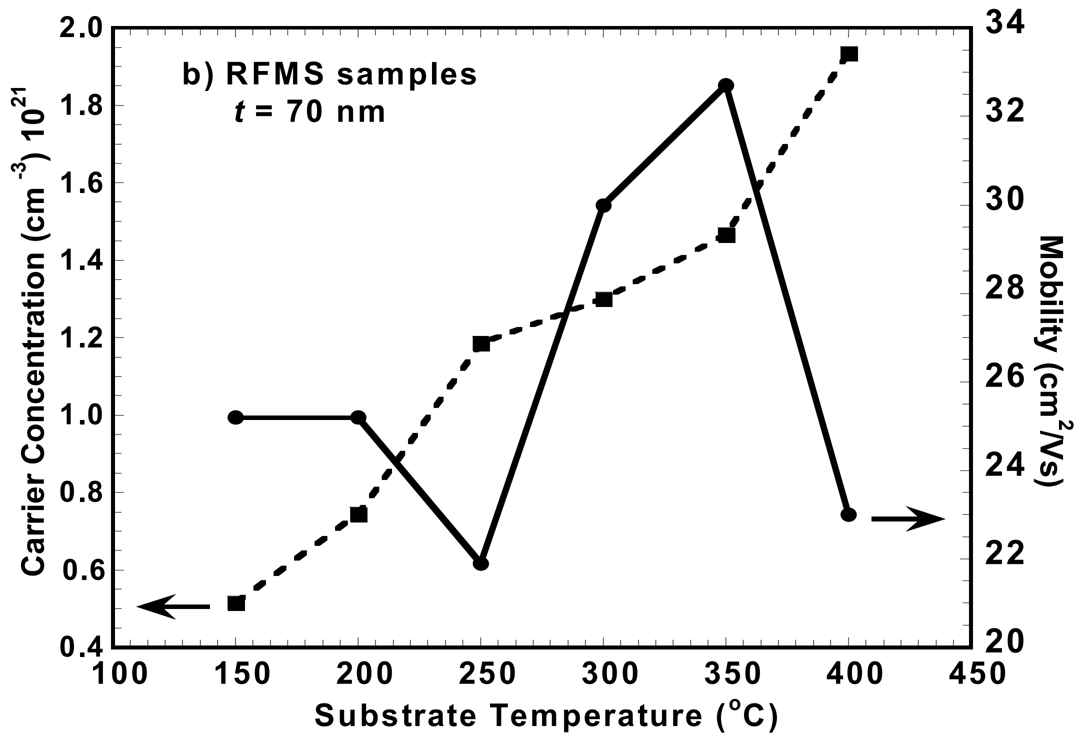

Figure 4. 14. Variation of carrier concentration and Hall mobilities of RF sputtered ITO thin films with respect to the substrate temperature.

4.4. Optical Results

4.4.1. Optical Transmission of Indium Tin Oxide Thin Films

The optical transmissions of DCMS and RFMS grown ITO thin films were measured by a spectroscopic ellipsometer. Before measured the transmission of the samples, we had measured the pure glass substrate transmission to compare and found only films' effect on transmission. We investigate that the samples were 80-85 % transparent in the visible region without glass effect for both 40 nm and 70 nm thick samples shown in Figure 4.15a and b and Figure 4.16a and b in order DCMS 70 nm and 40 nm and RFMS 70 nm and 40 nm samples. These high transmissions in the visible region are based on large band gap and crystallinity of thin ITO films. In Figure 4.15a and Figure 4.16a we saw slow wave rather than figure 4.15b and figure 4. 16b. Its reason should be the thickness of the films. As the thickness of the films is increased the probability of the scattering of light from layers are increased.

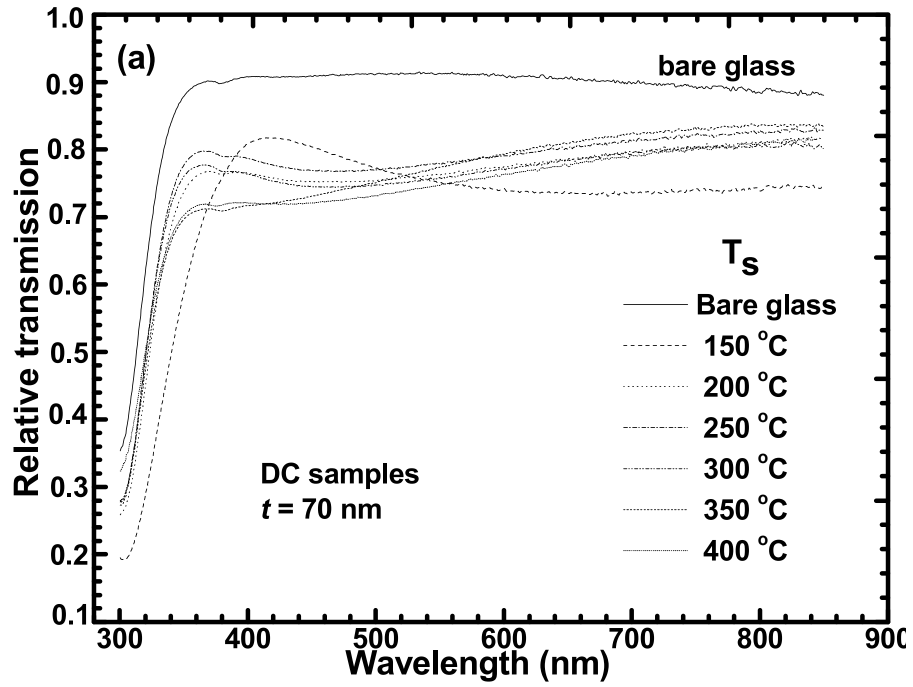

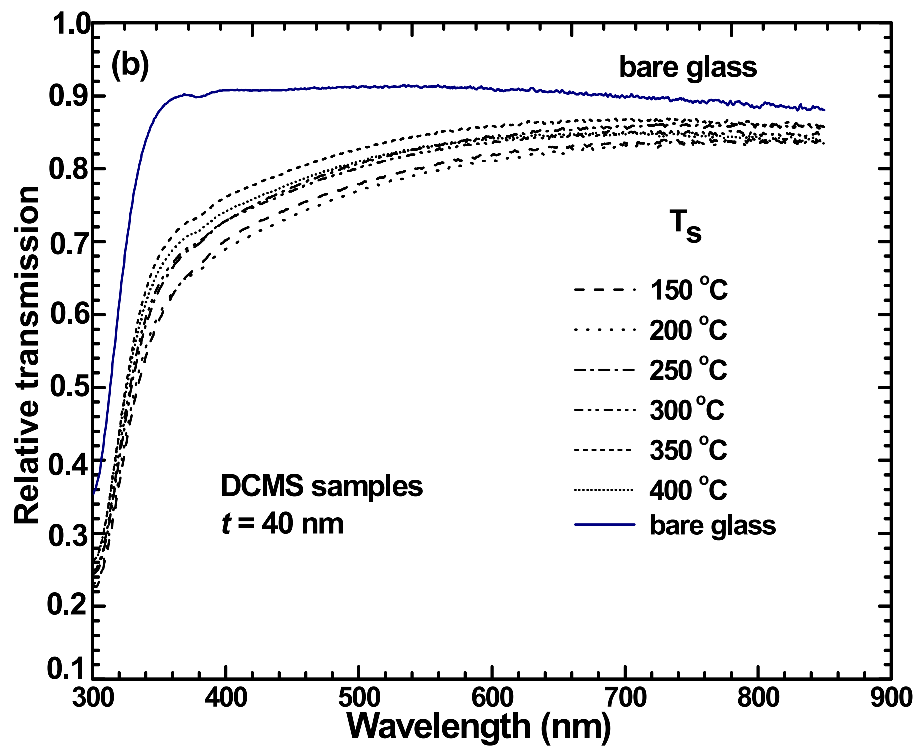

Figure 4. 15. Transmittance spectrum of a) 70 nm and b) 40 nm thick DC sputtered ITO thin films grown at different substrate temperatures (t is thickness).

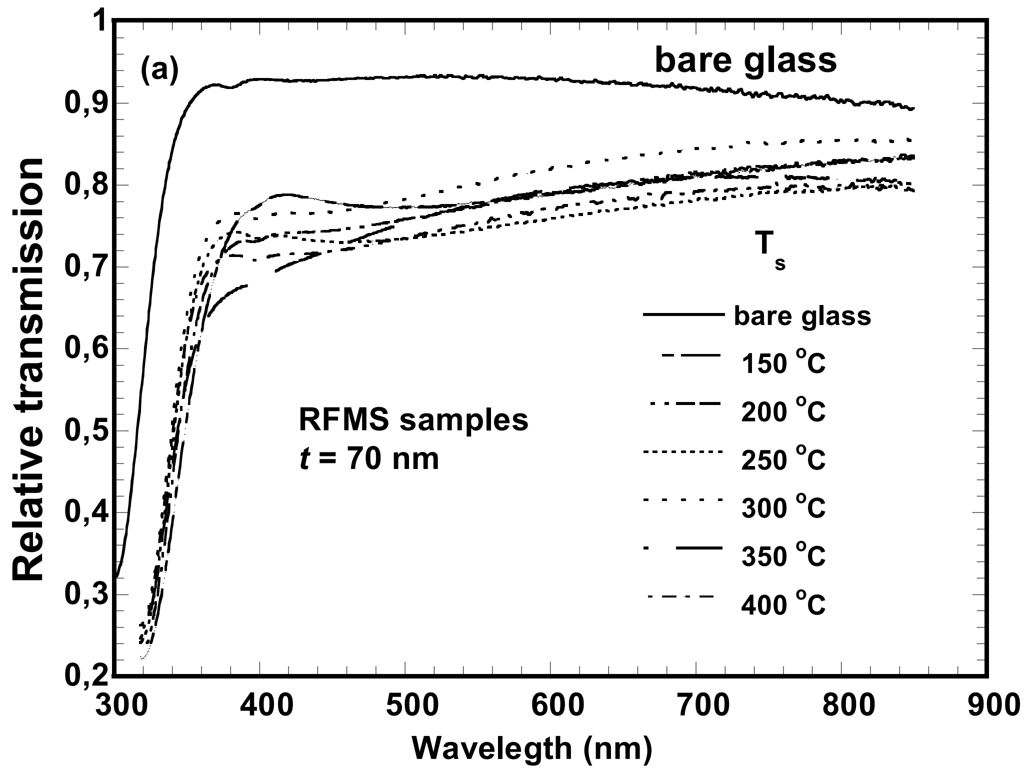

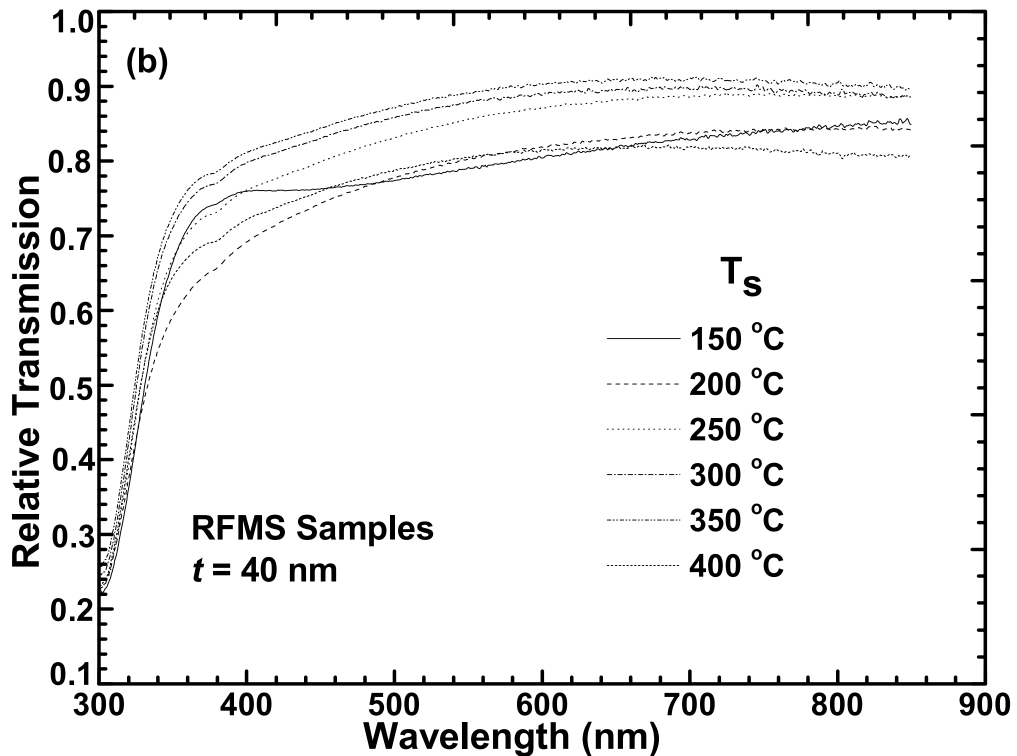

Figure 4. 16. Transmittance spectrum of a) 70 nm and b) 40 nm thick RF sputtered ITO thin films grown at different substrate temperatures (*t* is thickness).

4.4.2. Bandgap of Indium Tin Oxide Thin Films

The band gap of ITO thin films was calculated using transmittance spectrum of them. Actually in order to calculate band gap we should have used transmittance and reflectance spectrum of ITO thin films but in the visible and UV regions 'as many authors supported' reflectance of conducting oxide thin films is very low so to a good approximation it can be neglected. (Kerkache, et al. 2006). In my study, I used this approximation due to the transmittance of my films were more than 85%. In the view of this approximation I used the the absorption coefficient (α) versus energy graph to find the band gap of ITO thin films. Absorption energy can be calculated using the formula (Kerkache, et al. 2006, Meng and santos 1998):

$$T - R = \exp(-\alpha t)$$

Where T and R are the transmittance and reflectance and t is the thickness of the film. Using above mentioned approximation R can be taken zero so we can write absorption coefficient as:

$$\alpha^2 = \frac{[\ln T]^2}{t^2}$$

The optical band gap of the films were calculated by extrapolating linearly increasing portion of α^2 (absorption coefficient) versus *hυ* curve and obtaining the value corresponding to 0 for α^2. For x axis I used the well known formula;

$$E = \frac{hc}{\lambda}$$

Where *h* is Planck constant, *c* is light velocity, λ is wave length and E is energy. The optical band gap of the films were calculated by extrapolating linearly increasing portion of α^2 (absorption coefficient) versus *hυ* curve and obtaining the value corresponding to 0 for α^2 shown in figures 4.17a and b for DCMS and Figure 4.17a and b for RFMS samples.

Band gap variation of ITO thin films with respect to substrate temperature is given in Figure 4.18a and b and also written in Tablo 5.1. It is obviously seen these figure that band gap of ITO thin films were further increased with increased substrate temperature can be explained Burstain-Moss shift (Zhang, et al. 2007) which I mentioned in chapter 2. That shift is due to increment in number of carrier increases with increasing to substrate temperature which, leads to filling the lowest energy state in the conduction band as reported by Zhang et al. 2007. The fact that the band gap is getting lowered at 300 - 350 ^{o}C temperatures for RF sputtered film with the thickness of 70 nm that might be based on decreasing grain size at these temperatures (Tablo 5.1.) and increasing scattering from increased grain boundaries.

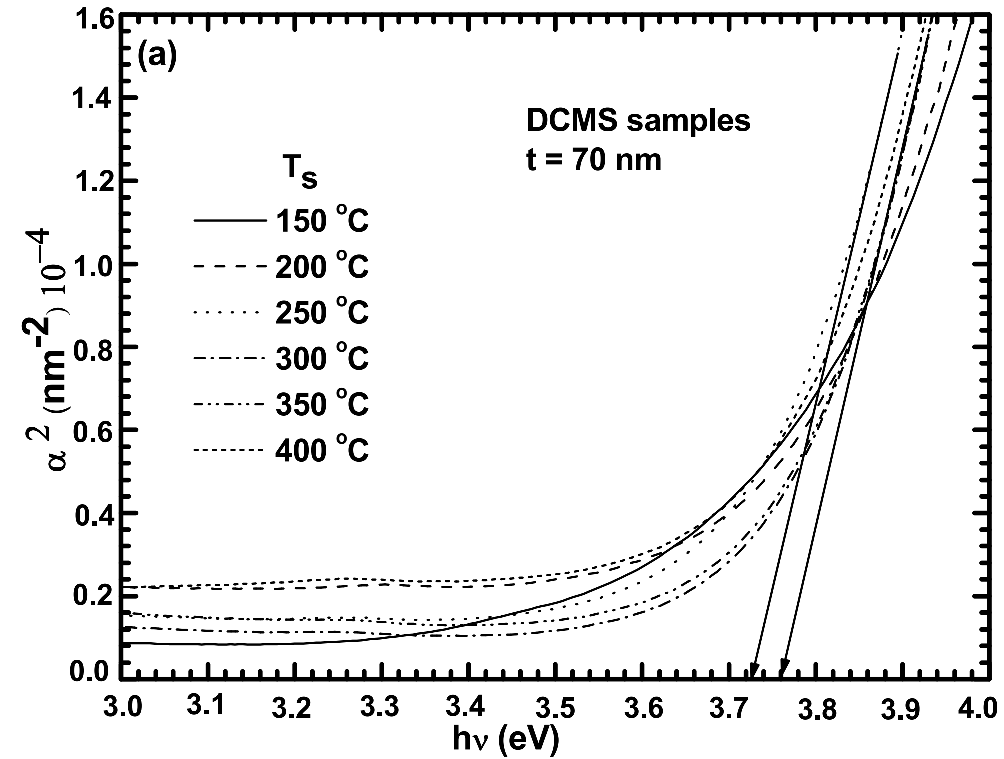

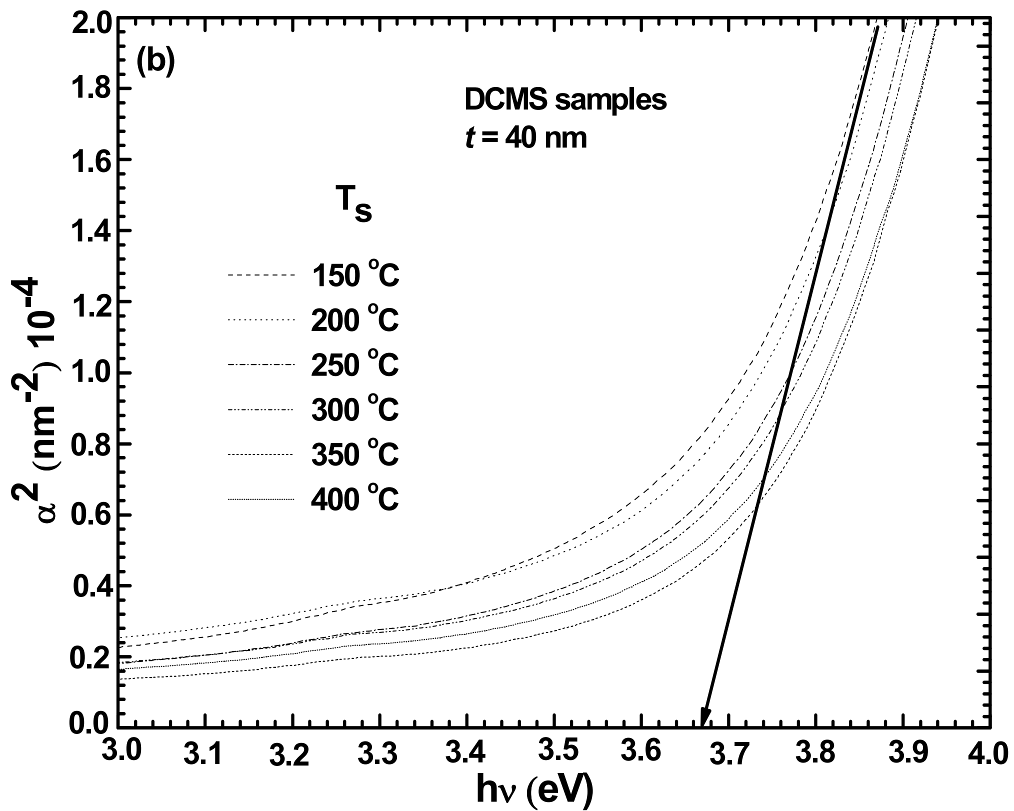

Figure 4. 17. Plot of α^2 versus $h\upsilon$ for DCMS samples with thickness of a) 70 nm and b) 40 nm grown at various substrate temperatures (t is thickness).

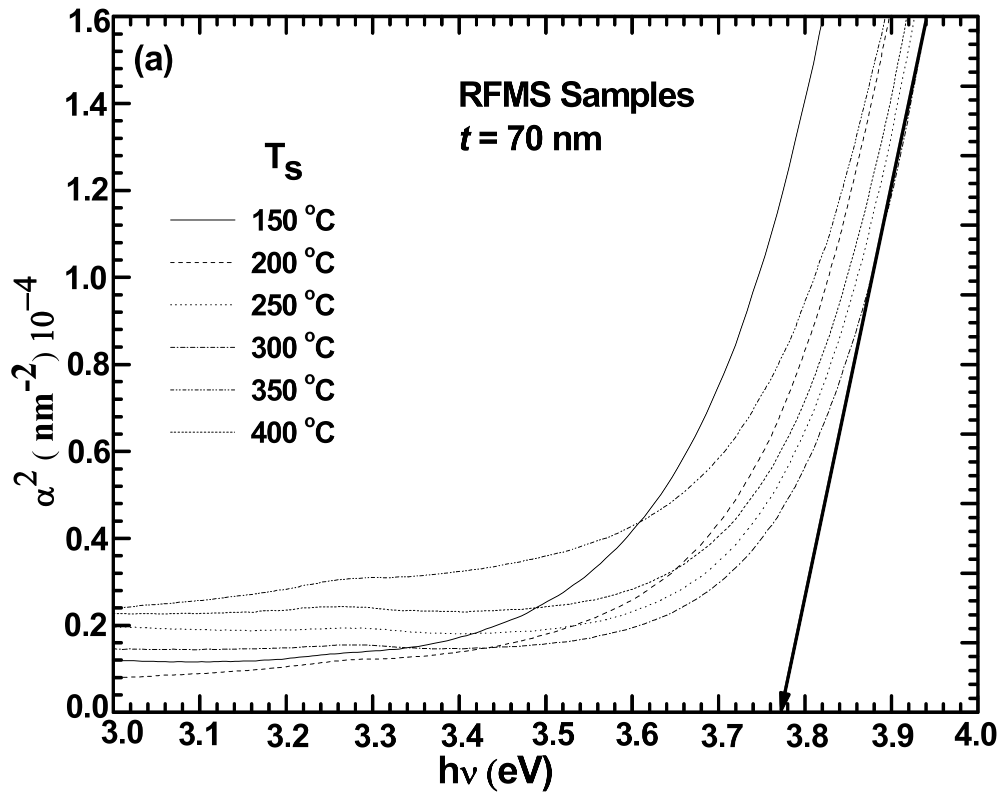

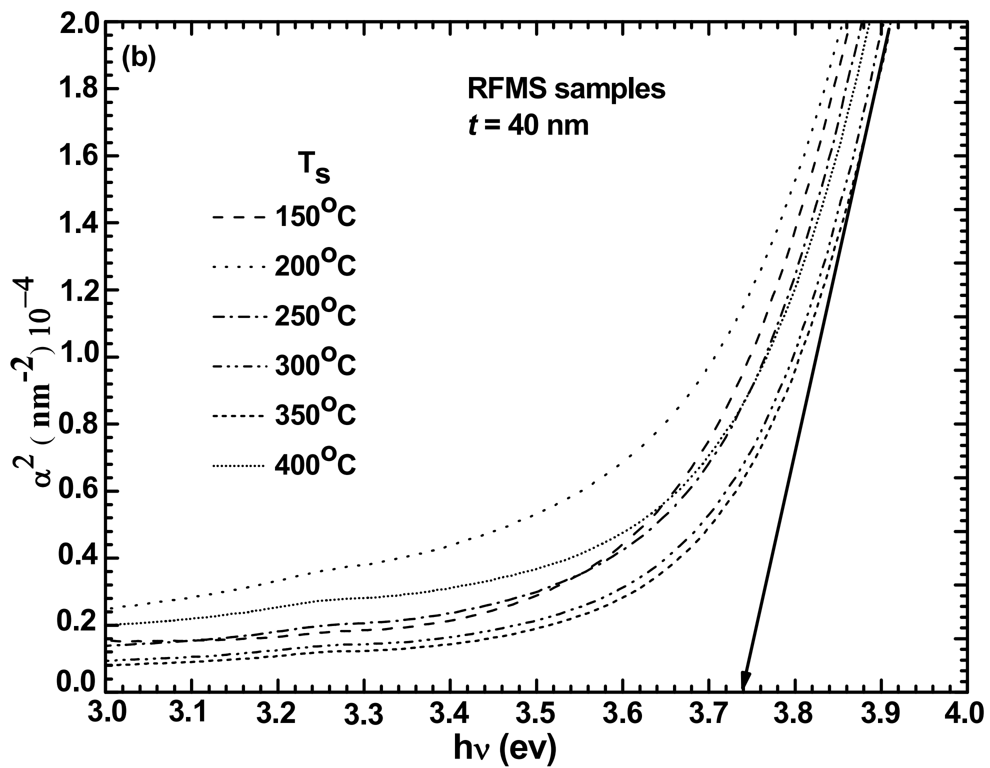

Figure 4. 18. Plot of α^2 versus $h\upsilon$ for RFMS samples with thickness of a) 70 nm and b) 40 nm grown at various substrate temperatures (*t* is thickness).

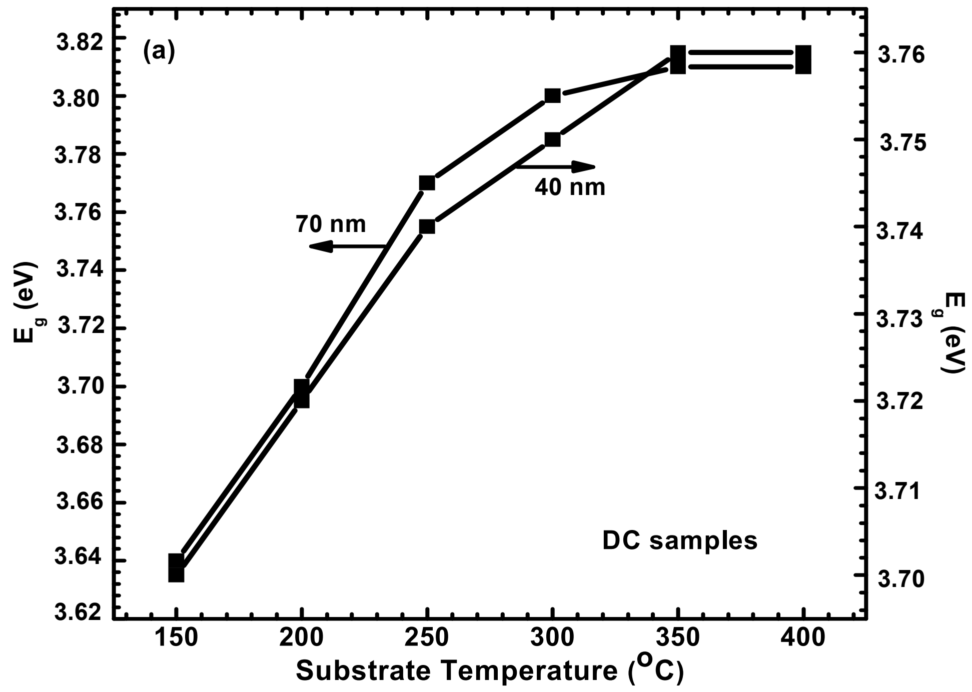

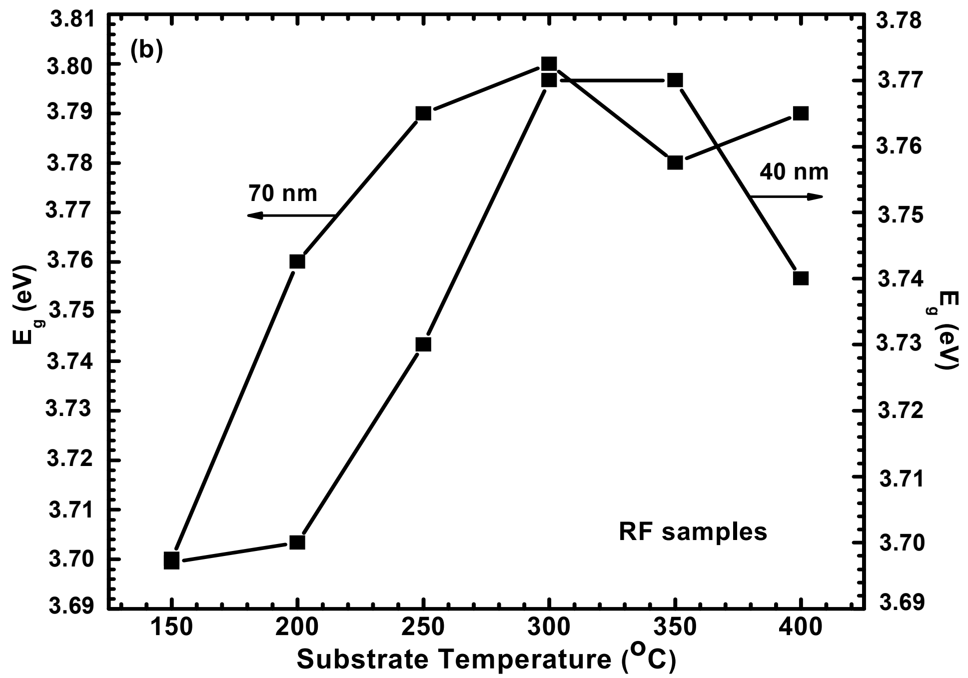

Figure 4. 19. Variation of band gap with respect to substrate temperature a) DCMS samples, b) RFMS samples.

Tablo 5. 1. Properties of the DCMS/RFMS sputtered ITO thin films. (T_s substrate temperature, E_g band gap, ρ resistivity, n carrier concentration, μ Hall mobility, d grain size. Note that : The results are for 70 nm thick samples.

Growth method	Sample Code	T_s(°C)	$\rho(10^{-4}\ \Omega\ cm)$ 300K	$\rho\ (10^{-4}\ \Omega cm)$ 78K	$n(cm^3 10^{21})$	$\mu(cm^2Vs)$	$E_g(eV)$	d(nm)
DCMS	ITO1	*150*	2.67	5.64	0.43	53.9	3.64	–
DCMS	ITO2	*200*	2.53	2.66	0.60	*40.0*	*3.70*	6.4
DCMS	ITO3	*250*	2.39	2.23	0.81	*31.9*	*3.77*	6.8
DCMS	ITO4	300	1.42	2.29	1.39	31.4	3.80	7.5
DCMS	ITO5	*350*	1.28	1.16	1.89	25.7	3.81	16.6
DCMS	ITO6	*400*	1.68	1.53	2.00	18.5	3.81	19.5
RFMS	ITO1	150	4.49	4.04	0.51	25.2	3.70	–
RFMS	ITO2	200	3.29	3.01	0.74	25.2	3.76	15.4
RFMS	ITO3	250	2.40	2.20	1.18	21.9	3.79	17.0
RFMS	ITO4	300	1.40	1.81	1.30	30.0	3.80	17.1
RFMS	ITO5	350	1.29	1.15	1.46	32.7	3.78	16.0
RFMS	ITO6	400	1.40	1.27	1.93	23.0	3.79	17.8

4.5. Large Area Coating Magnetron Sputtering Results

4.5.1. X-Ray Diffiraction Result of Annealed LA-ITO Samples

The X-Ray diffiraction result of annealed large area ITO thin films shown in figure 4.20 and as the result shows ITO has polycrytal structure which is refered to cubic bixybite structure. While the annealing temperature increased the crystallizatization increased with the planes of (222) and (400) mostly and the other crystallization planes also seen but not much intensive. The improvement of the crystallization can be explained by increasing vibration of atoms with temperature and that may result in sitting atoms on most densely planes like (222) and (400). For this measurement we used grazing incidence method that is why we did not see any roughness might come from glass substrate.

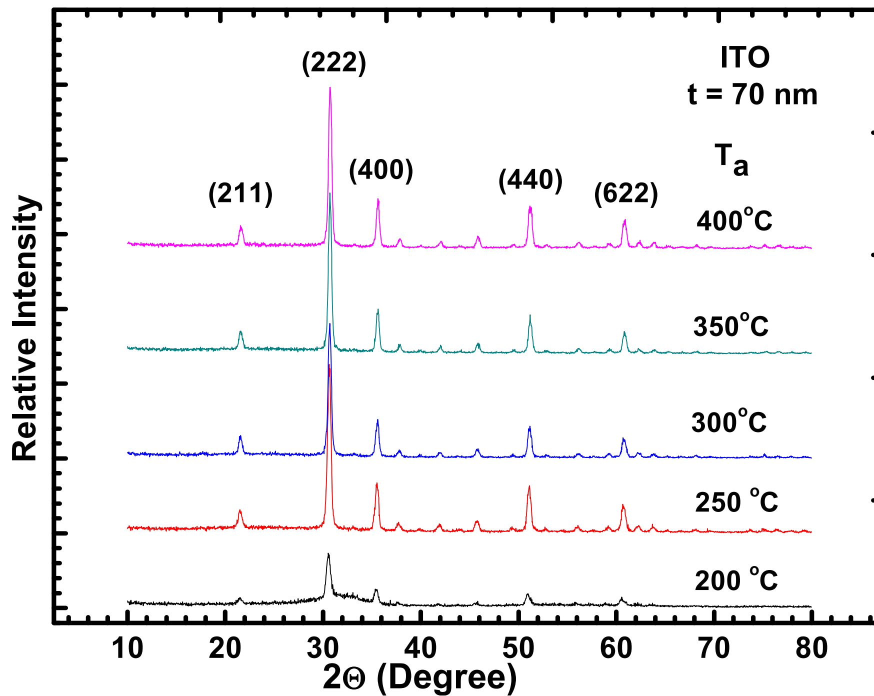

Figure 4.20. X-Ray Diffiraction Results of LA-ITO Thin Films

4.5.2. Electrical Results

4.5.2.1. Room Temperature Resistivity versus Annealing Temperature

Room temperature resistivities were measured by van der Pauw method. As it is clear from figure 4.21 resistivity of the films decrease with increaing annealing temperature because with increasing annealing temperature the grain size of the films were also increase and also with increasing annealing temperature carrier concentration of he films were increase. The lowest resistivity value was measured at the annealing temperature of 450 ^{o}C with the value of 3.12×10^{-4} Ω-cm.

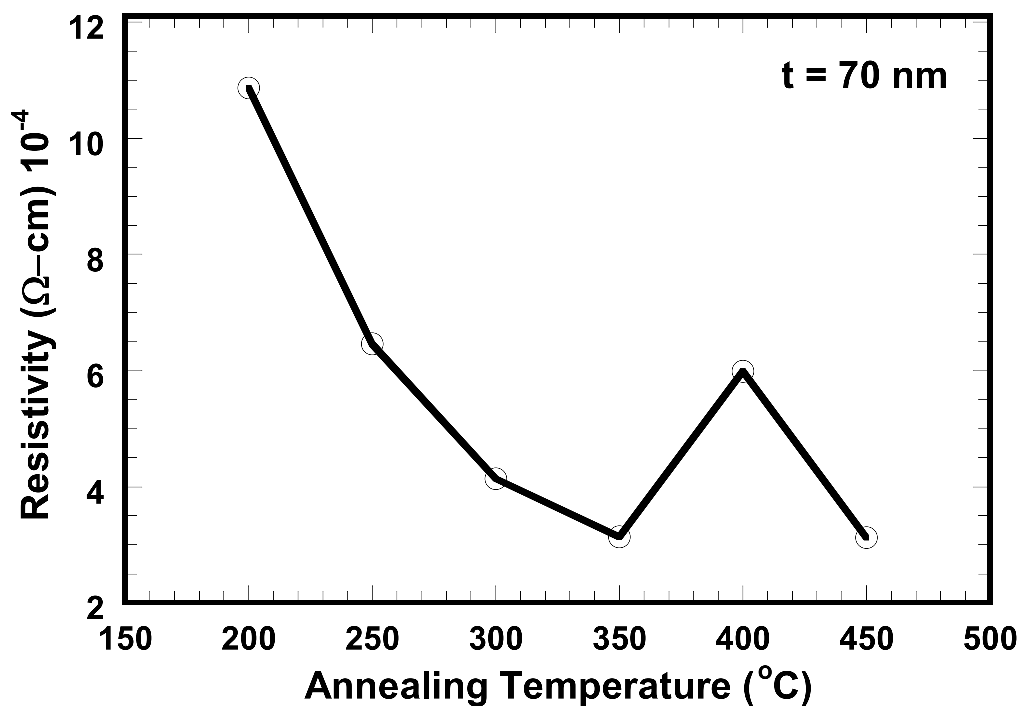

Figure 4.21. Annealing temperature dependence resistivity of LA-ITO thin films

4.5.2.2. Temperature Dependence Resistivity

Temperature dependence resistivity show that ITO behaves like a metal with temperature because its resistivity increased with temperature. The lowest that we found was 4.6×10^{-4} Ω-cm at the annealing temperature of 350 °C and its behavior with temperature shown in figure 4.22.

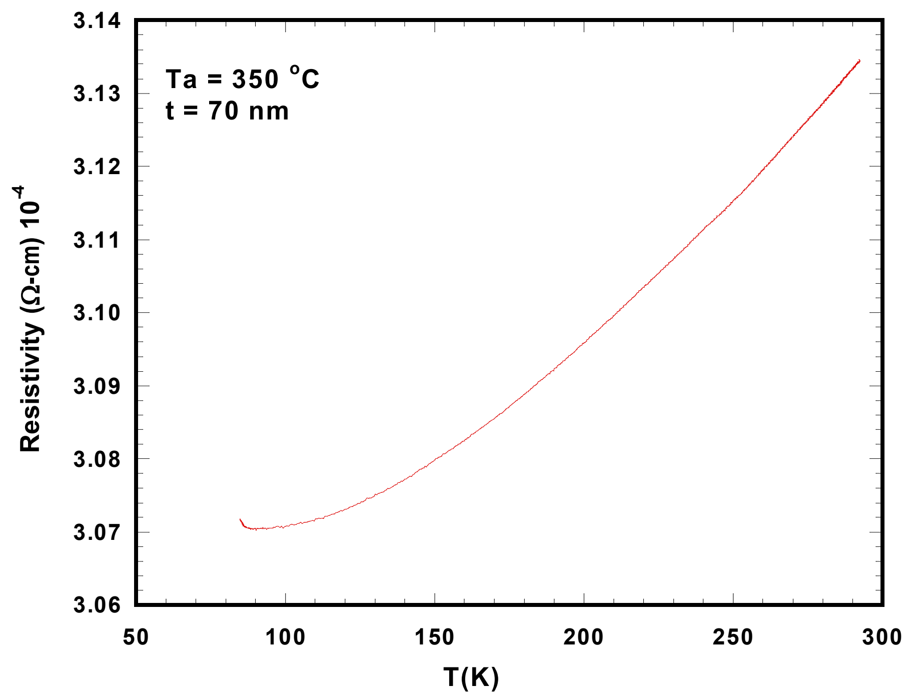

Figure 4.22. Temperature dependence resistivity of annealed LA-ITO

4.5.2.3. Temperature Dependence Hall Coefficient

Temperature dependence Hall coefficient result illustrated in figure 4.23. as it is clear from the figure hall coefficient don not change so much with temperature because

ITO has highly degenerate band gap structure due to large amound of carrier concentration.

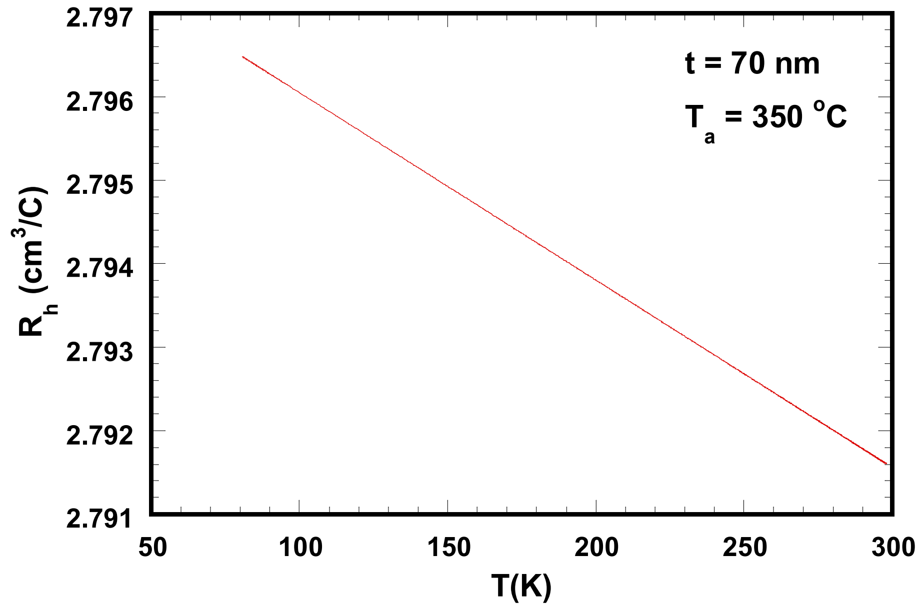

Figure 4.23. Temperature Dependence Hall Coefficient of LA ITO Thin Films

4.5.2.4. Carrier Concentration and Hall Mobilities versus Annealing Temperature

As I mentioned before oxygen vacancy and the activated Sn in In site are the two main sources of the free electrons. Crystallinity of the films are increased with annealing temperature so higher degree of crystallinity results in the lessen oxygen vacancy and, therefore, Sn atoms would have a higher possibility to produce free electrons as Lee and Park 2006 suggested and the other source of free alectrons are diffusivity of tin atoms with four valance electrons in interstitial and grain boundaries, replacing In atoms with three valance electrons as reported earlier by Reddy, et al. 2006. The variation of carrier concentration and Hall mobilities versus annealing temperature

is shown in figure 4.24 and with increasing annealing temperature carrier concentration are increase and Hall mobilities are decrease. The decreasing of Hall mobilities can be explained by scattering in semiconductors mentioned in chapter 1.

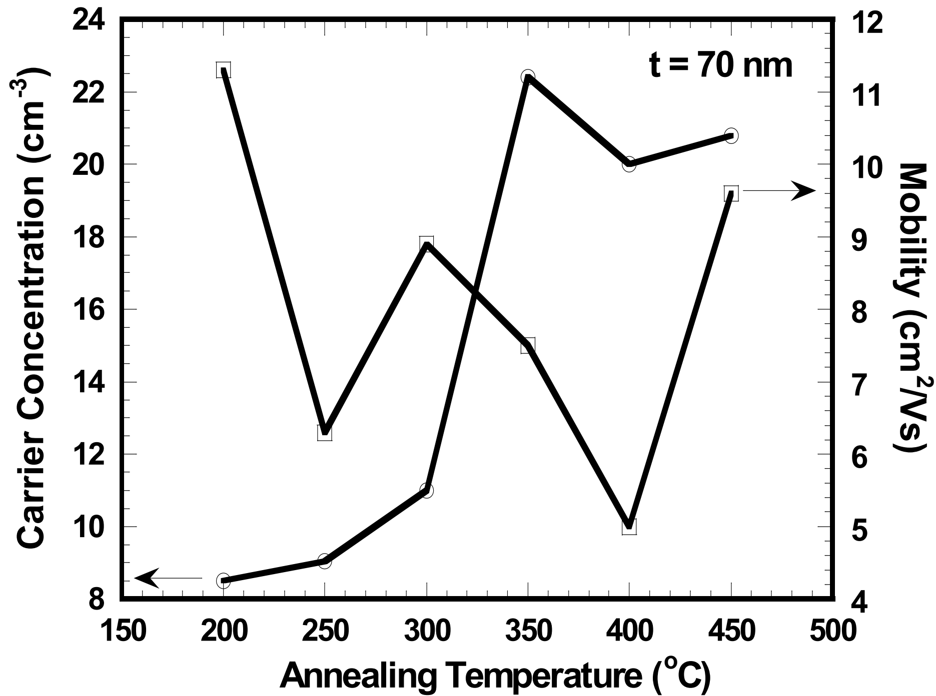

Figure 4. 24. Variation of carrier concentration and Hall mobilities with annealing temperature

4.5.3. Optical Results

4.5.3.1. Optical Transmission of LA-ITO Thin Films

Variation of LA-ITO thin films optical transmission illustrated in figure 4.25. and with increasing the annealing temperature the transmittance was increased. The increasing visible transmittance can be explained by crystal qualith of the films and

band gap values of ITO thin films that is increase with increasing annealing temperature due to Burstain Moss shift. Mentioned before the crystal quality of the films were increased with annealing temperature.

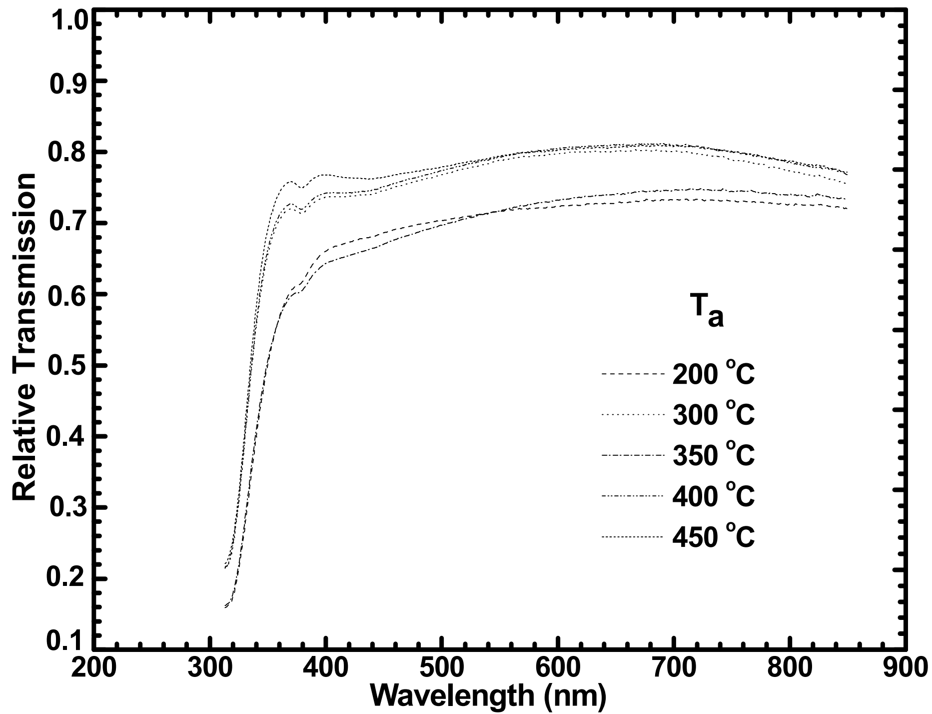

Figure 4.25.Transmission spectrum of LA-ITO thin films

4.5.3.2. Annealing Temperature Dependence Band Gap of LA-ITO Thin Films

As mentioned in sub title 4.4.4 band gap of ITO thin films can be calculate using transmission spectrum of ITO thin films. For this calculation again the reflectance of the films in the visible region were eliminated due to high transmission in that region. As seen in figure 4.25 visible transmissions of the films were above 75%. The behavior of band gap is depending on the variation of carrier concentration because band gap widening and narrowing depend on the carrier cocentration. Band gap values were

measured from absorption spectrum of the films which is shown in figure 4. 26. Band gap of annealed films increased with annealing temperature (Figure 4. 27.) because of the fact that with increasing temperature carrier concentration of the films are increase so it leads to increasing band gap.

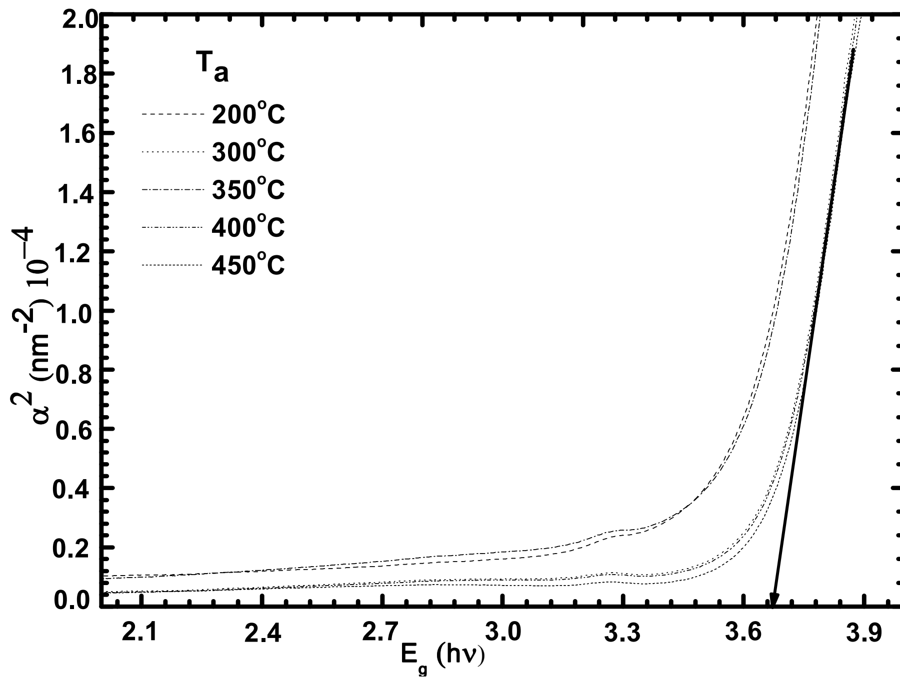

Figure 4.26. Absorption coefficient versus energy gap of LA-ITO samples

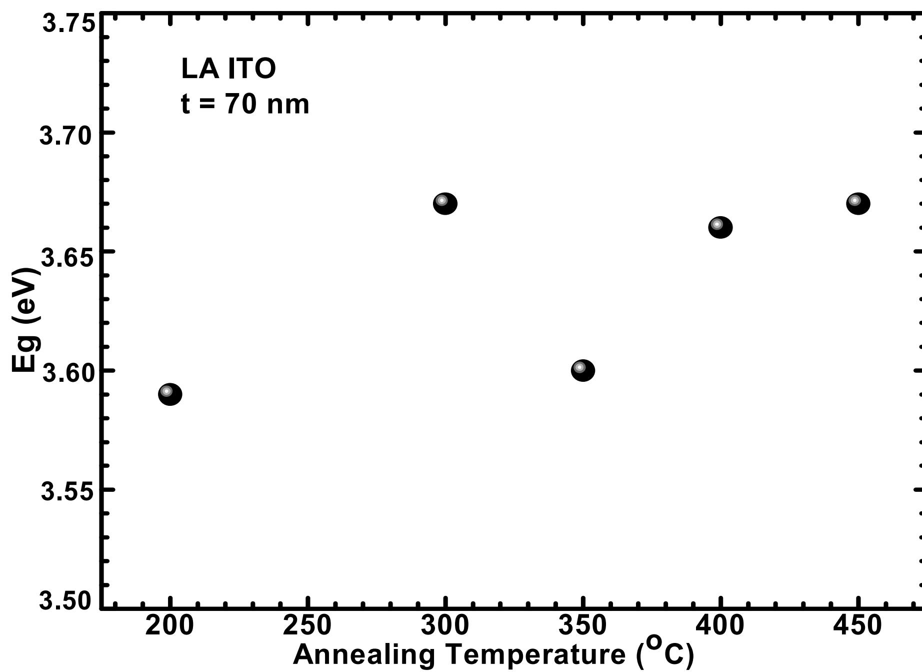

Figure 4.27. Variation of bandgap of LA-ITO thin films versus annealing temperature

CHAPTER 5

SUMMARY AND CONCLUSION

In this thesis I studied growth and characterization of Indium Tin Oxide (ITO) thin film grown by DC and RF magnetron sputtering. Growing process occur under high vacuum condition that is as low as 2×10^{-6} torr. Structural, temperature dependence electrical i.e. Hall effect and R-T measurements and optical characterization were done. Atomic Force Microscopy (AFM), Scanning Electron Microscopy (SEM), X-Ray Diffiraction (XRD), Ellipsometer and Cryostat were used to charactarize samples. Our aim was figure out effect of the substrate temperature and film thickness on film properties. Wan der Pauw method was used for electrical measurements and to use this method properly we patterned film using photolithograph and Ion beam etching. To take take contact on patterned films and also eliminate ohmic contact problem, we evaporate gold on patterned films. From the analysis of our measurements, we deduced that substrate temperature substentially affect all film properties especially electrical and structural properties. While for DCMS grown samples crystallization direction change from (222) to (400) and (440), for RFMS grown samples it changes from (222) to (211) and (440) with increased substrate temperature. The reasons of these changes were mobility of ad-atoms, clusters and also density of crystal planes. The effects of substrate temperature on electrical properties were notable. Resistivities of the grown samples we decreased with increased substrate temperature. The reasons of this decreasing ware increasing grain size and carrier concentration of the films with subtrate temperature. The films deposited at a substrate temperature of 350 ^{o}C by DC and RF magnetron sputtering showed lowest resistivities that were 1.28×10^{-4} Ω-cm, 1.29×10^{-4} Ω-cm, respectively. Band gap of grown films increased with increasing subtrate temperature which was explained with Burstain-moss shift. The largest band gap for DCMS samples was observed at the substrate temperature of 350 ^{o}C and 400 ^{o}C with the value of 3.81 eV and for RFMS grown samples it was observed at the subtrate temperature of 300 ^{o}C with the value of 3.80 eV. The band gap differences between DCMS and RFMS grown

samples can be explained with different scattering mechanism in RFMS grown films such as ionized impurity scattering, neutral defect scattering and grain boundary scattering. The effective one was grain baundary scattering due to at substrate temperature of 350 ^{o}C, grain size of RFMS grown films were decreased. Subtrate temperature is also substantially effective on carrier concentration and Hall mobilities. Carrier concentration increament was observed with subtrate temperature increament. It is known that oxygen vacancy and the activated Sn in In site are the two main sources of the free electrons in ITO thin films. As discussed above the crystallinity of ITO film increased with substrate temperature. This higher degree of crystallinity results in the lessen oxygen vacancy and, therefore, Sn atoms would have a higher possibility to produce free electrons. The other reason of this increase may due to increase in the diffusivity of tin atoms with four valance electrons in interstitial locations and grain boundaries, replacing In atoms with three valance electrons. Temperature dependence of Hall coefficient measurements was done and the results show that Hall coefficient was not change much with temperature. The slow change was related to highly degenerate band structure of ITO. It is known that ITO thin films are highly degenerate *n*-type semi conductors; the variation of electrical properties with temperature is small. The other important results of ITO thin films were transmission in the visible range. One of important properties of ITO is high infrared reflectivity and high visible transmission in the light spectrum. Substrate temperature was not much effective on transmission but film thickness was directly affected it. Substrate temperature is also affect crystallinity and resistivity of the films. For instance resistivity decreased with increased thickness. Resistivities of the films were calculated by multiplying sheet resistance and film thickness therefore it was expected that result. Crystallinity detection of films increased with film thickness because it is related with penetration depth of the light. When the thickness of the films increased, the light can not penetrate into substrate and we can observe films effect on crystallinity.

REFERENCES

Adurodija, F.O., Izumi, H., Ishihara, T., Yoshitoka, H., Yamada, K., Matsui, H., Motoyama, M. 1999. Highly Conducting Indium Tin Oxide (ITO) Thin Films Deposited by Pulsed Laser Ablation. Thin Solid Films 350:79-84.

Ali, H.M., Mohamed, H.A., Mohamed, S.H. 2005. Enhancement of the Optical and Electrical Properties of ITO Thin Films Deposited by Electron Beam Evaporation Technique. Jornal Apply Physics 31:87-93.

Akkad, F. E., Punnoose, A., Prabu, G. 2000. Properties of ITO films prepared by rf magnetron sputtering. Apply Physics A 71:157-160.

Akkad, F.E., Marafi, M., Punnoose, A., Prabu, G. 2000. Effect of Substrate Temperature on the Structural, Electrical and Optical Properties of ITO Films Prepared by RF Magnetron Sputtering. Physics State solution 177: 445-452.

Azens, A., Granqvist, C. G. 2003. Electrochromic Smart Windows: Energy Efficiency and Device Aspects. Journal Solid State Electrochemical 7:64-68.

Ammerma, D., Böhler, A., Kowalsky, W. 1995. Multilayer Organic Light Emitting Diodes for Flat Panel Display. Institute of Hochfrequenztechnik, TU Braunscweig.

Adorodija, F. O., Izumi, H., Ishihara, T., Yoshioka, H., Matoyama, M., Murai, K. 2000. Influance of Substrate Temperature on the Properties of Indium Oxide Thin Films. Journal Vacuum Science Technology 18:814-818.

Brauer, G. 1999. Large Area Glass Coating. Surface and Coating Technology 112:358-365.

Comini, E., Faglia, G., Sberveglieri, G. 2001. UV Light Activation of Tin Oxide thin Films for NO_2 Sensing at Low Temperature. Sensor and Actuatory 78:73-77.

Chrisa, X. P. 1998. Growth and Characterization of Indium Oxide (InOx) Films. Ph.D.'s Thesis, University of Crete.

Campet, G., Geoffroy, C., Wen, S. J., Portier, J., Keou, P., Salardenne, J., Sun, Z. W.1991. Influance of Thermal Treatment on the Electronic Properties of ITOThin Films Obtained by RF Cathodic Pulverization. Study of Solar Cells Based on Silicon/(RF Sputtered) ITO Junctions. Active and Passive Electronic Company 14:151- 161.

Chen, Y., Zhou, Y., Zhang, Q., Zhu, M., Liu, F. 2007. The Correlation Between Prefered Orientation and Performance of ITO Thin Films. Journal Matter Science:Matter Electron 18:411-414.

Das, D., Banerjee, R. 1986. Properties of electron beam evaporated tin oxide Films. Thin Solid Films 147:321-331.

Diao, X, Hu, Y., Wang, C., Hao, W., and Wang, T. 2004. Effect of heat treatment on properties of ITO films prepared by rf magnetron sputterin. Vacuum 75:183-188.

Ding, F. L., Jow, L. Y., Lau, J. J., Su, S. L., Pavol, S. 2005. Effects of annealing on the properties of indium-tin oxide films prepared by ion beam sputtering. Surface Coating Technology 192:106-111.

Dutta, J., Ray, S. 1988. Variations in structural and electrical properties of magnetron sputtered Indium Tin Oxide films with deposition parameters. Thin Solid Films 162:119-127.

Donald, N. 1997. Semiconductor Physics and Devices (3rd ed.). University of Mexico: McGraw-Hill.

Elfallal, I.,Rilkington, R. D., Hill, A. E. 1993. Formation of a Statistical Thermodynamic Model for the Electron Concentration in Heavily Doped Metal Oxide Semiconductors Applied to the Tin-Doped Indium Oxide System. Thin Solid Films 223:303-310.

Friend, R. H., Gymer, R. W., Holmes, A. B., Burroughes, J. H., Marks, R. N., Taliani, C. D., Bradley, D. C., Santos, D. A. D., Bredas, J. L., Lögdlund, M. W., Salaneck, R. 1999. Electroluminescence in Conjugated Polymers. Nature 397:121-127.

Guillen, C.,Herrero, J. 2006. Influance of oxygen in the deposition and annealing atmosphere on the charecteristic of ITO thin films prepared by sputtering at room temperature. Vacuum 80:615-620.

Gupta, L., Mansingh, A., Srivastava, P. K. 1998. Band Gap Narrowing and the Band Structure of Tin Doped Indium Oxide Films. Thin Solid Films 176:33–44.

Jianming, Z. 2005. Indium Tin Oxide (ITO) Deposition, Patterning and shottky Contact Farication. Ph.D.'s Thesis. Rochester Institute of Technology.

Jayaraj, M. K., Nisha, M., Anusha, S., Antony, A., Manoj, R. 2005. Effect of Substrate Temperature of ITO Thin Films. Applied Surface Science 252:1430-1435.

Kerkache, L., Layadi, A., Dogheche, E., Remiens, D. 2006. Physical Properties of RF sputtered ITO Thin Films and Annealing Effect. Applied Physics 39:184 - 189.

Kittel., C. 2004. Introduction to Solid State Physics. New York:John Wiley and Sons INC.

Lee, H. C., Park, O.O. 2004. Electron Scattering Mechanism in Indium Tin Oxide thin Films: Grain Boundary and Ionized Impurity Scattering. Vacuum 75:275-282.

Lii, D. F., Huang, J. L., Jen, L. J., Lin, S.S., Sajgalik, P. 2005. Effect of Annealing on the Properties of Indium Tin Oxide Films Prepared by Ion Beam Sputtering. Surface and Coating Technology 192:106-111.

Lee, H. C., Park, O. O. 2004. Behaviors of carrier concentration and mobilities in indium tin oxide thin films by dc magnetron sputtering at various oxygen flow rates. Vacuum 77:69-77.

Lee, H. C., Seo, J. Y., Choi, Y. W., Lee, D. W. 2004. The growth of indium-tin-oxide thin film on glass substrate using DC reactive magnetron sputtering. Vacuum 72:269-276.

Licciulli, D. A., Lisi, D. 2001. Electrochromic Glass. University of Degli.

Lee, H. C., Park, O. 2006. The Evoluation of the Structural, Electrical and Optical Properties of Indium Tin Oxide Thin Film on Glass Substrate by DC Reactive Magnetron Sputtering. Vacuum 80:880-888.

Matin, M. A., Jezierski, A. F., Bashar, S. A., Locklisan, D. E., Benson, T. M., Cheng, T. S., Roberts, J. S., Sale, T. E., Orton, J. W., Foxon, C. T., Rezazadeh, A. A. 1994. Optically Transparent Indium-Tin-Oxide (ITO) Ohmic Contacts in the Fabrication of Vertical-Cavity Surface-Emitting Lasers. Electronic Letters 30:318-320.

Meng, L. J., Santos, M. P.D. 1998. Properties of indium tin oxide films prepared by rf reactive magnetron sputtering at different substrate temperature. Thin Solid Films 322:56-62.

Meng, L. J., Dos, M. P. 1998. Prpperties of Indium Tin Oxide Films Prepared by Reactive magnetron Sputtering at Different Substrate Temperature. Thin Solid films 322:56-62.

Marazio, M. 1965. Refinement of the Crystal Structure of In_20_3 at two Wavelengths. Acta Crystal 20:723-728.

Nisha, M., Anusha,S., Antony, A., Manoj, R., and Jayaraj, M. K. 2005. ''Effect of substrate temperature on the growth of ITO thin films'', Applied Surface Science. Vol. 252, pp. 1430-1435.

Piromreun. P., Oh, H., Shen, Y. L., Malliaras, G. G., Scott, J. C., and Brock, P. J. 2000. Role of CsF on electron injection into a conjugated polymer. Applied Physics Letter 77:2403-2409.

Reddy, V. S., Das, K., Dhar, A., Ray, S. K. 2006. The Effect of Substrate Temperature on the Properties of ITO Thin Films for OLED Aplications. Semicondors Science Technology 21:1743-1747.

Reddy, V., Sivaji, K., Das, A., Dhar and Ray, S. K. 2006. The effect of substrate temperature on the properties of ITO thin films for OLED applications. Semiconductor Science Technology 21:1747-1752.

Sahabbir, A. B., 1998. Study of Indium Tin Oxide for Novel Optoelectronics Devices. Ph. D.'s Thesis, University of London.

Sanon, G., Raj, R., Abhai, M. 1991. Band-gap Narrowing and Band Structure in degenerate Tin Oxide (SnO_2) films. Physical Review B 44:5671-5680.

Tang, C. W., Vanslyke, S. A. 1987. Organic Electroluminescent Diodes. Apply Physics Letter 51:913-920.

Tang, Z., Chan, P. C. H., Sharma, R. K., Yan, G., Hsing, I. M., Sin, J. K. O. 2001. Investigation and Control of Microcracks in Tin Oxide Gas Sensing Thin Films. Sensor and Actuatory 79:39-47.

Whang, K. W., Kim, J. K. 2005. Discharge Physics of Alternating Current PlasmaDisplay Panels (PDPs). Journal Display Technology 1:295-303.

Zhang, Q., Yuqin Z., Yao C., Meifang, Z.,Fengzien, L. 2007. The correlation between prefered orientation and performance of ITO rhin films. J mater sci:Mater Electron 18:411-414.

Zhao, L., Zhou, Z., Peng, H., Cui, R. 2005. Indium Tin Oxide Thin Flms by Bias Magnetron RF Sputtering for Heterojunction Solar Cells Application. Applied Surface Science 252:385-392.